HYPERSPECTRAL IMAGERY FOR LARGE AREA SURVEY OF ORGANOPHOSPHATE PESTICIDES

THESIS
MARCH 2015

Daniel R. Baseley, Captain, USAF

AFIT-ENV-MS-15-M-203

DEPARTMENT OF THE AIR FORCE
AIR UNIVERSITY

AIR FORCE INSTITUTE OF TECHNOLOGY

Wright-Patterson Air Force Base, Ohio

AFIT-ENV-MS-15-M-203

HYPERSPECTRAL IMAGERY FOR LARGE AREA SURVEY OF ORGANOPHOSPHATE PESTICIDES

THESIS

Presented to the Faculty

Department of Systems Engineering and Management

Graduate School of Engineering and Management

Air Force Institute of Technology

Air University

Air Education and Training Command

In Partial Fulfillment of the Requirements for the

Degree of Master of Science in Industrial Hygiene

Daniel R. Baseley, BSE

Captain, USAF

March 2015

AFIT-ENV-MS-15-M-203

HYPERSPECTRAL IMAGERY FOR LARGE AREA SURVEY OF ORGANOPHOSPHATE PESTICIDES

Daniel R. Baseley, BSE

Captain, USAF

Committee Membership:

Dr. W. F. Harper
Chair

Dr. G. P. Perram
Member

Dr. K. C. Gross
Member

Abstract

Current detection of organophosphate pesticides in residential settings involves taking swipe samples at locations of potential contamination and conducting lab analysis. This method provides results that are applicable only to the points where samples were taken. A standoff detection method utilizing hyperspectral imaging would allow for analysis of a larger area without the need for lab analysis. This report demonstrates a proof of concept experiment that shows the applicability of hyperspectral imaging for the detection of organophosphates. The differences in detection on reflective and non-reflective surfaces are also explored. To the author's knowledge, this research is the first to use the Telops longwave infrared hyperspectral imager to positively identify and locate dimethyl methylphosphonate on both reflective and non-reflective surfaces.

Acknowledgments

I would like to convey my thanks to my faculty advisor, Dr. Willie Harper, for his guidance and patience throughout this thesis process. I would also like to thank Dr. Kevin Gross and the ENP Remote Sensing Group for their support. Finally, I would like to thank my sponsor, the US Environmental Protection Agency National Homeland Security Research Center, for their invaluable insights and support.

Daniel R. Baseley

Table of Contents

Page

List of Figures

Page

List of Tables

Page

HYPERSPECTRAL IMAGERY FOR LARGE AREA SURVEY OF ORGANOPHOSPHATE PESTICIDES

I. Introduction

General Issue

Organophosphate (OP) pesticides are commonly used to eliminate or control insect infestations. However, over-application in residential settings, in some cases, has led to unhealthy living conditions. In particular, it has been identified that some companies, while treating bedbug infestations, have contaminated the living space of their clients. The current sampling methods applied rely on swipe sampling. This method is only effective if swipes are taken in a contaminated area, which makes it difficult to identify all contaminated surfaces. A standoff detection method would allow large area screening for OP chemical contamination and identify specific areas where decontamination is required.

Problem Statement

Current sampling techniques for OP pesticides in residential settings rely on swipe sampling and lab analysis. Swipe samples are a proven method, but they only give results from the exact area the swipe was taken. A screening technique that covers a wide area would be of great benefit to ensuring decontamination is conducted on all surfaces that require it.

Research Questions

1. Can hyperspectral imaging be used to detect organophosphate pesticides on a surface in a lab setting?
2. What, if any, illumination technique will be required to detect organophosphate pesticides?
3. Can organophosphate pesticides be detected on various building materials in a lab setting?
4. What is the limit of detection when using hyperspectral imaging to detect organophosphate pesticides on various building materials?
5. Can hyperspectral imaging be used to quantitate contamination levels of organophosphate pesticides on building materials?

Research Focus

This research will focus on the detection of dimethyl methylphosphonate (DMMP). The materials used for this study are stainless steel and formica laminate. These materials represent both reflective and non-reflective surfaces. The data collected will be analyzed to determine if quantification of surface contamination is possible.

Methodology

As a proof of concept, a representative OP will be chosen and applied to both a stainless steel and Formica laminate surface. These surfaces effectively represent both reflective and non-reflective materials. A blackbody source will be used to illuminate the surface and the longwave infrared (LWIR) Telops camera will be set up at the specular angle to collect a hyperspectral image of the surface.

Once the data has been collected, the data cubes for each scene will be averaged and calibrated using the internal blackbodies on the Telops. Further data analysis includes averaging the spectra over the contaminated area of the surface and comparing the spectra for each concentration, as well as comparing the spectra over each image to a representative spectrum of the chemical used to positively identify where contamination exists in each image.

Assumptions/Limitations

There were various limitations and assumptions made in the course of this research. Some of these were due to the nature of conducting experiments in the lab. Others arose from the need to limit the scope of the research to make the data collection and analysis process practical for the purposes of proving the concept.

The intended application of this research is to conduct a large area screening for OP chemical contamination of surfaces inside a residential building. Due to limited space in the protective lab hoods, analysis was only conducted on small samples. This necessitated the use of optics and placing the Telops imager close to the samples to fill as much of the field of view as possible.

It was also deemed necessary to limit the analysis to one OP chemical. There are too many OP chemicals to practically test all of them. This decision was arrived at due to limited availability of equipment and the time necessary to collect data for different concentrations applied. All OP chemicals contain spectral features in the LWIR range. The methods used in this research relies on using the spectrum for this specific chemical

in identifying where contamination is present. Therefore, the method would need to be adjusted to make it applicable to a wide range of OP candidates.

The chemical applied in the lab setting was in a pure form, without the additives present in commercial pesticide products. Because of this, in a real-world application, there may be interferences from other chemicals present. The more volatile nature of these additives may lessen this effect, but was not explored in the course of this research.

Implications

This research would provide a proof of concept for the ability to detect and/or quantify OP chemical contamination on a surface using the Telops LWIR hyperspectral imaging camera. It would show the applicability of the technique for detection on both reflective and non-reflective surfaces.

Preview

It will be shown that it is possible to identify spectral features OP chemicals in the LWIR region using the Telops hyperspectral imager. This was successfully done on both reflective and non-reflective surfaces. A method will be shown that allows one to identify where on the surface contamination exists.

II. Literature Review

Chapter Overview

The purpose of this chapter is to lay a foundation that the research is built upon. The review includes information on why this research is important from a human health perspective. The background and current uses of the technology used in this research will be discussed. The current sampling techniques this proof of concept is meant to improve upon will also be presented.

Relevant Research

Organophosphates are esters of phosphoric acid that are widely used as herbicides, insecticides and chemical warfare agents. As a pesticide, they are primarily used in agriculture, but in some cases, are used in residential and industrial applications (Munoz-Quezada et al., 2013). Organophosphates are effective at eliminating certain insects, but they are also highly toxic to mammals, to include humans. Where there is little control of the use of organophosphate pesticides, such as in developing countries, there are many overexposures to organophosphates. There are an estimated 3 million organophosphate pesticide poisonings worldwide each year (Carey et al., 2013). Developing easy to use detection methods for organophosphates is therefore a very important and worthwhile endeavor.

At high enough exposures to organophosphates, humans may experience acute toxic effects. These effects are due to the inhibition of the acetylcholinesterase (AchE) enzyme. This leads to overstimulation as acetylcholine (Ach) accumulates in the cholinergic brain synapses. The symptoms of acute exposure include salivation, nausea,

vomiting, lacrimation, respiratory depression, seizures, and death (Carey et al., 2013; Munoz-Quezada et al., 2013). Exposure may occur from inhalation, dermal absorption, or ingestion. The binding to acetylcholinesterase is irreversible and chronic exposure to even low concentrations of organophosphates can lead to illness and possible death (Fu et al., 2012).

In addition to the acute effects of organophosphate exposure, research has been done to study the developmental effects exposure may have on children. A review of epidemiological studies showed that in 26 of 27 studies, exposure to organophosphate pesticides was a risk to neurodevelopment, especially for prenatal exposure (Munoz-Quezada et al., 2013).

Studies have been conducted in residential settings to determine the extent of pesticide contamination in the average home. In one study, 27 different pesticides were sampled for. These included three OP pesticides (chlorpyrifos, diazinon and malathion). Samples were taken on the floor and the 95th percentile concentrations were 0.70ng/cm^2 for chlorpyrifos, 0.15ng/cm^2 for diazinon, and 0.05ng/cm^2 for malathion. The maximum detected concentrations were 135ng/cm^2 for chlorpyrifos, 1.1ng/cm^2 for diazinon, and 4.1ng/cm^2 for malathion (Stout et al., 2009.

Fourier transform infrared (FTIR) spectroscopy is a well-established method for chemical identification. In FTIR spectroscopy, a sample spectrum can be compared to a reference spectrum to determine if the sampled chemical is the same as the reference. Problems arise when attempting to use FTIR spectroscopy to detect mixtures or when water is present. However, in most cases FTIR spectroscopy is a powerful tool that provides fast data collection and results with high sensitivity (Smith, 2011).

The chemical bonds between atoms in a compound can be thought of as a sort of spring. These bonds allow for vibrations within the molecule. Vibrations can occur from either stretching or bending of the bond. These modes of vibration have corresponding frequencies which they can absorb. When the molecule is exposed to infrared radiation, the energy of these frequencies are absorbed. This is what created the unique spectral signatures for each compound (Stuart, 1996).

Hyperspectral imaging is a stand-off detection method involving spatial imaging and spectral analysis. Advantages of hyperspectral imaging are that it allows detection without making contact and risking contamination or destruction of the contaminated medium. It has been used in the fields of food safety and quality, pharmaceuticals, and medical diagnostics and has potential for non-contact forensic analysis. Hyperspectral imaging can be used for various parts of the electromagnetic spectrum (e.g. ultraviolet, visible, and infrared) (Edelmen et al., 2012). Because of this, the technique has a wide range of possible applications. The data collected through hyperspectral imaging is in the form of 3-D hyperspectral cubes. The image dimensions consist of the 2-D spatial image and the wavelength associated with each pixel (Qin et al., 2013).

Hyperspectral imaging requires a light source to collect the spectral images. This can be accomplished through illumination or excitation of the target area. The most common illumination sources are halogen lights. Lasers have been used as an excitation source for fluorescence and Raman imaging (Qin et al., 2013).

OP detection methods that have been proved to be reliable with high sensitivity include gas chromatography, liquid chromatography, and mass spectroscopy. While highly effective, these methods require specialized equipment, trained personnel, and are

time consuming (Dutta and Puzari, 2013; Liu et al., 2008). Because of this, these methods are generally not feasible in the field when large numbers of samples or real-time monitoring are required.

Enzyme based biosensors using inhibition of cholinesterase, immunoassays, and organophosphorus hydrolase have been studied and have been found to be effective in detecting organophosphate vapors and particulates. Cholinesterase-based biosensors are highly sensitive and have lower detection limits. However, they have poor selectivity, are one-use detectors, and require a multi-step process. Organophosphorus-hydrolase-based biosensors have potential as continuous environmental detectors (Lee et al., 2009; Liu et al., 2008;Luckarift et al., 2007; White and Harmon, 2004). Immunoassays are selective, sensitive and have a low cost but also have only one use.

Advances have been made in nanotechnology for the detection of chemicals including organophosphates. Carbon nanotube electrodes have shown to be promising in their ability to detect OP chemicals in a liquid medium (Musameh et al, 2012). Initial research into nanoparticle-based enzyme biosensors has shown the method to be possible (Simonian et al., 2004). Nanotechnology has the potential for the development of handheld, real-time, and accurate OP detectors (Goltz et al., 2011).

An overall drawback to the developed detection methods for OP chemicals is the need to either capture it in aerosol form or know where to take environmental samples. Because of this, they may be ineffective in determining residual concentrations after contamination has occurred. A rapid, standoff method of detection, which could cover large surface areas would be advantageous for detecting residual contamination.

Summary

FTIR spectroscopy is a powerful tool for the detection of chemicals. However, most applications of this technology are limited to individual samples collected from a scene or detection at a discreet location. The Telops camera combines the power of FTIR spectroscopy with the ability to spatially interpret the results. This shows promise in improving field detection methods for contaminated surfaces.

III. Methodology

Chapter Overview

The purpose of this chapter is to describe the methods used for data acquisition and analysis. Some trial data collection methods led to the method to be discussed in this chapter. An initial attempt at passive sampling, with malathion applied to a floor tile, showed no spectral change. Another method analyzing OP chemicals absorbed into cardboard showed an ability to spatially differentiate between differing spectra, but the representative spectral features of OP chemicals were not present after analysis of the data. Further details on the trial methods are shown in Appendix A. Finally, data collection was performed using active illumination on two non-absorptive materials: stainless steel and formica laminate. These materials effectively represent reflective and non-reflective surfaces. Absorption spectra were collected for various OP chemicals on both materials using a Bomem MB FTIR spectrometer. From these results, a representative chemical was selected for data collection using the Telops hyperspectral imager.

Equipment and Materials

The Telops LWIR hyperspectral imager utilizes a Michelson interferometer, creating an interferogram for each pixel of the scene. A Michelson interferometer consists of two perpendicular mirrors, where one of them oscillates a distance, δ. A beamsplitter is located in the path of both mirrors. With an ideal beamsplitter, 50% of the radiation passed into it will be transmitted to each mirror. The two resulting beams are reflected back to the beamsplitter, where they combine and interfere with each other. He

resulting beam emerging from the interferometer is detected by the sensor. Figure 1 shows the layout of a Michelson interferometer (Stuart, 1996).

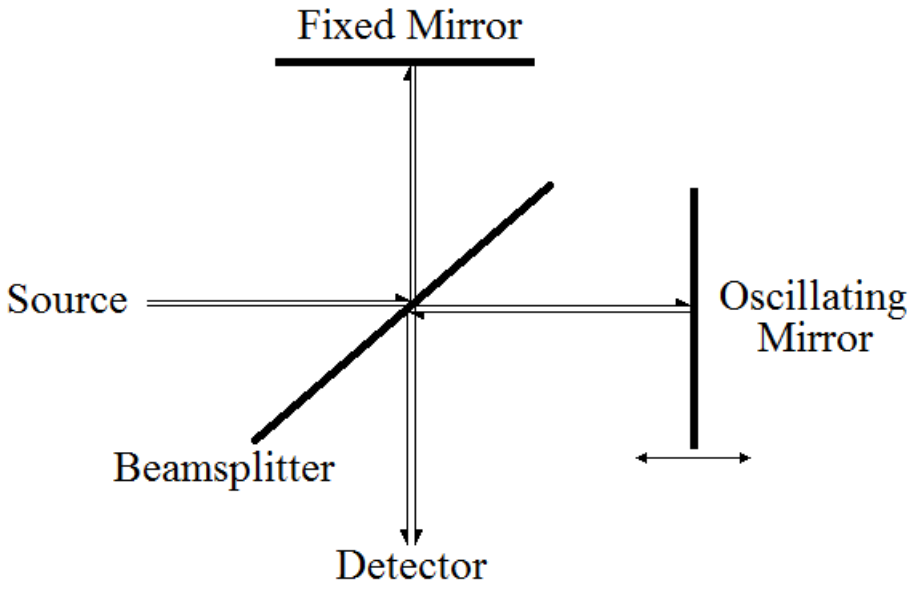

Figure 1 - Michelson Interferometer

To positively identify DMMP in the samples, the spectra obtained must be compared to a reference spectra for DMMP. Figure 2 shows a reference spectra as well as the wavenumbers of the characteristic peaks obtained from Japan's National Institute of Advanced Industrial Science and Technology (SDBSWeb). The LWIR region being sampled should include the four peaks located at 914, 1032, 1186 and 1244 cm^{-1}. Some major features are highlighted on the spectra with the colors matching the bond they correspond to (Reusch, 2013). In addition to the wavenumbers, the shape of the peaks will also be compared.

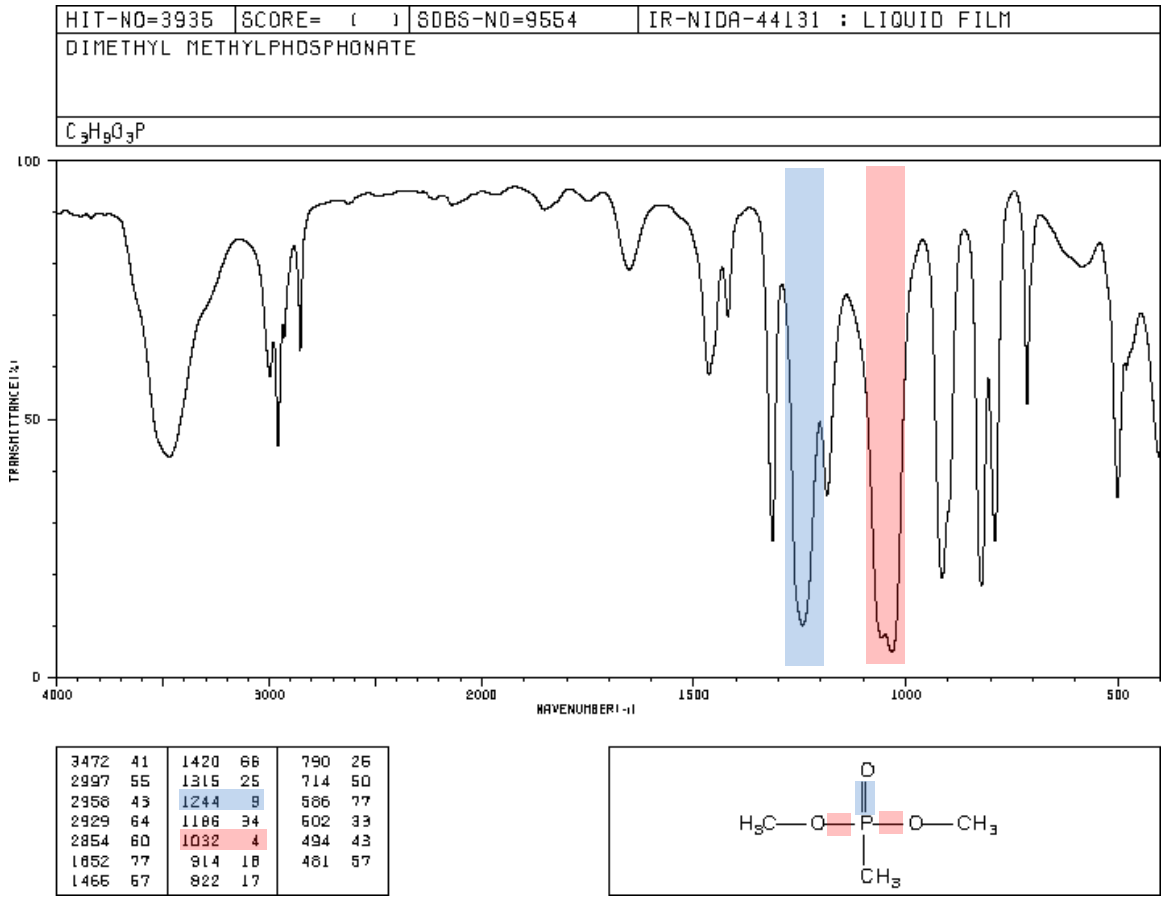

Figure 2 – Reference spectrum for DMMP.

Data Collection

The surfaces for analysis consist of 4" x 4" coupons made of polished stainless steel and formica laminate. DMMP is applied to half of the coupon in different amounts. Two methods of application are used. First, 10, 25 and 50µL are applied by smearing the chemical across the surface with the tip of a pipette. An additional sample of each material is prepared by applying 10µL in an "X" pattern in the center of the coupon. Next 1, 5 and 10µL are applied by creating a solution in methanol and covering half the surface, then allowing the methanol to evaporate.

The coupon is set vertically in a lab hood at a 45° angle relative to the face of the hood. The blackbody illumination source is placed inside the hood, facing the sample at a 45° angle. The Telops LWIR camera is situated outside of the lab hood, also at a 45° angle to the surface. Figure 3 shows a sketch of the experiment layout. Since the Telops is located within 3m of the contaminated surface, a 1.5x optical lens is installed.

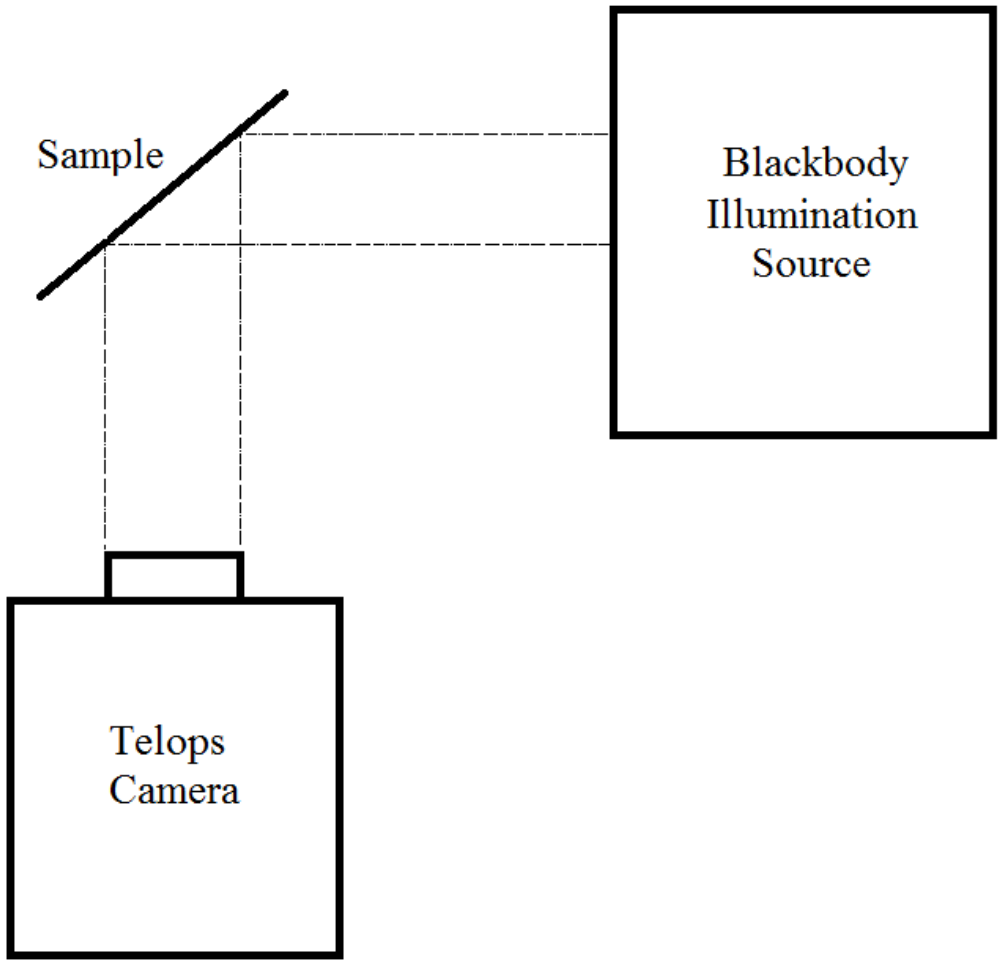

Figure 3 - Sketch of experimental layout

For each image collected, an equal number of acquisitions for each blackbody are also collected for calibration purposes. The internal blackbodies on the Telops are set at

25 and 50°C. Once the sample is in place, the illumination blackbody is adjusted so the signal in the contaminated area is between that of the two internal blackbodies. Table 1 shows the details of each scene collected for analysis.

Table 1 - Scenes for analysis

Scene Number	Surface Material	Amount of DMMP Applied (μL)	Application Method	Acquisitions
1	Stainless Steel	0	-	40
2	Stainless Steel	1	Methanol Solution	40
3	Stainless Steel	5	Methanol Solution	40
4	Stainless Steel	10	Methanol Solution	40
5	Stainless Steel	0	-	20
6	Stainless Steel	10	Smear	20
7	Stainless Steel	25	Smear	20
8	Stainless Steel	50	Smear	20
9	Formica Laminate	0	-	40
10	Formica Laminate	1	Methanol Solution	40
11	Formica Laminate	5	Methanol Solution	40
12	Formica Laminate	10	Methanol Solution	40
13	Formica Laminate	0	-	20
14	Formica Laminate	10	Smear	20
15	Formica Laminate	25	Smear	20
16	Formica Laminate	50	Smear	20

Data Analysis

Before further analysis can begin, the datacubes for all the acquisitions collected for each scene are averaged. This reduces signal noise in the data. The scene is then calibrated using the averaged datacubes for each of the blackbodies collected with the scene. The blackbodies have a known temperature and emissivity which allows the scene data to be calibrated. A significant portion of the signal detected by the instrument is due

to the heat generated by the instrument itself. The calibration process effectively corrects for this. An example of an interferogram, taken from the uncalibrated scene data for 25µL DMMP on stainless steel, is shown in Figure 4. The interferogram's optical path difference (OPD) is the position of the oscillating mirror. The full OPD range is from -800 to 800; the interferogram in Figure 4 was shown for a smaller range to make the waves of the interferogram clearer. The intensity at the OPD extremes is the broadband intensity that will be used to generate the broadband image.

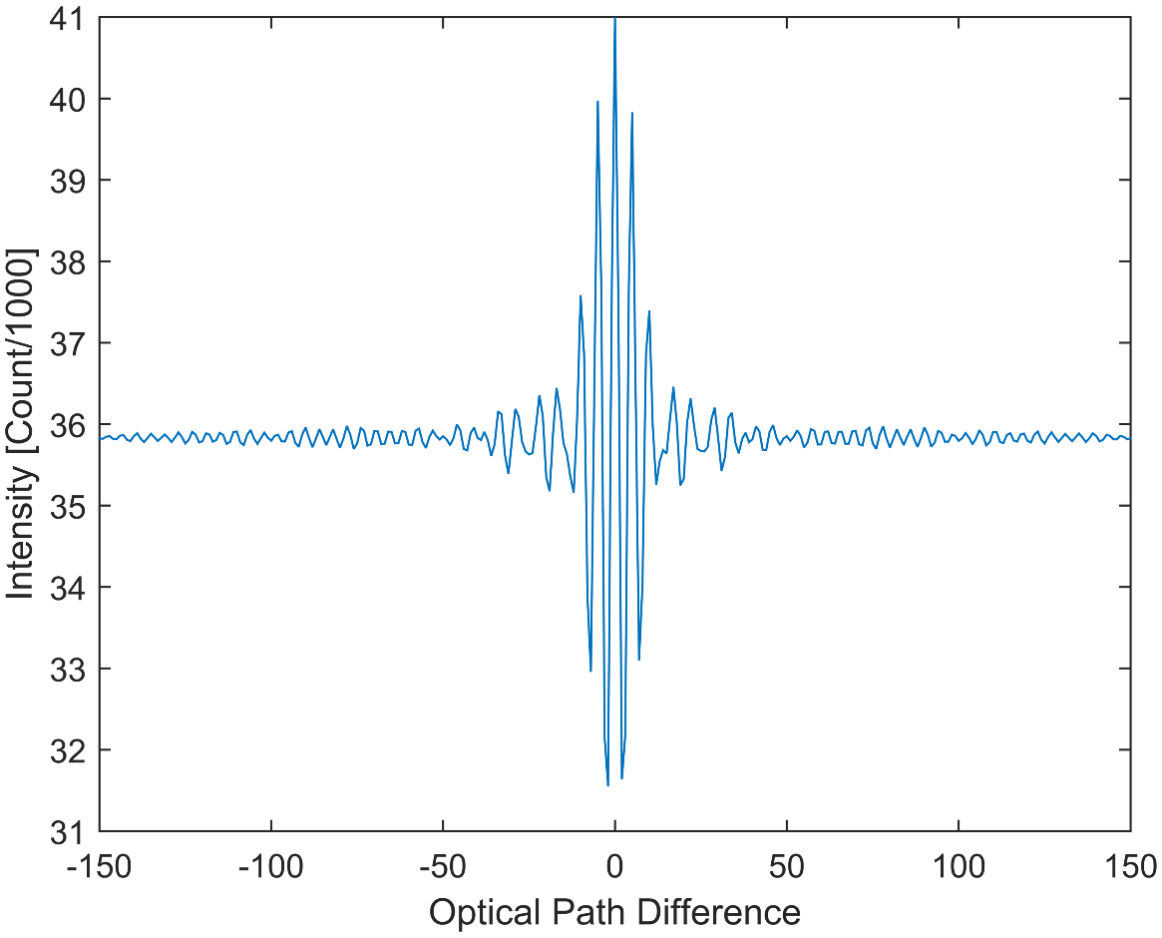

Figure 4 –Interferogram from 25µL DMMP on stainless steel.

The interferograms are converted to spectra by performing a Fourier Transform as shown in Equation 1, where $B(\bar{\nu})$ is the spectral power density, $I(\bar{\nu})$ is the intensity of

the interferometer intensity, and $\bar{\nu}$ is the wavenumber. Because of the complexity of this operation and the number of interferograms to transform, a computer with high processing power is required.

$$B(\bar{\nu}) = \int_{-\infty}^{\infty} I(\partial)\, cos2\pi\bar{\nu}\partial\, d\partial\ \ \bar{\nu} \tag{1}$$

From the calibrated data, a plot is generated, showing the mean spectra at each pixel. This plot can be used to determine if contaminated areas can be observed at this point in the data processing.

There are two types of spectra possible in this analysis. First, there is an absorptive spectra, where the spectral features of the chemical are shown as less intense than the baseline, as the chemical absorbs energy at the frequencies corresponding to its modes of vibration. Secondly, there may be an emissive spectra, where the chemical emits energy that is greater than that which is being reflected due to excitation of the chemical after absorbing energy at those frequencies. Two methods are used to calculate the spectral angle between the spectrum of each pixel and a reference spectrum. The difference is that in one method, the absorption spectrum will be used to calculate the angle for all scenes, regardless if the spectra present are absorptive or emissive. In the other method, an absorptive reference spectrum is used for scenes with absorptive spectra and an emissive reference spectrum is used for scenes with an emissive spectrum. Both methods will show their ability to qualitatively identify where contamination is present.

A background spectra is found by averaging the calibrated spectra over the surface of a non-contaminated surface. This is done for both types of surfaces and is used to generate spectra corrected for atmospheric and surface interferences. This

background spectra is subtracted from the spectra in the scene. The resulting spectra are each subtracted by their respective means, which eliminates any intensity shifts present and brings their mean to zero. This corrected spectra is then compared with the reference spectra to determine the spectral angle using Equation 2, where the angle, θ, is the ant cosine of the dot product of the spectra divided by the product of their magnitudes.

$$\theta = cos^{-1} \frac{A \cdot B}{\|A\|\|B\|} \quad (2)$$

To attempt to quantitate the concentrations present, the spectral intensities are used. A representative spectra for the scene is obtained by taking the mean of the spectra across the contaminated area. These spectra are shifted so, for each scene, they have the same reference point. For absorptive spectra, the spectra is subtracted by the maximum spectral intensity. For emissive spectra, if the spectra is subtracted by the minimum intensity, an issue arises due to the fact there is a feature near the low end of the wavelength range, causing the spectra for different scenes to have shifts in intensity. To get around this, each spectra is subtracted by the intensity at a wavelength with no feature present, in this case 1142 cm^{-1}. Next the emissive spectra are all corrected by adding the minimum intensity from the lowest concentration. The spectra for each surface than can all be plotted on the same axis for comparison. The mean value for each of these averaged spectra is used to observe the trend of intensity vs concentration. To determine the statistical limit of detection, three times the standard deviation of the spectral means of each bare material is used. To get these values, the spectra from each pixel of the bare samples are manipulated as described above. The mean spectra for each pixel is

produced and from these, the overall mean and standard deviation of each bare material is calculated.

Summary

This methodology allows for a small scene in a lab setting to be analyzed for contamination. Each step of the data analysis is used to improve the clarity of the scene and improve the ability to positively detect the chemical of concern. Finally, the construction of a calibration curve provides a means to quantitatively analyze the scene.

IV. Analysis and Results

Chapter Overview

The analysis of the data showed that it is indeed possible to identify where contamination exists using the Telops hyperspectral imager. Figures generated throughout the analysis can be used to see how each step in the methodology is improving the clarity of the results.

Results of Data Analysis

After averaging each scene, a broadband image was generated. This image is a color plot where the colors represent the logarithm of the broadband intensity (counts). This image shows the intensity of the edge of the interferogram for each pixel. This provides a rough image of the scene before any calibration has taken place. Figures 5 and 6 show the broadband images for the stainless steel and formica laminate scenes with 5μL of DMMP applied. The remaining figures are shown in Appendix B.

Once calibration was complete, calibrated images were generated. These images show the average spectral intensity over the sampled range for each pixel. Heavily contaminated areas of the image can be seen more clearly in these than the broadband images. Figures 7 and 8 show these calibrated images for the 5μL scenes. The other scenes' calibrated images are found in Appendix C.

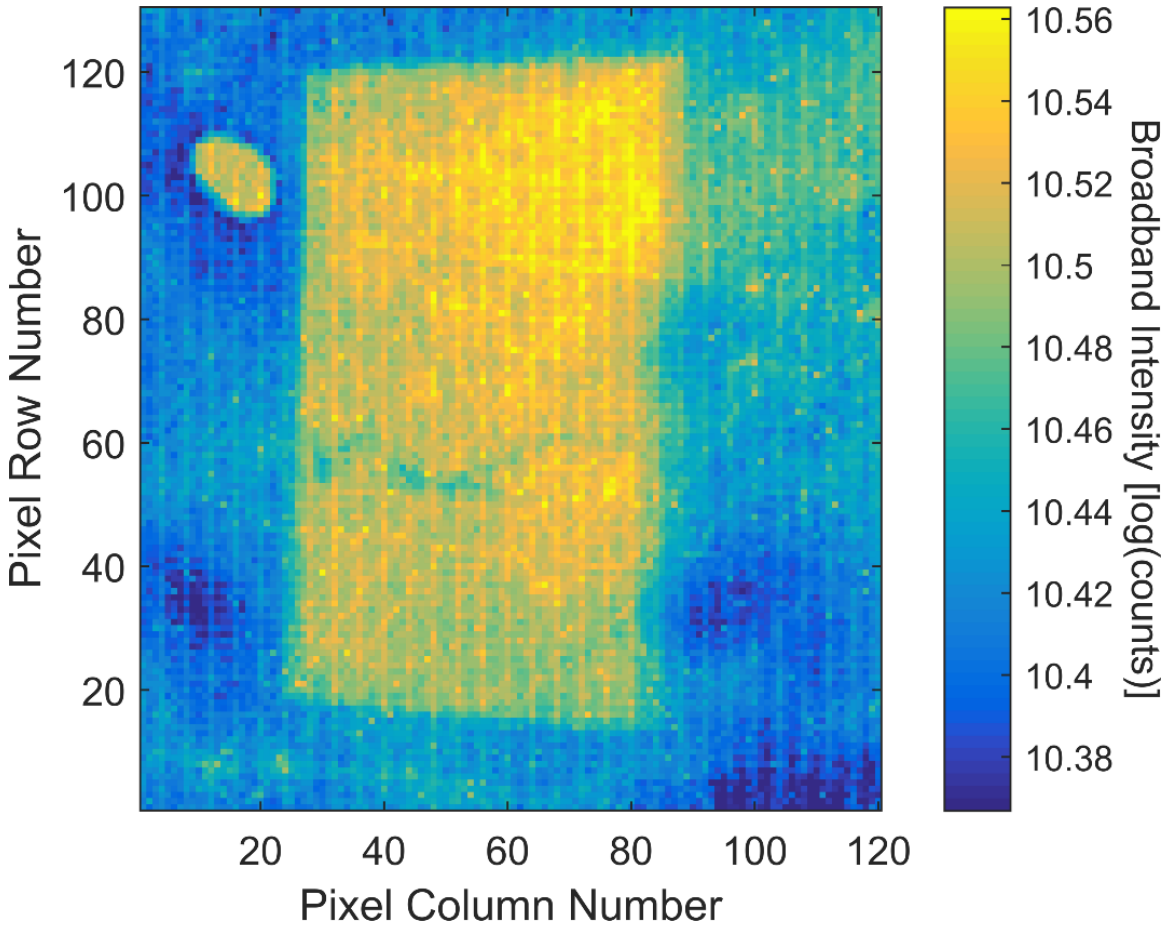

Figure 5 - Broadband image of 5µL DMMP applied to stainless steel.

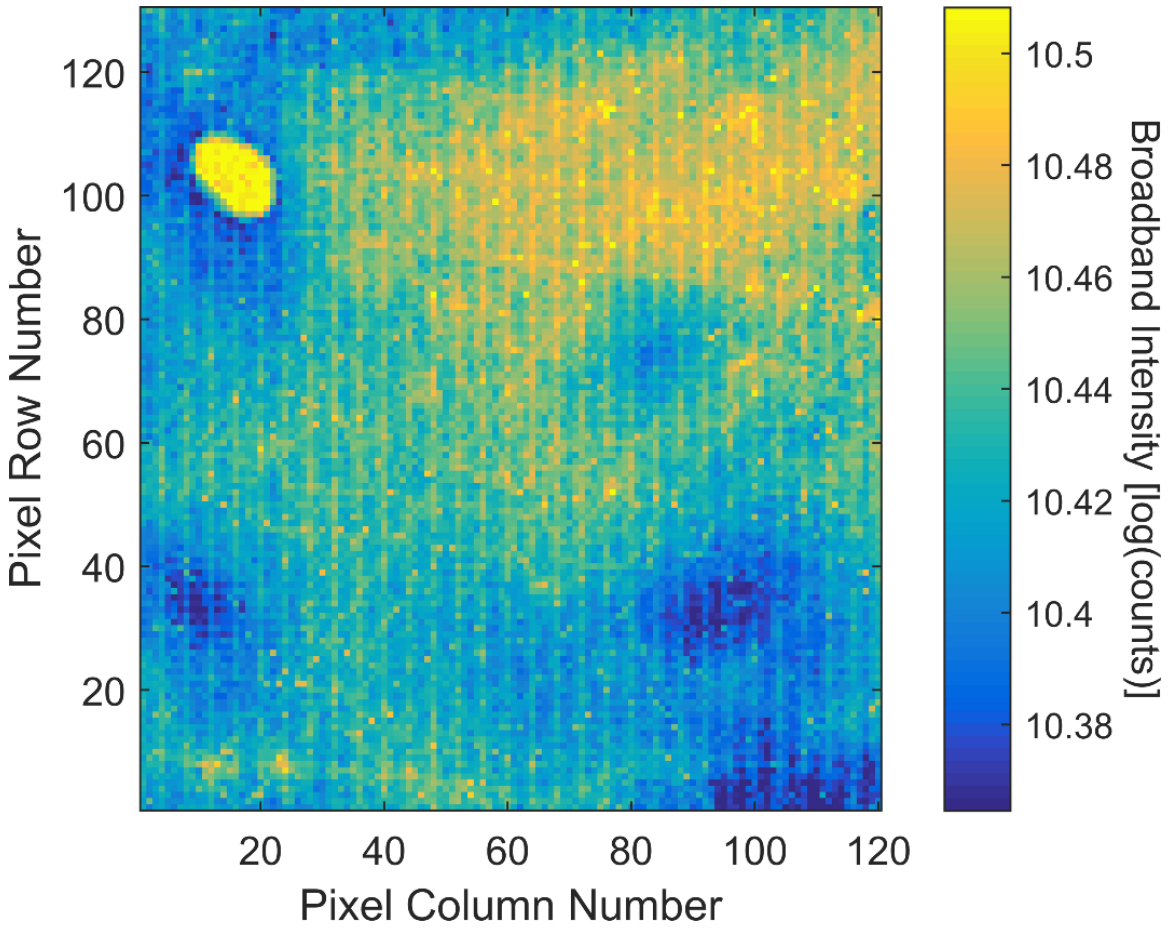

Figure 6 - Broadband image of 5µL DMMP applied to laminate.

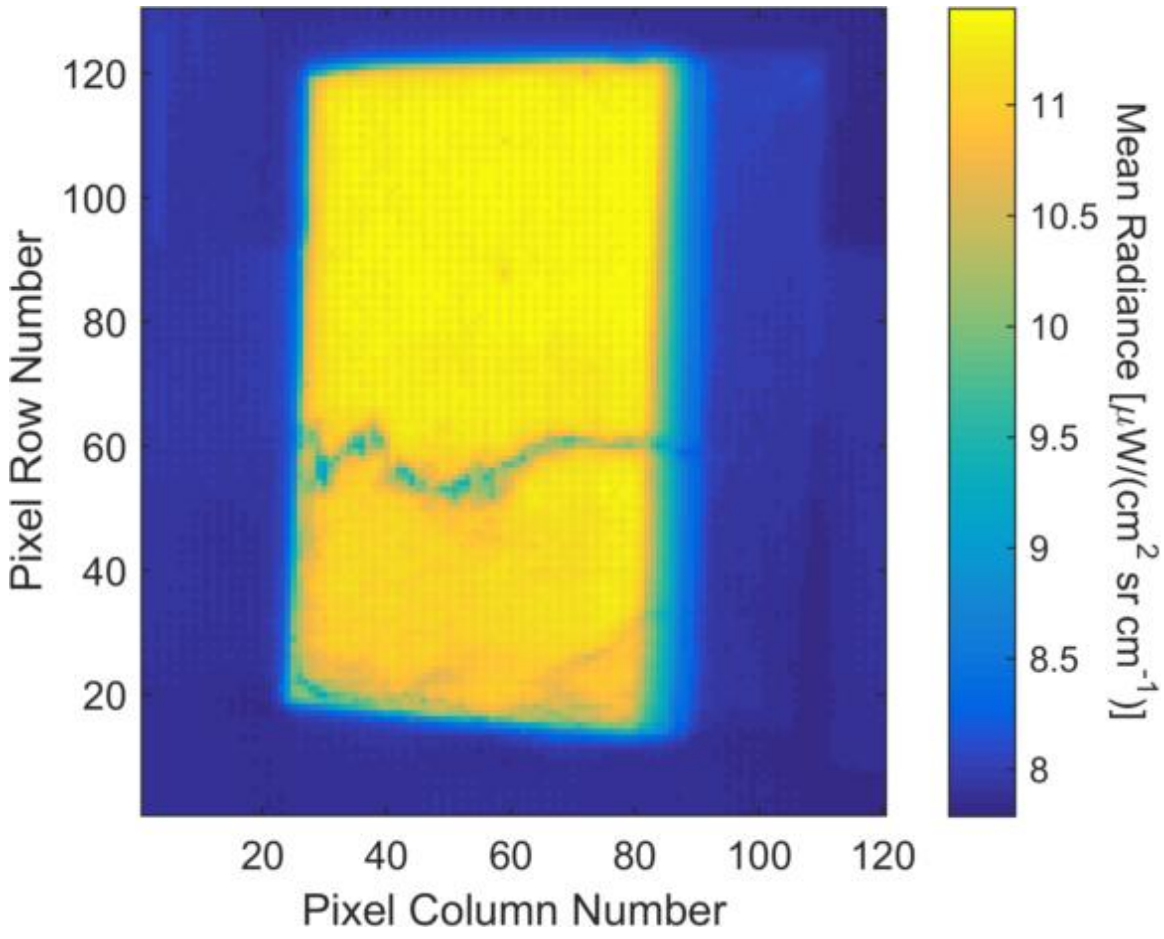

Figure 7 - Calibrated image of 5µL DMMP applied to stainless steel.

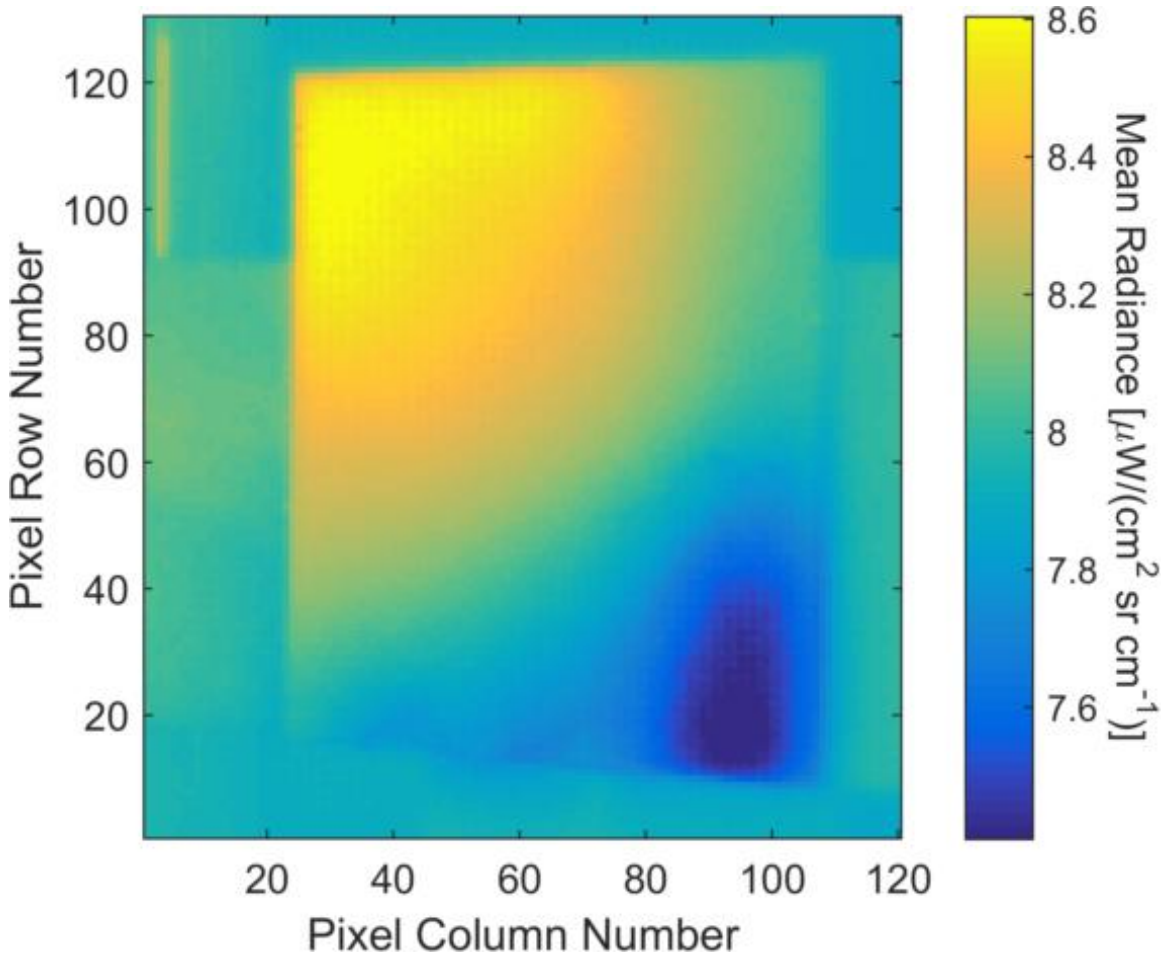

Figure 8 - Calibrated image of 5μL DMMP applied to laminate.

Next, spectral angles were calculated and plotted on a color map. The color maps were forced to have a range of 0 to 150°. This created consistency in the color scheme, however the method of using the absorptive spectrum for the emissive scenes generated less contrast so forcing the bounds on the color scale was not done for these. Figures 9 and 10 show the images generated for 5μL DMMP applied to stainless steel and laminate, respectively. The entire collection of spectral angle plots can be found in Appendix D. It can be seen that contaminated areas of the image, as well as level of contamination, are more distinguishable than in the calibrated images. The blue colored sections of the

image indicate DMMP contamination, with the darker blue being closer to the reference spectra.

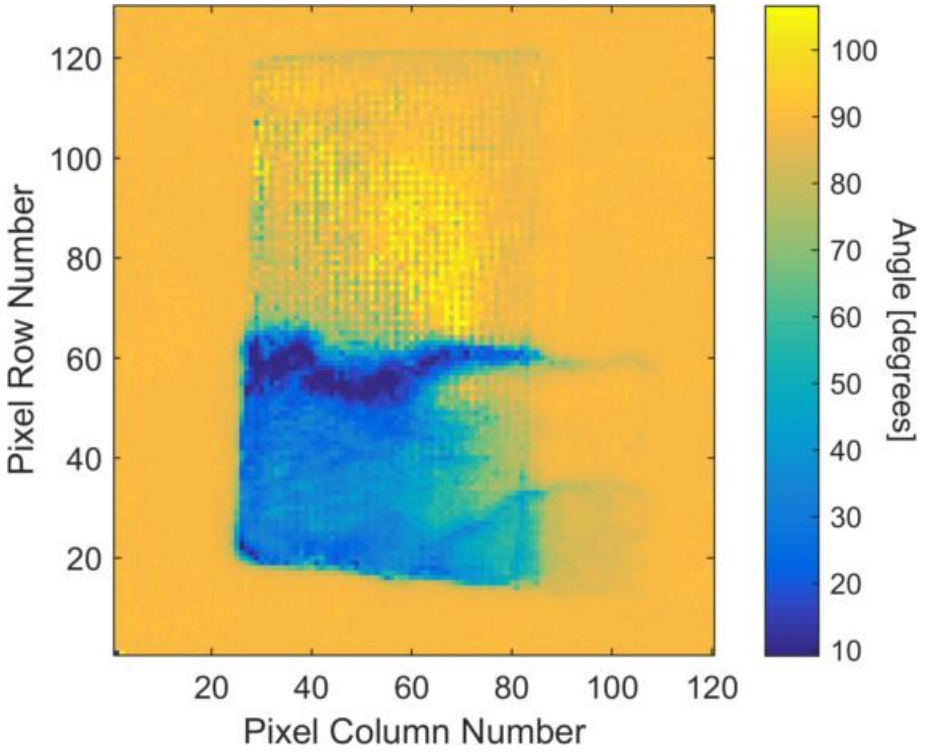

Figure 9 - Spectral angle plot of 5µL DMMP applied to stainless steel.

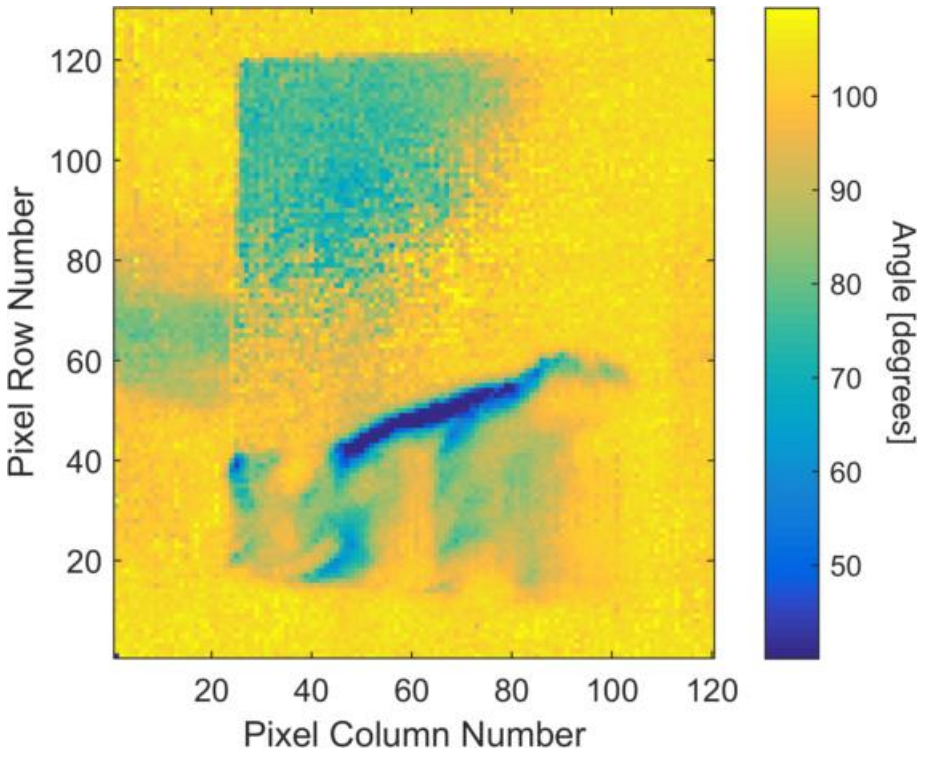

Figure 10 - Spectral angle plot of 5µL DMMP applied to laminate.

The spectra from the contaminated areas of each scene were averaged. The spectra for the first application method, spreading of neat DMMP onto the surface, are shown in Figures 11 and 12. The spectra for the second application method, applying a solution of DMMP and methanol, are shown in Figures 13 and 14. Finally, the spectra for both methods are consolidated and shown in Figures 15 and 16. The individual spectra may be found in Appendix E.

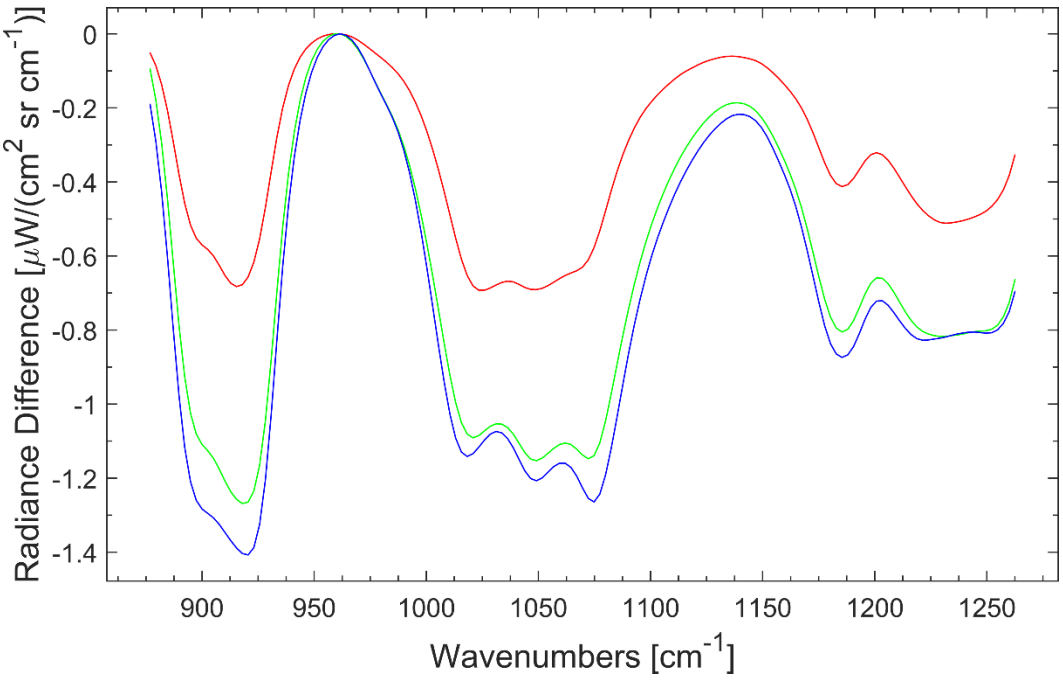

Figure 11 - Average spectral difference for stainless steel with 10µL (red), 25µL (green) and 50µL (blue) DMMP applied.

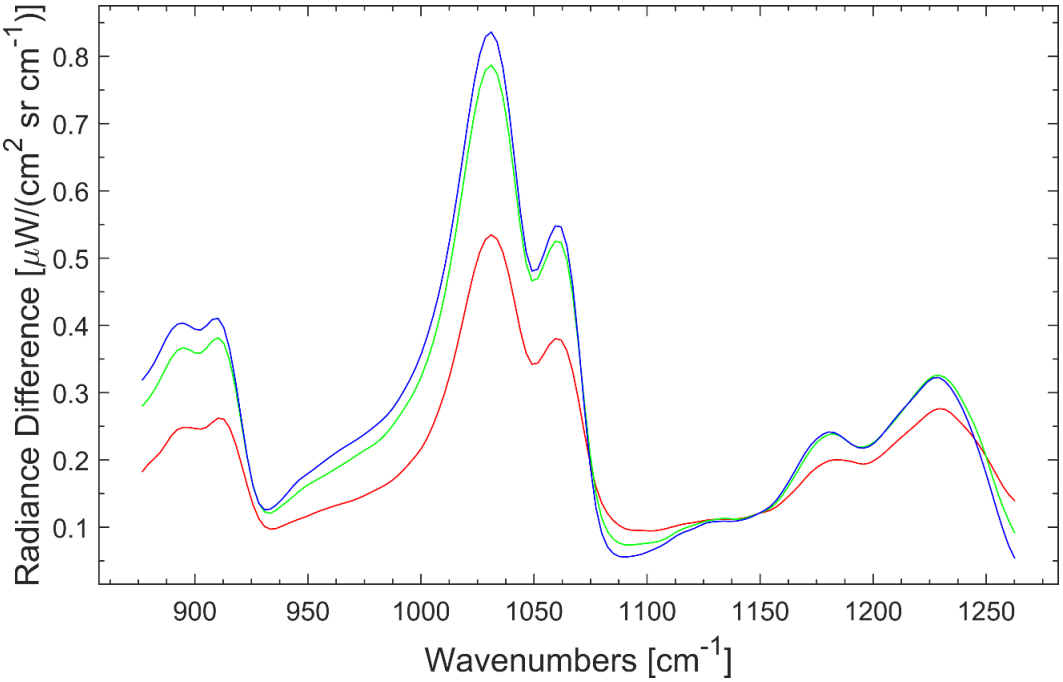

Figure 12 - Average spectral difference for laminate with 10µL (red), 25µL (green) and 50µL (blue) DMMP applied.

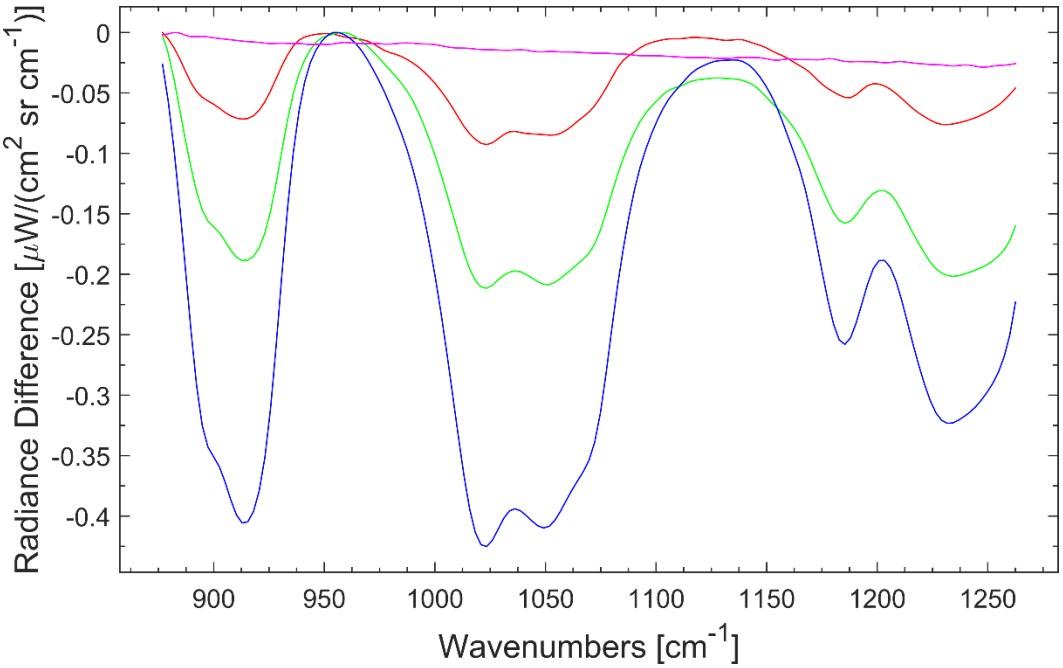

Figure 13 - Average spectral difference for stainless steel with 0µL (magenta), 1µL (red), 5µL (green) and 10µL (blue) DMMP applied.

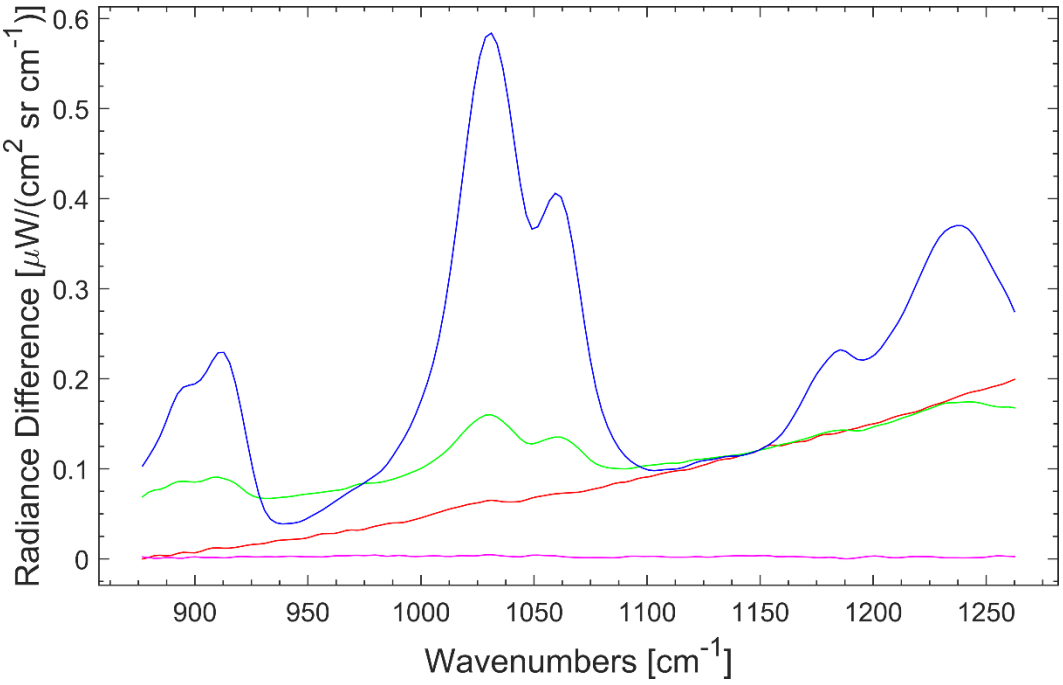

Figure 14 - Average spectral difference for laminate with 0µL (magenta), 1µL (red), 5µL (green) and 10µL (blue) DMMP applied.

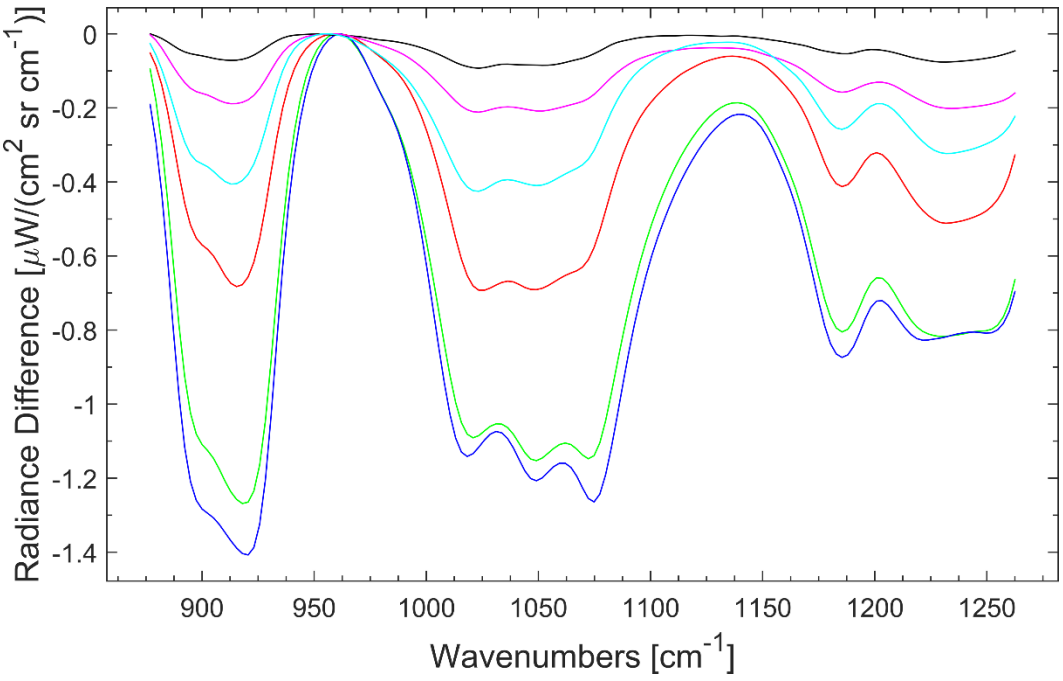

Figure 15 – Consolidated plot of averaged spectral differences for 1-50µL DMMP applied to stainless steel.

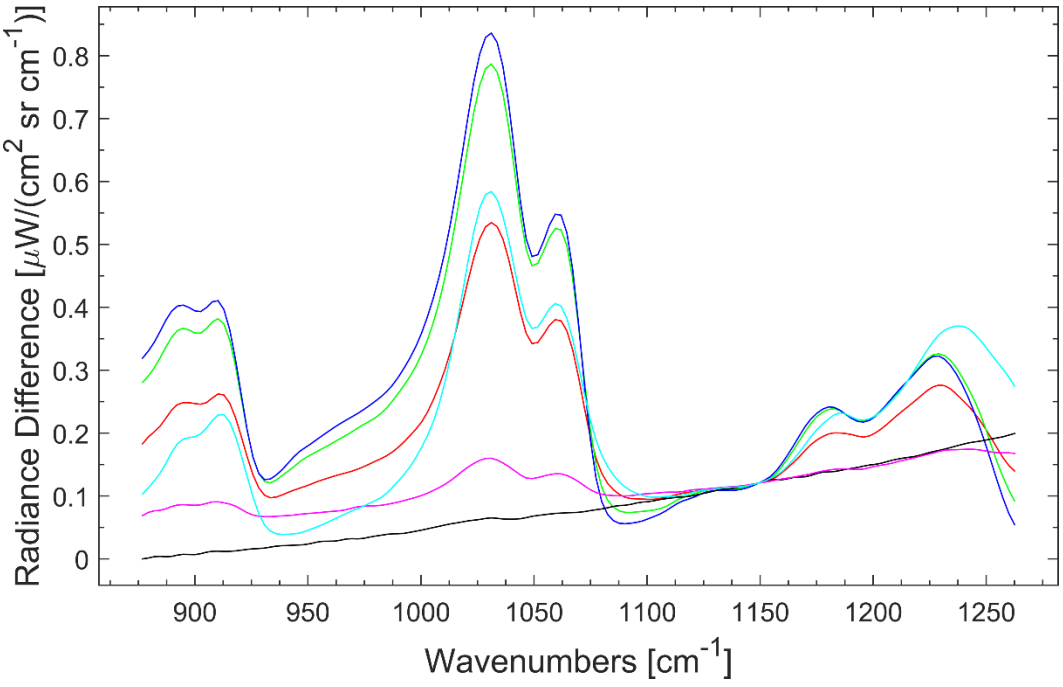

Figure 16 - Consolidated plot of averaged spectral differences for 1-50µL DMMP applied to laminate.

It can be noted from the spectra generated that the spectra for the scenes with 25 and 50μL applied had similar intensities for both surface materials. This is likely due to the fact that they were applied at the same thickness due to the application method. Because of this, only the scenes where DMMP was applied using the solvent will be used for the preliminary quantitative analysis. The mean intensity for each of these spectra are shown in Table 2. A negative spectral difference represents absorbance, while a positive spectral difference represents emission. The surface contamination level was calculated with the assumption that the chemical was applied evenly over exactly on half the coupon ($8in^2$) and a density of 1.145 g/mL for DMMP. The mean spectral differences were plotted against the approximate surface contamination level and a trend line was fitted, as shown in Figures 17 and 18. Trend lines forced through the zero intercept, are shown in Figures 19 and 20. This prevents the statistical limit of detection from being a negative concentration, and the equations generated from these fits are used to calculate limits of detection.

Table 2 – Mean radiance difference of scene spectra

Surface	DMMP Applied (μL)	Approx Concentration ($\mu g/cm^2$)	Mean Spectral Difference ($\mu W/(cm^2\ sr\ cm^{-1})$)
Stainless Steel	1	22	-0.041478
Stainless Steel	5	111	-0.11660
Stainless Steel	10	222	-0.20612
Formica Laminate	1	22	0.084123
Formica Laminate	5	111	0.11692
Formica Laminate	10	222	0.21199

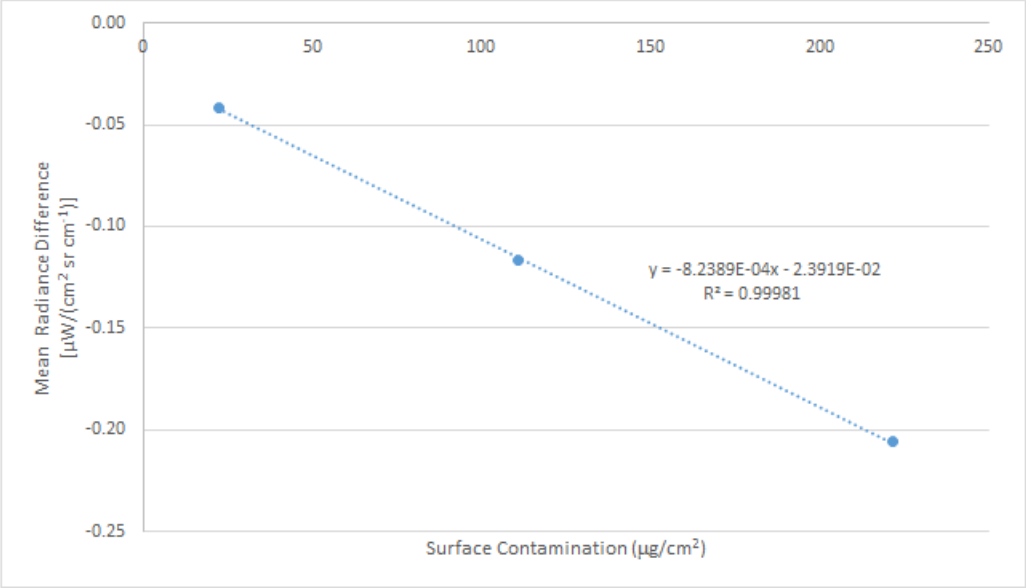

Figure 17 - Mean spectral differences plotted against surface concentration of DMMP on stainless steel

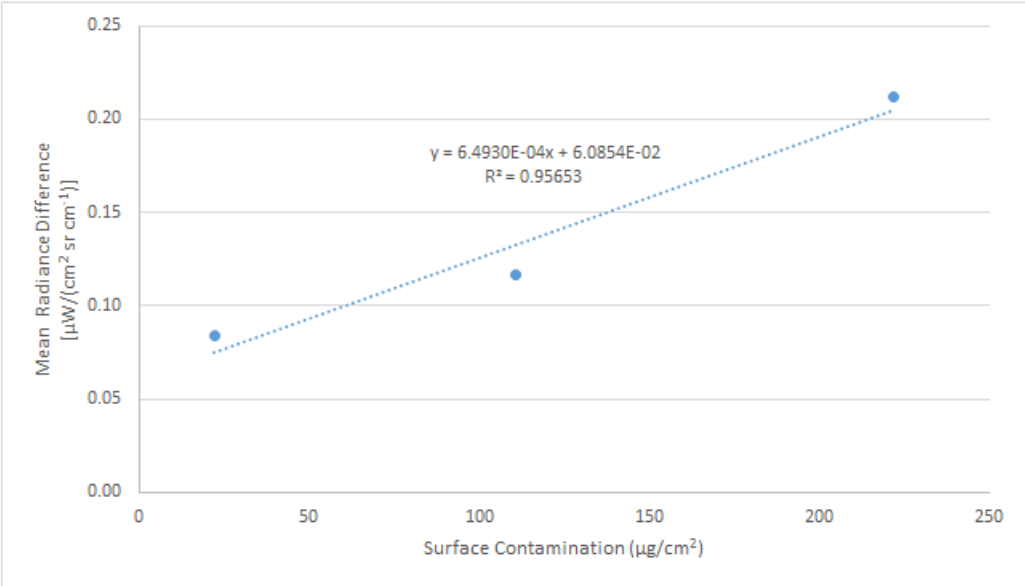

Figure 18 - Mean spectral differences plotted against surface concentration of DMMP on laminate

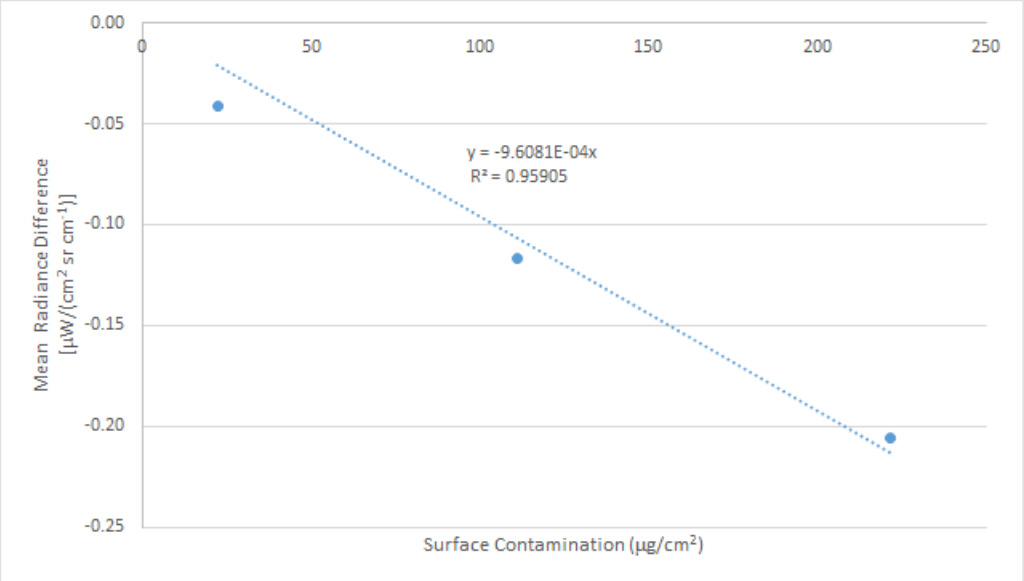

Figure 19 - Mean spectral differences plotted against surface concentration of DMMP on stainless steel. The trend line is forced through the zero intercept.

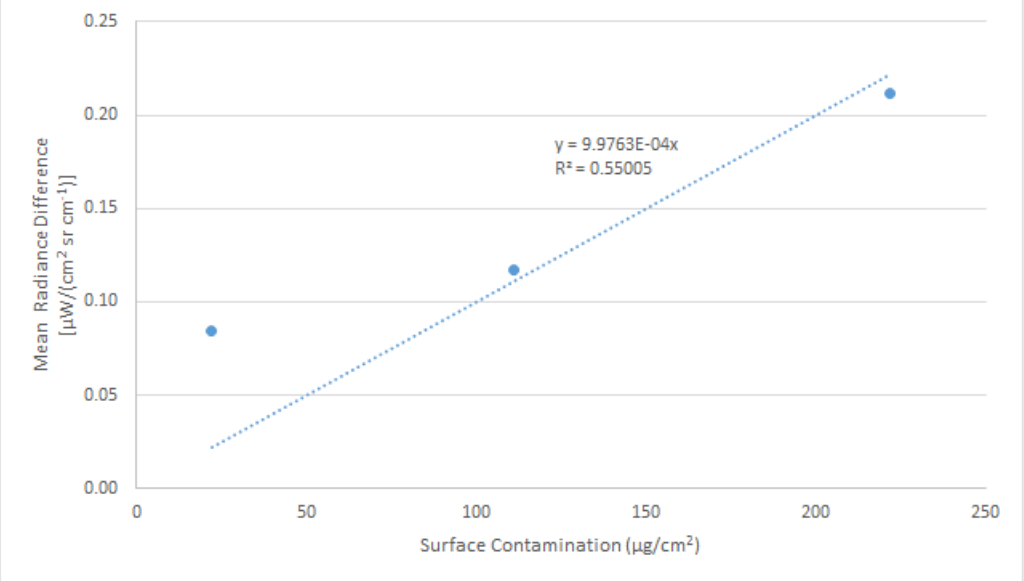

Figure 20 - Mean spectral differences plotted against surface concentration of DMMP on laminate. The trend line is forced through the zero intercept.

While the generated trend lines show promise in developing a linear calibration curve, the use of a single sample average does not allow proper statistical confidence intervals to be generated. It was attempted to separate each scene into sections to allow for several averages, but the uneven deposition of chemical on the surface made this difficult, as there were areas of higher and lower concentrations.

The mean spectral intensity difference of the bare stainless steel scene was -2.9473E-5 μW/(cm^2 sr cm^{-1}) with a standard deviation of 1.8168E-3 μW/(cm^2 sr cm^{-1}). The mean difference for the bare formica laminate scene was 6.5439E-6 μW/(cm^2 sr cm^{-1}) with a standard deviation of 4.2560E-4 μW/(cm^2 sr cm^{-1}). Adding three standard deviations to each mean yields -5.4799E-3 μW/(cm^2 sr cm^{-1}) for stainless steel and 1.2833E-3 μW/(cm^2 sr cm^{-1}) for formica laminate. Solving the trend line equations shown in Figures 18 and 19 for the x variable gives Equations 3 and 4 for stainless steel and formica laminate, respectively, where x is the surface contamination in μg/cm^2 and y is the mean spectral intensity. Inputting the limits of detection for each material, the statistical limits of detection were found to be 5.70μg/cm^2 for stainless steel and 1.29μg/cm^2 for formica laminate.

$$x = -\frac{y}{9.6081*10^{-4}} \quad (3)$$

$$x = \frac{y}{9.9763*10^{-4}} \quad (4)$$

Investigative Questions Answered

This research showed that OP pesticides can be detected using hyperspectral imaging. It was shown that illumination is necessary. For a reflective surface, active illumination allows an absorptive spectra to be obtained. For a non-reflective surface, it

is suspected that the illumination source heated the chemical at a higher rate than the surface, which allowed an emissive spectra to be seen. A rough limit of detection was obtained for both reflective and non-reflective surfaces, which made it possible to quantitate contamination levels in this experimental setup.

Summary

Each step in the data analysis made the location of the contamination clearer, improving the qualitative results. Using the spectral angle method with a reference spectra allows one to identify the contaminated pixels as they have smaller angles than the background pixels. The quantitative analysis shows linearity in the absorptive spectra, which suggests that the calibration curve is applicable. The 1μL scene on laminate, however, was outside the linear calibration curve. This may be due to poor distribution of the chemical over the surface. Another issue with the 1-10μL scenes was that the blackbody was not properly aligned with the coupon, cutting off the right edge of the sample. This would have negligible effects if the chemical were uniformly distributed, but could be a cause of the elevated intensity for the 1μL scene.

V. Conclusions and Recommendations

Chapter Overview

As a proof of concept, this research showed that hyperspectral imaging is a potential candidate for OP detection in the field. It shows more promise for detection on reflective surfaces. To duplicate the results in the field for non-reflective surfaces, a method of heating a large area to cause emission would be required. The instrument would not allow for real-time analysis of a scene, but would allow for data collection, and with the proper code in place, would allow for fairly rapid analysis.

Conclusions of Research

It could be observed that for every step of analysis, the surface contamination became more distinctive in the images generated. The spectral angle method appears to be a good qualitative option for identifying where contamination is present.

As a proof of concept, this research showed that it is indeed possible to detect OP chemical contamination using the Telops hyperspectral imager. However, the method of detection between reflective and non-reflective surfaces differ. Detection on a reflective surface is relatively straight-forward. An illumination source reflects radiation off of the surface and into the Telops, while any chemical on the surface absorbs radiation at certain wavelengths. However, the spectra obtained from the non-reflective surface were not absorptive spectra. This likely indicates that the illumination source was causing heating of the scene. If the DMMP was heating faster than the surface, it would show emission, which may be the case here. While this led to successful detection in the lab, it

is unclear from this research how one would go about heating surfaces in this manner in the field.

The analysis of the spectra showed that the features present matched those the reference DMMP spectrum. There were also no additional peaks. The peaks are at approximately the same wavelength, with a small shift in two of the cases. The shifts may be attributed to differing sampling techniques. There were likely interferences at the boundaries of the chemical film, which caused the shifts. The shapes of the peaks also match. Table 3 shows the peak location comparison and peak descriptions. The peak locations were consistent throughout the scenes collected.

Table 3 – Spectral feature comparisons.

Peak Description	Reference Wavenumber (cm^{-1})	Experimental Wavenumber (cm^{-1})	Peak Shape Match?
Strong peak with shoulder	914	913	Yes
Strong feature with two peaks	1032	1023	Yes
Weak peak	1186	1186	Yes
Strong peak	1244	1244	Yes

The solvent used for application, methanol, was allowed to evaporate prior to scene collection. There was a chance that methanol would interfere with the spectra due to a strong peak at $1030cm^{-1}$. The spectra for methanol is shown in Figure 21 (SDBSWeb). However, the spectra analyzed matched that of the reference DMMP spectra, so interference was minimal, if any. It would have been prudent to select a different solvent that does not have any spectral features in the LWIR range sampled.

Some examples would be carbon tetrachloride (Figure 22), which has no substantial features in this range or xylene (Figure 23), which has weaker features.

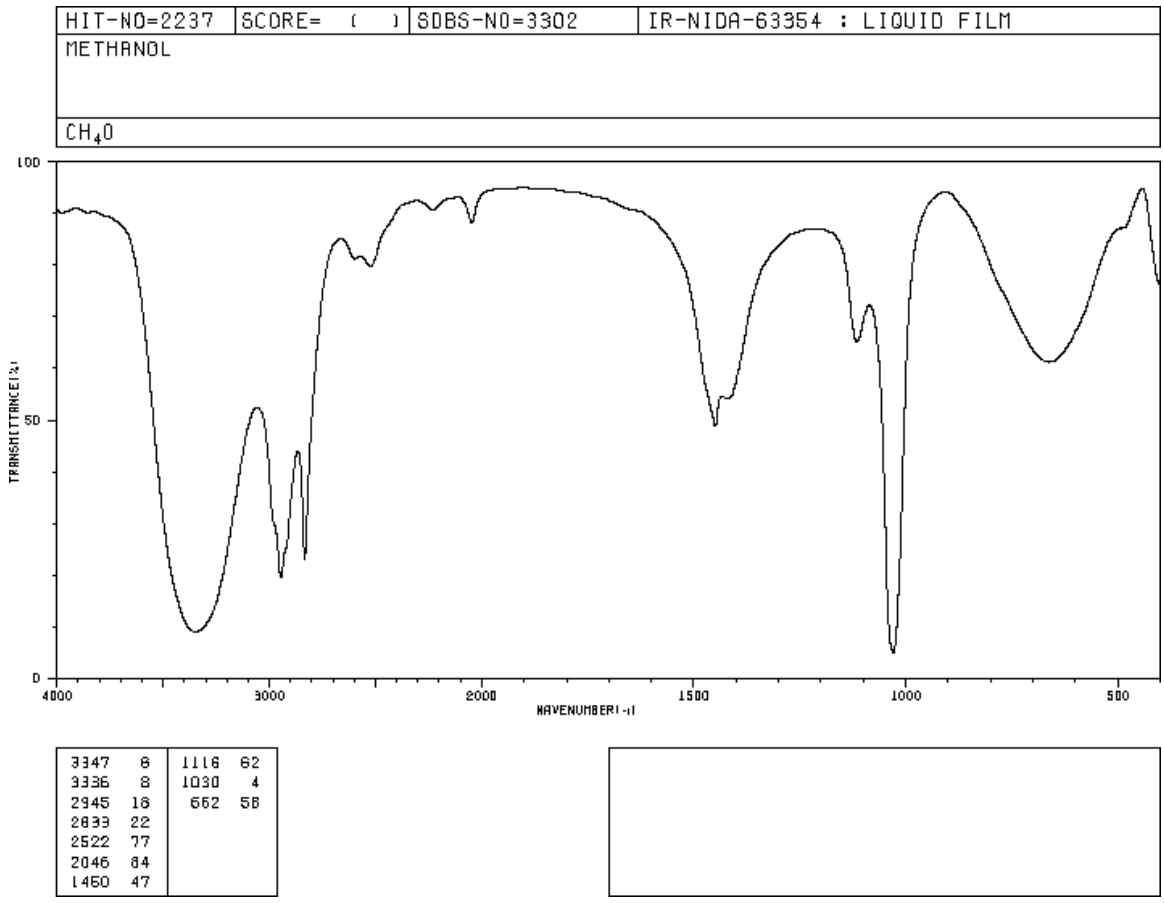

Figure 21 – IR spectrum for methanol.

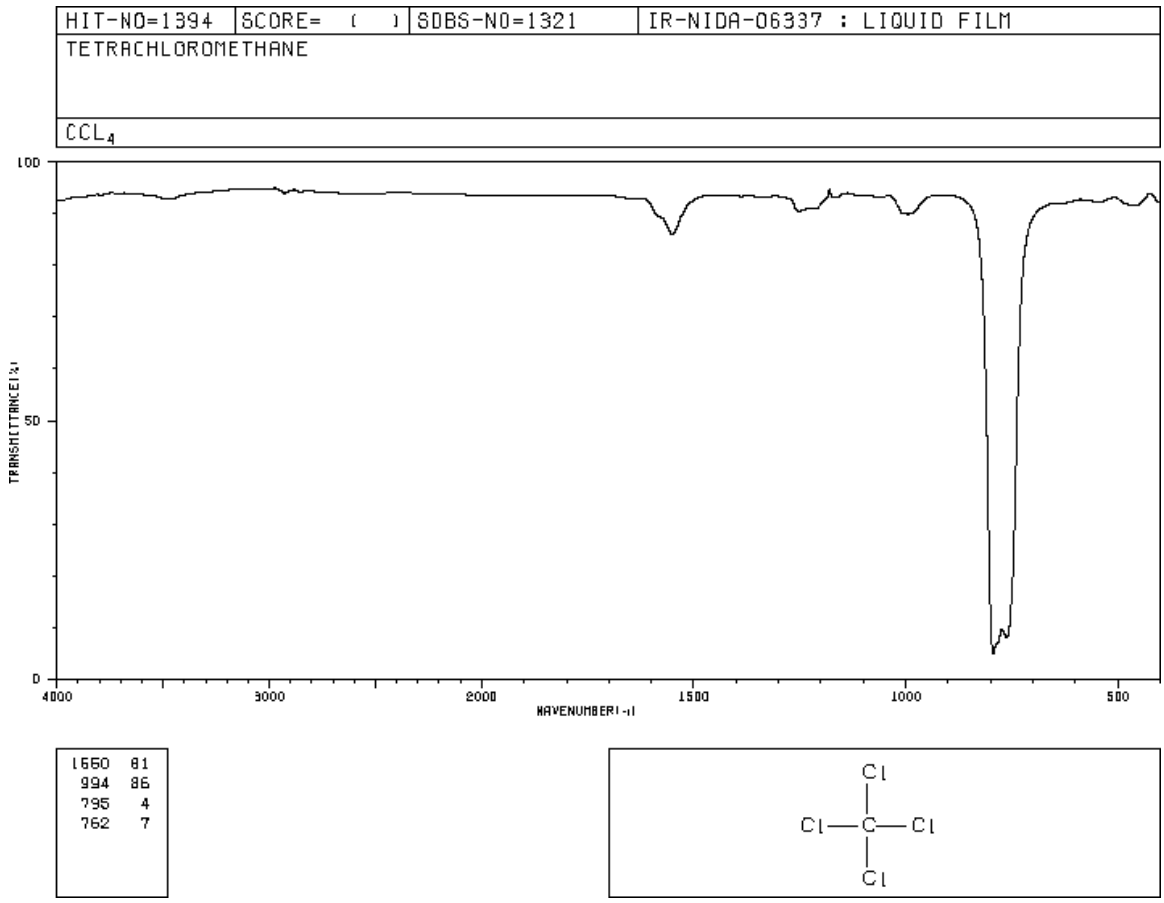

Figure 22 – IR spectrum for carbon tetrachloride

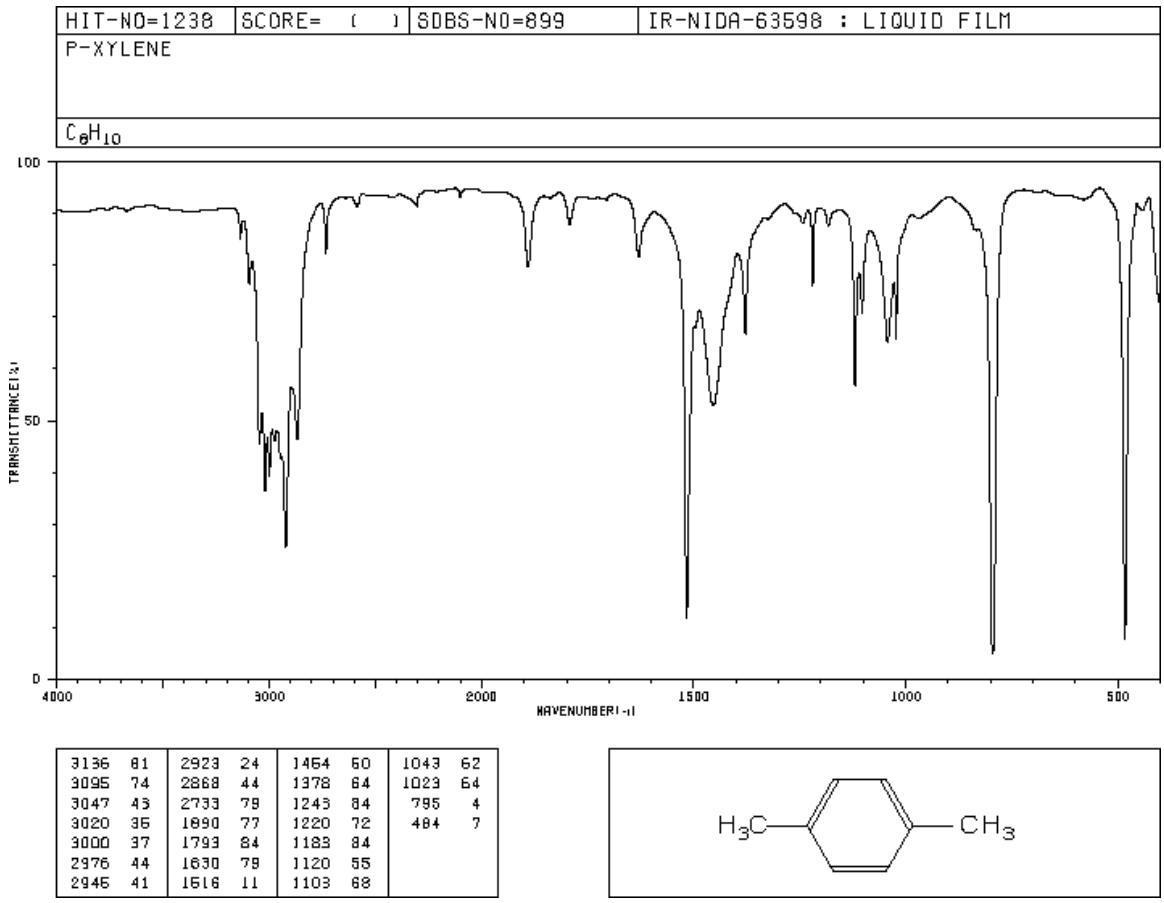

Figure 23 – IR spectrum for xylene.

The method used relied on knowing what OP chemical was applied to the surface. It is possible that other OP chemicals could be seen, but the spectral angles would not be as close. However, with chemical other than the reference spectrum present, the spectral angle of the contaminated areas would still be relatively grouped, making it possible to be able to qualitatively identify where it is present. If the chemical of concern is known, the method can be altered to apply the applicable reference spectrum.

The quantitative results for DMMP applied to stainless steel yielded a very good linear fit to the plotted mean spectral intensities (R^2=0.9998). The results for DMMP applied to Formica laminate were also fairly good (R^2=0.9565). However, when forcing

the trend line to intercept at zero intensity for zero concentration, the fit was 0.9591 and 0.5501 for stainless steel and laminate, respectively. The trend line for the laminate surface fit the data points where 5 and 10μL applied. The 1μL spectral intensity difference was greater than the trend line, which greatly reduced the fit. Since the spectra are averages over a large area of the scene, it is possible that the greater amounts were more accurately averaged because they were applied more evenly over the coupon. If the whole 1μL of DMMP deposited on the illuminated section, it would be more concentrated than if it had spread over the entire half of the coupon. There was an issue of the blackbody illumination being out of line on these samples, causing the edge of the coupon to not be illuminated. If the 1μL sample all settled in the illuminated area, it is possible that the averaged spectra intensity would increase, since it would be concentrated in a smaller area.

One issue with applying this methodology in the field is that there is no known non-contaminated sections of the surface. To overcome this, a section of each surface being analyzed could be cleaned prior to scene collection. This would provide the bare section needed to obtain the background spectra. Another problem is that the quantitative analysis performed during this research may not be directly applicable to another data collection setup. Since linearity in the calibration curve has been shown, it may be possible to "spike" another clean section of the surface with a known amount of chemical to be used to generate a two-point calibration curve.

The qualitative analysis performed, which included developing the spectral angle plot to compare to the reference spectra, has limited usefulness. While is effectively showed the deposition pattern of the chemical, it lacks quantitative power. The method is

strictly qualitative and cannot assign concentrations to the angle between the spectral vectors.

Significance of Research

This research demonstrated a potential method for identifying areas of a scene that have a similar spectra. The specular angle method shown was effective for differentiating between clean and contaminated pixels with a cutoff point of about 60°. The identification of OP pesticides on surfaces was shown to be possible with the Telops camera. However, the methods used in this research will need to be further tested to show that they are viable in the field and a method for illuminating or heating non-reflective surfaces may need to be explored. While the initial quantitative analysis looks promising in developing a linear relationship, more testing is necessary to gain statistical confidence.

Recommendations for Future Research

1. Developing a method for quantitative analysis of OP contamination over a large surface area.
2. Method for detection of OP contamination over a large area on non-reflective surfaces.
3. Determining application of method to other OP pesticides and commercial products.

There are alternate data processing methods available that may produce improved selectivity. A more traditional absorbance or transmittance spectra analysis may benefit and have more success in developing a quantitative method. A limit of detection with

this method could be obtained by taking three times the noise of an absorption spectra. A quantitative image from this data may also be generated.

There are also research opportunities in improving equipment and data processing efficiencies. Since OP chemicals share the phosphate-oxygen bonds, equipment may be specialized to selectively scan these frequencies. This could allow for the development of a cheaper imager, faster acquisition times and faster, simplified data processing.

Appendix A – Trial Methodology and Results

The first attempt at detecting OP pesticides was to apply malathion to a section of composite floor tile. 1mL of 1mg malathion per mL methanol solution was applied in an approximately 1in diameter area. The tile was positioned vertically, with the Telops camera positioned normal to the surface. The scene is shown in Figure 24. This setup was not illuminated and had a blackbody source placed in the corner of the tile as a reference point in the scene. After calibration, spectra from 50 pixels in the contaminated area were observed to show no spectral features above background, as shown in Figure 25.

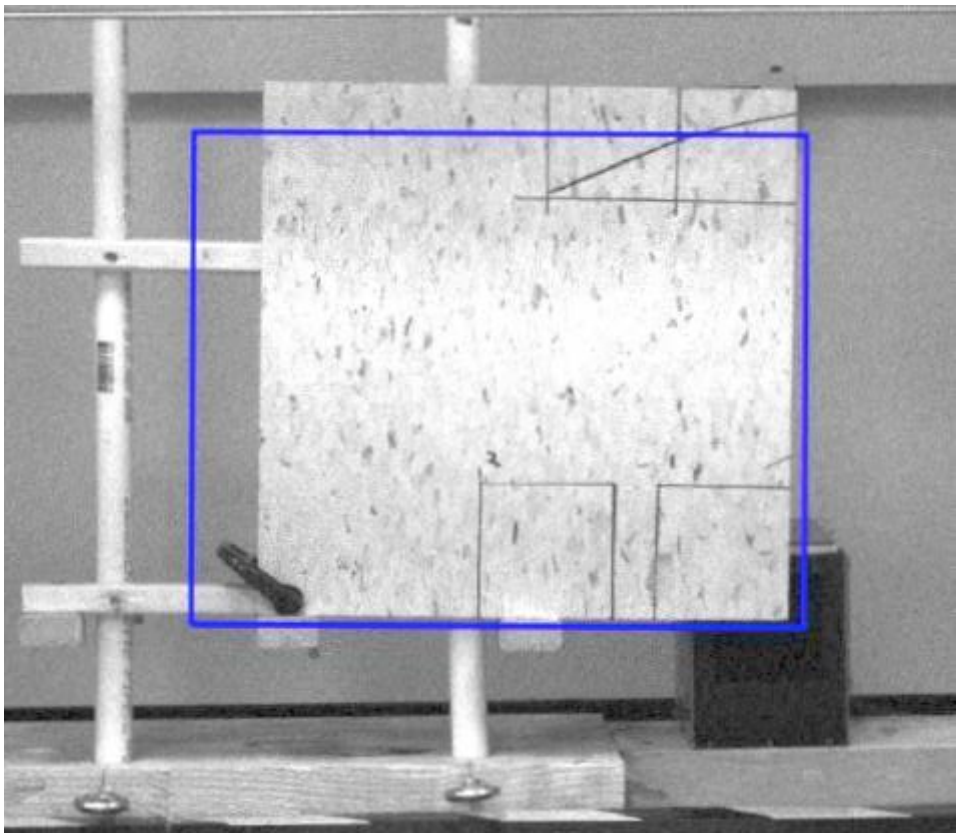

Figure 24 – Non-illuminated floor tile with malathion applied in lower right corner.

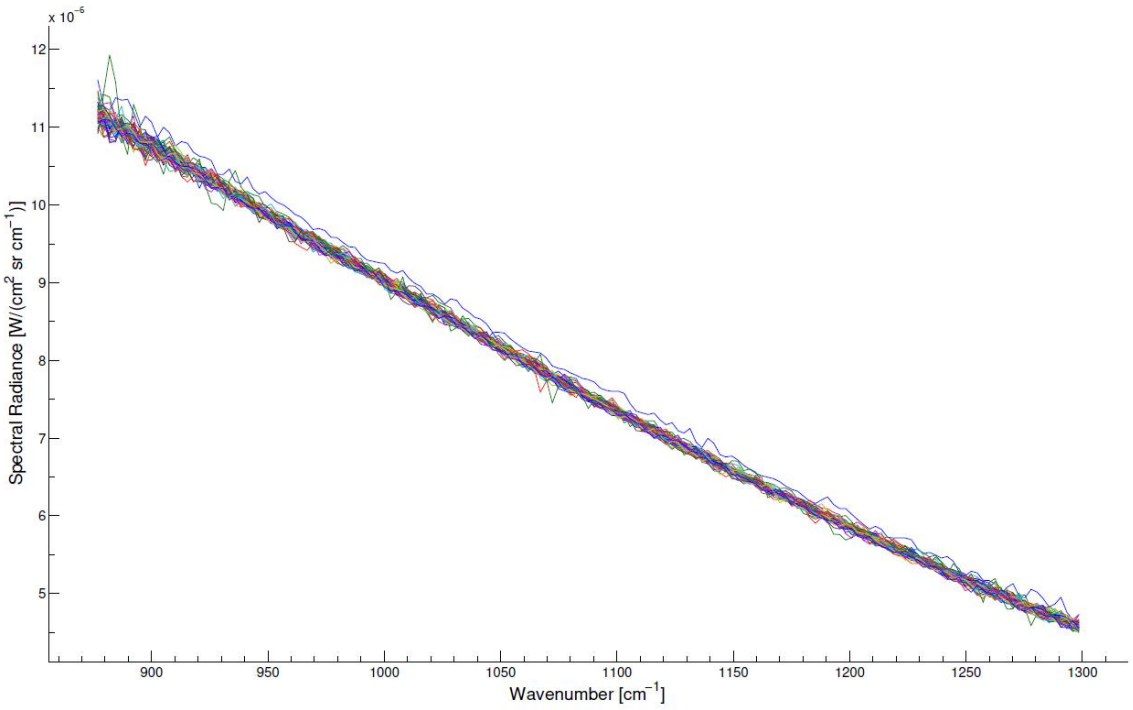

Figure 25 – Spectra from 50 pixels searching for spectral features of malathion.

The second method tried involved applying various OP chemicals to cardboard. The chemicals applied were diisopropyl methylphosphante (DIMP), DMMP, and malathion. The samples were arranged vertically with a blackbody illumination source, as seen in Figure 26. The non-calibrated spectral data was observed to change from the non-contaminated and contaminated sections of cardboard. However, the expected spectral features were not present, as shown in Figures 27-30. The spectral angle method was first used during the analysis of this data. While this experiment failed to positively identify presence of the OP chemical, it did demonstrate the ability of the spectral angle method to visually differentiate between pixels with differing spectra. Figures 31-33 show the spectral angle plots obtained from this experiment.

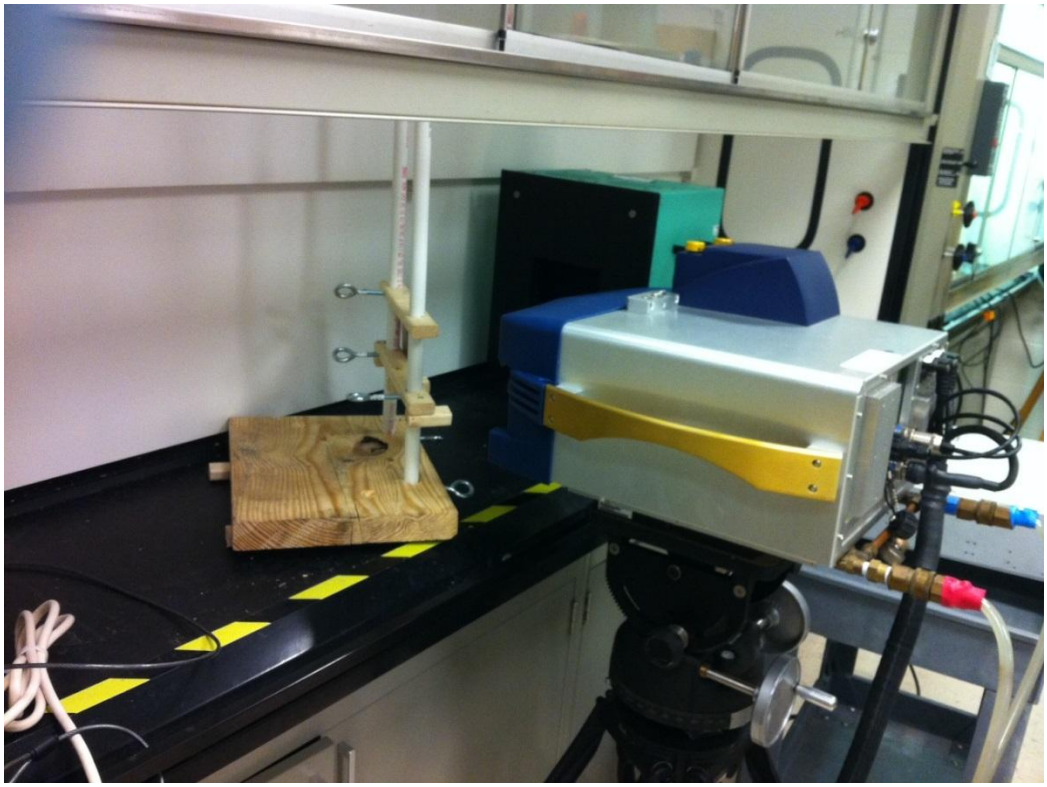

Figure 26 - Trial method setup utilizing contaminated cardboard.

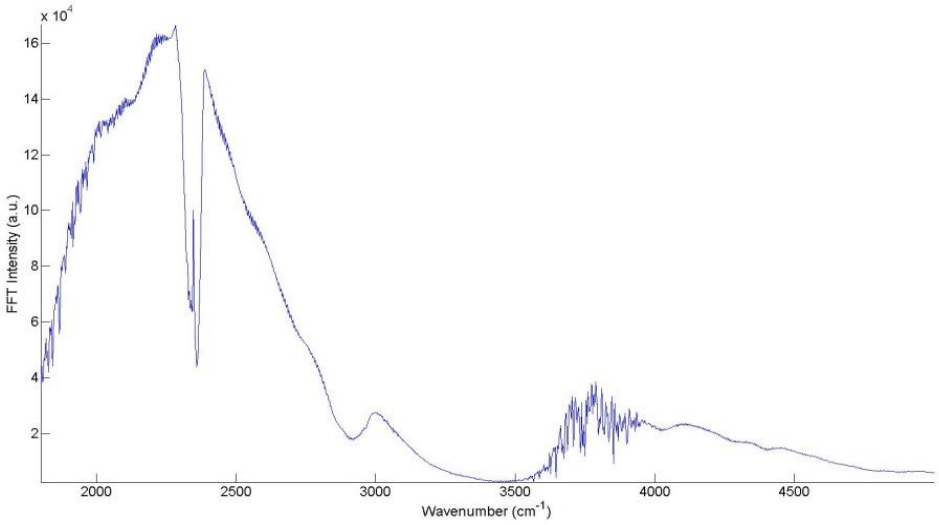

Figure 27 - Uncalibrated spectra for bare cardboard.

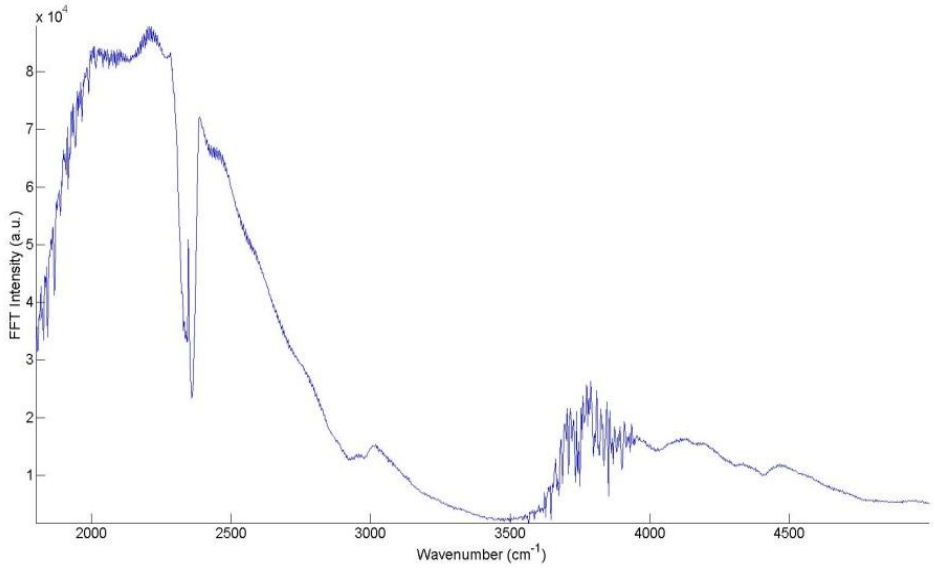

Figure 28 – Uncalibrated spectra for DIMP on cardboard.

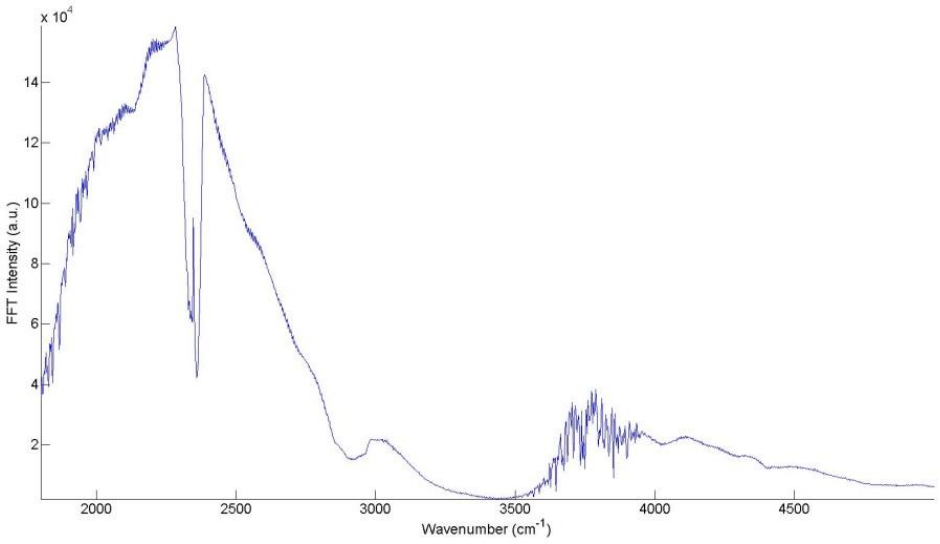

Figure 29 – Uncalibrated spectra for DMMP on cardboard.

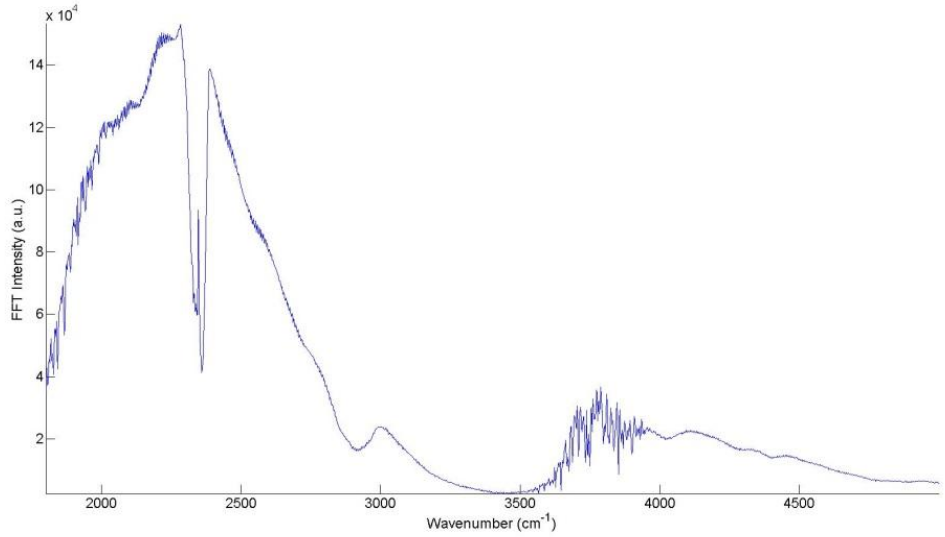

Figure 30 - Uncalibrated spectra for malathion on cardboard.

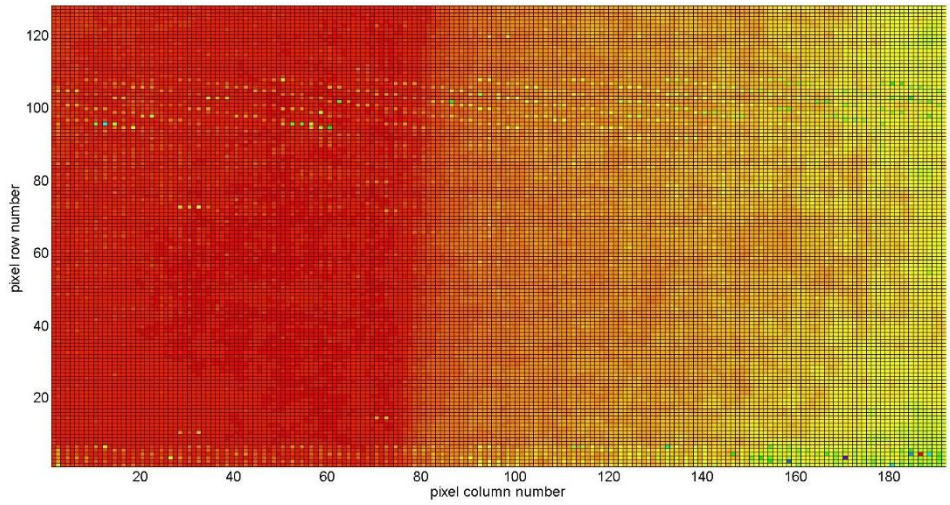

Figure 31 – Spectral angle plot for DIMP on cardboard.

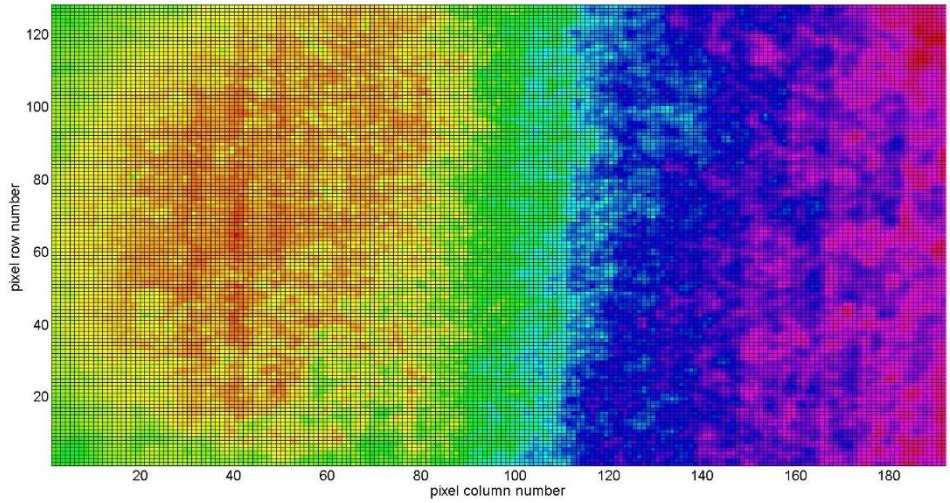

Figure 32 – Spectral angle plot for DMMP on cardboard.

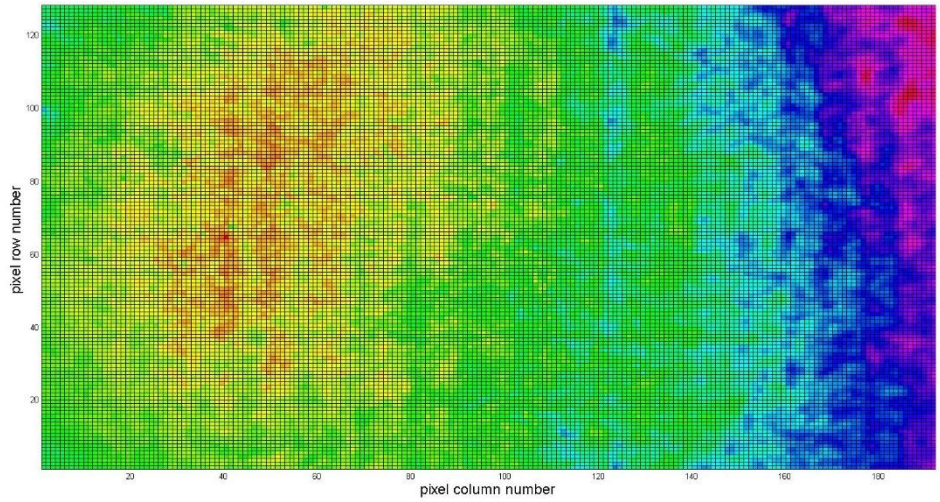

Figure 33 - Spectral angle plot for malathion on cardboard.

Appendix B – Broadband Images

The broadband images were generated by taking the logarithm of each interferogram broadband intensity. The interspersed bright yellow pixels and yellow dot at (20,100) are caused by bad pixels and will be corrected for during the calibration. Hardly any difference can be discerned between the contaminated and bare stainless steel broadband images as seen in Figures 34 and 35. In Figure 36, the DMMP can be seen as a wavy blue line around row 60. As more DMMP is applied, a larger area of blue can be seen as with the bottom half of the coupon in Figure 37.

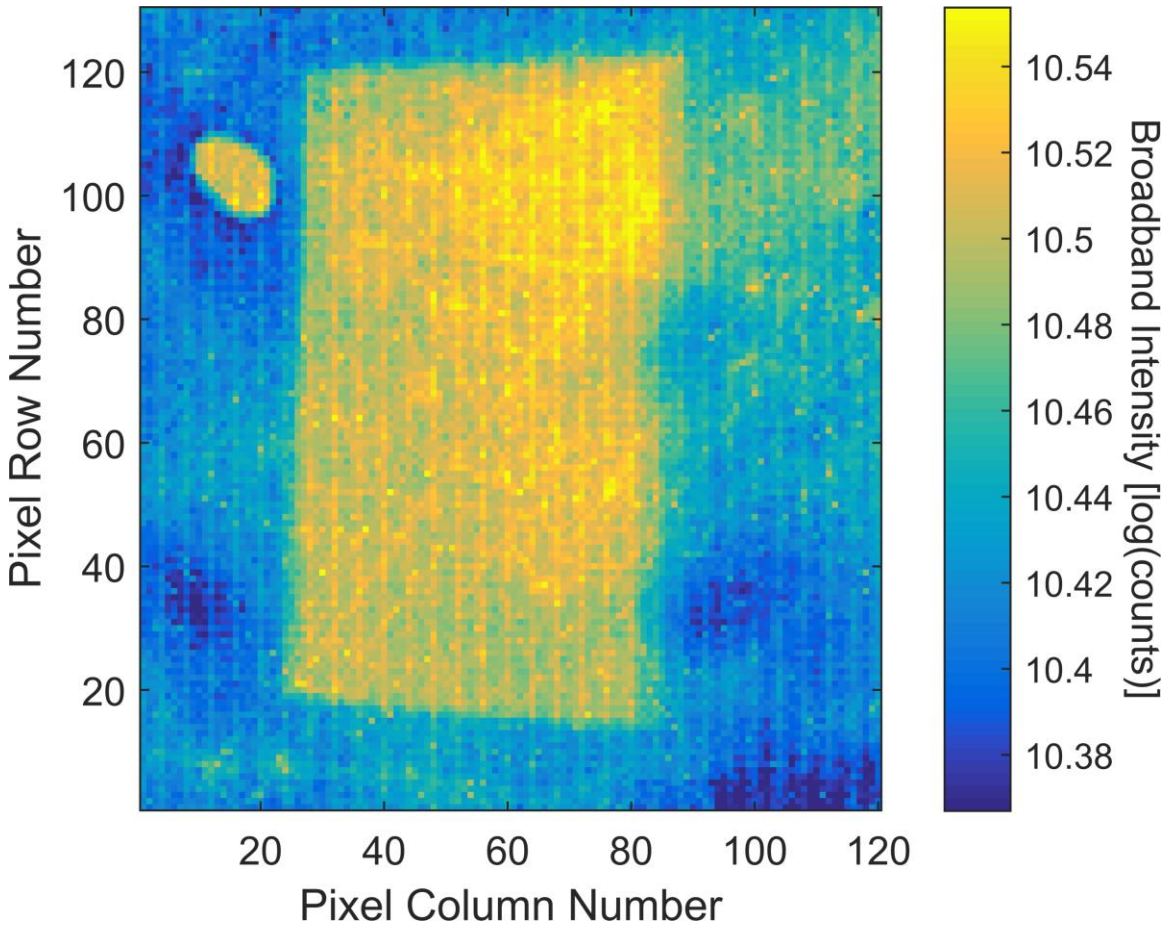

Figure 34 – Broadband image of bare stainless steel.

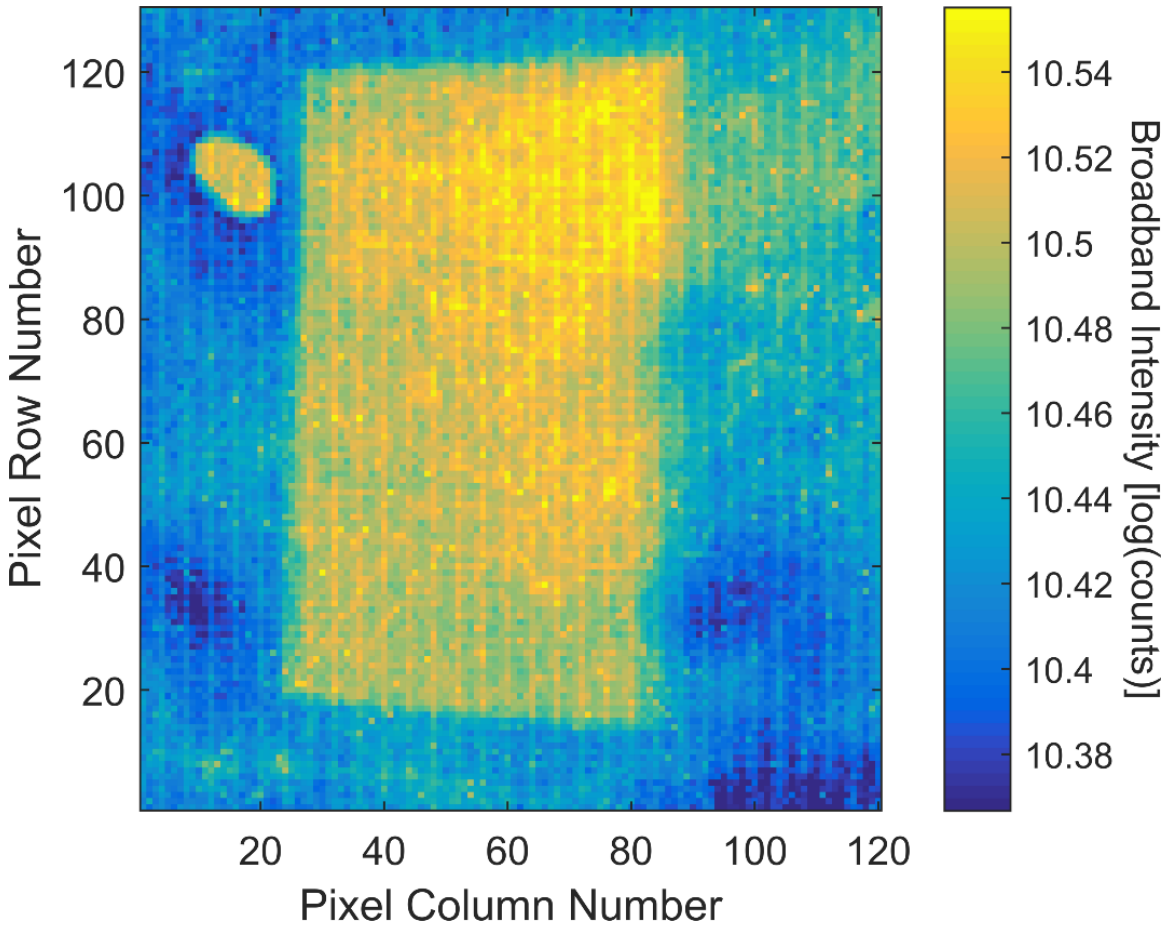

Figure 35 – Broadband image of stainless steel with 1µL DMMP applied.

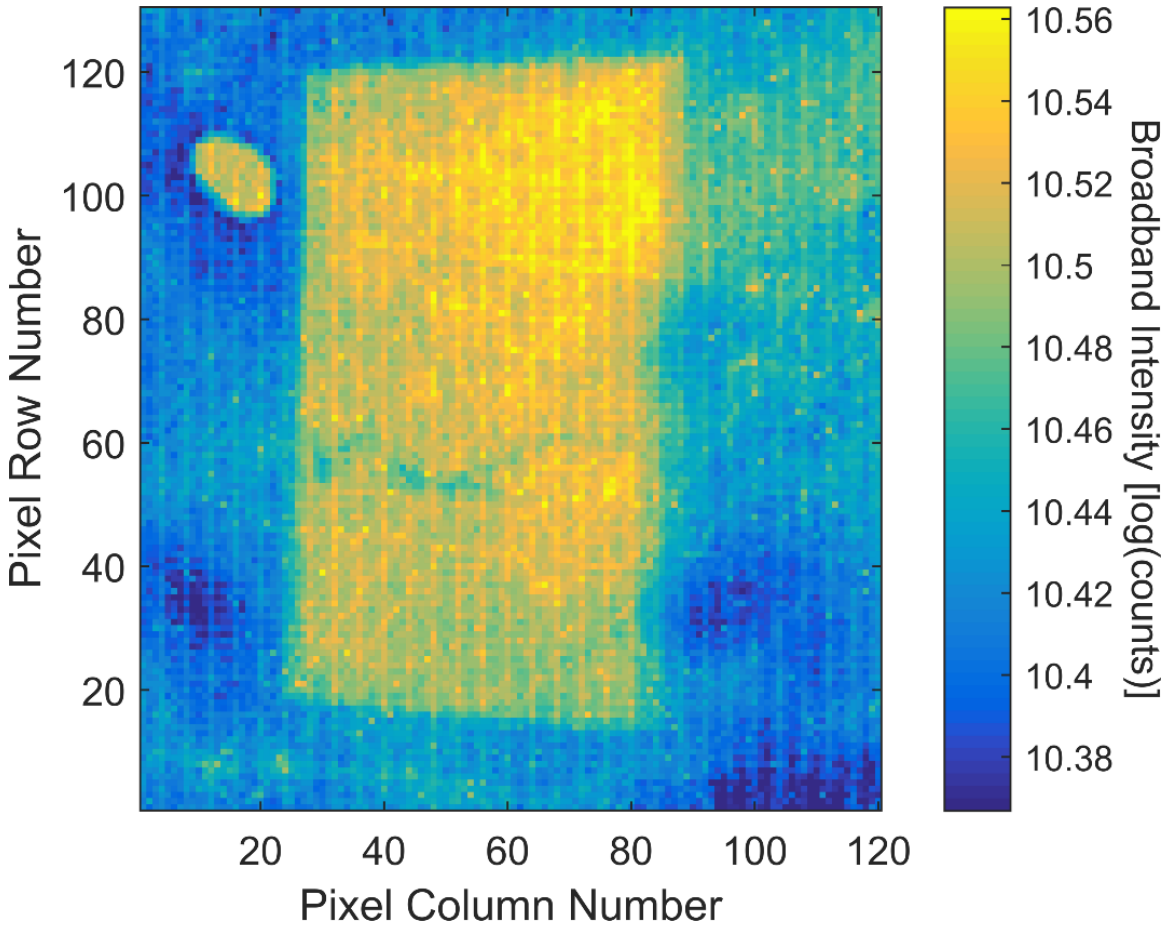

Figure 36 - Broadband image of stainless steel with 5µL DMMP applied.

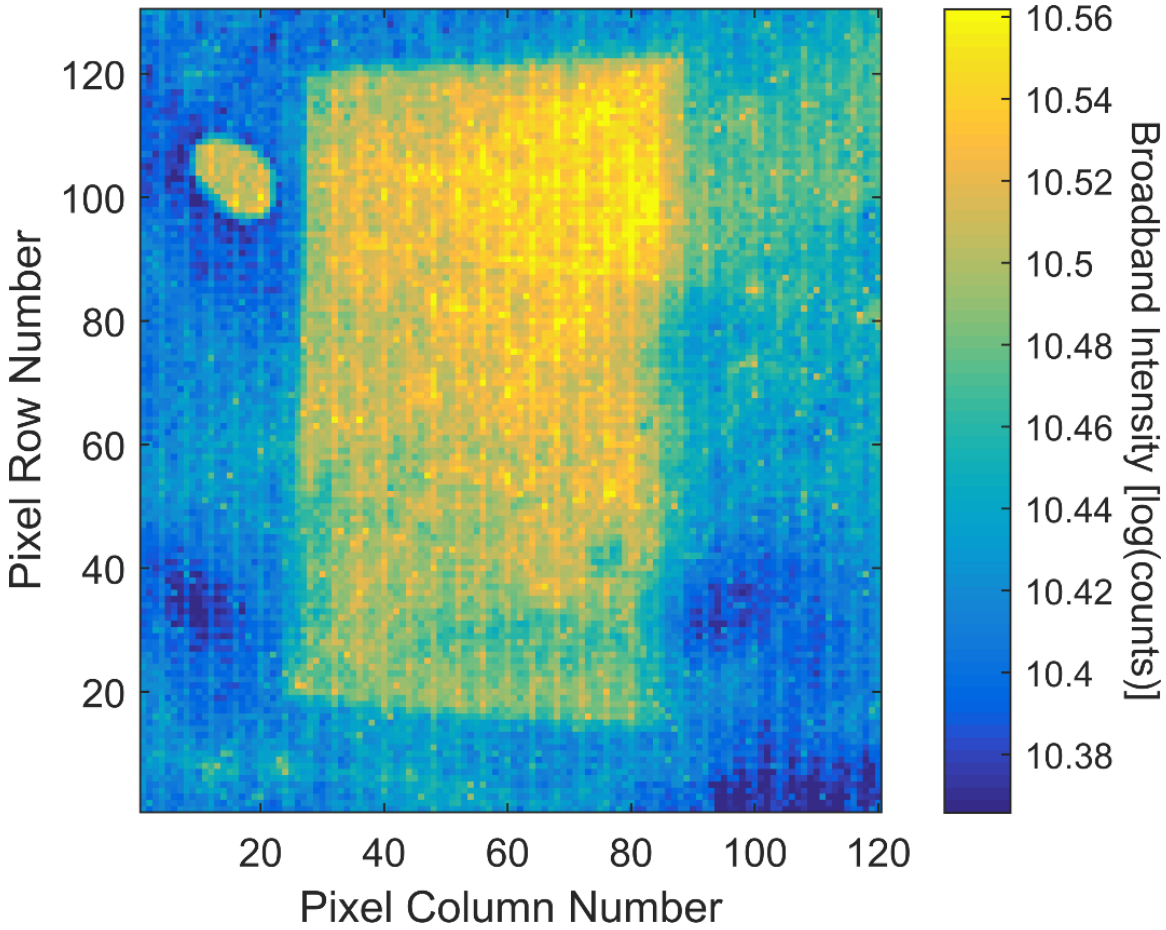

Figure 37 - Broadband image of stainless steel with 10µL DMMP applied by solution.

Another bare sample was taken for the higher concentrations of neat DMMP applied, as these were done at a different time. With these, it is much easier to see where contamination exists than with the lower concentrations. It is also noted that the coupons appear larger. This is because with the lower concentration tests, an alignment error was made with the blackbody, which prevented the entire coupon from being illuminated. This had little effect on most results, since a large area was still contaminated. However the 1µL DMMP formica laminate sample was highly affected due to poor chemical

deposition. Figure 42 shows an “X” pattern drawn onto the coupon. These scenes were added to show the ability to detect a deposition pattern on a sample.

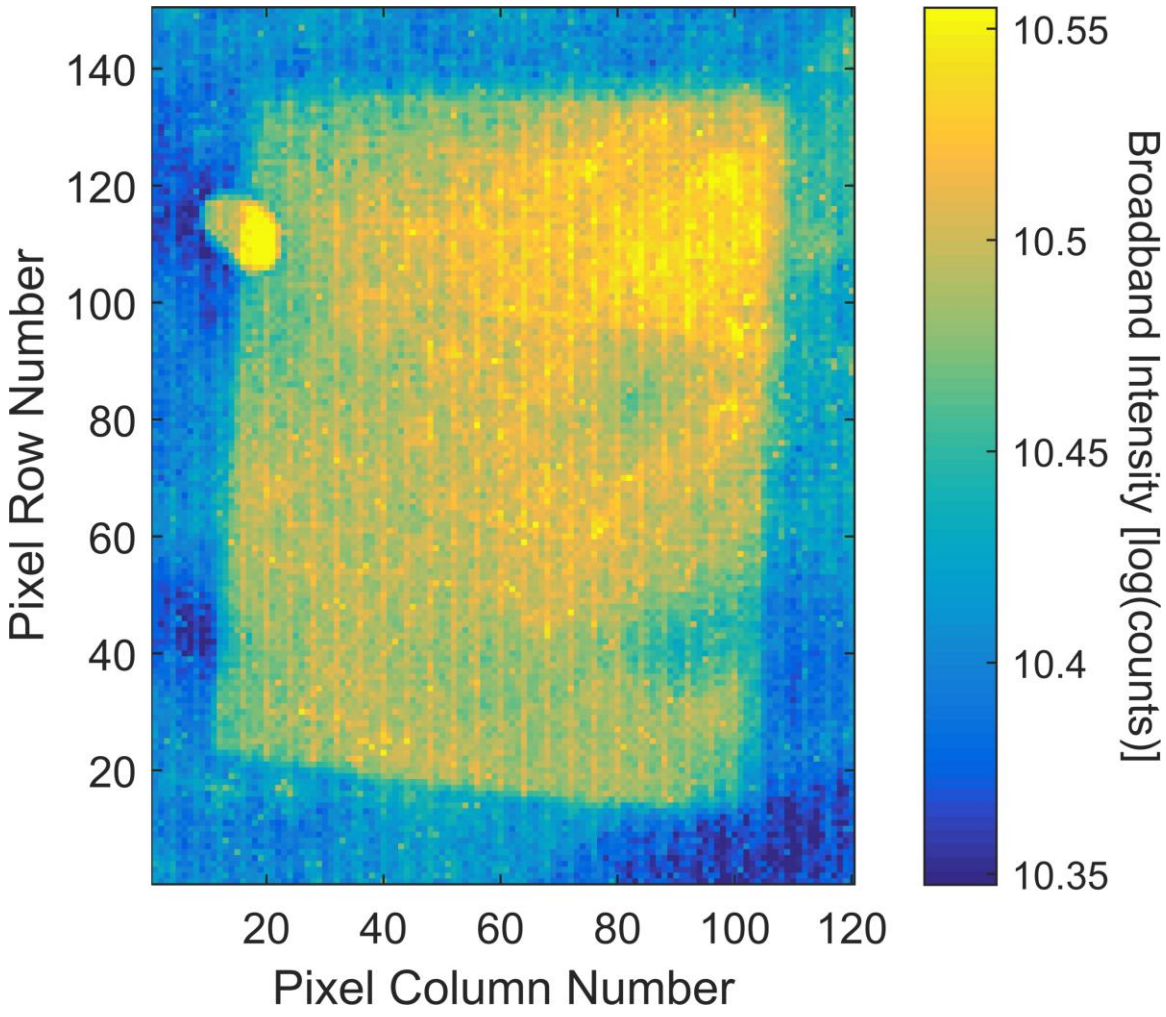

Figure 38 - Broadband image of bare stainless steel.

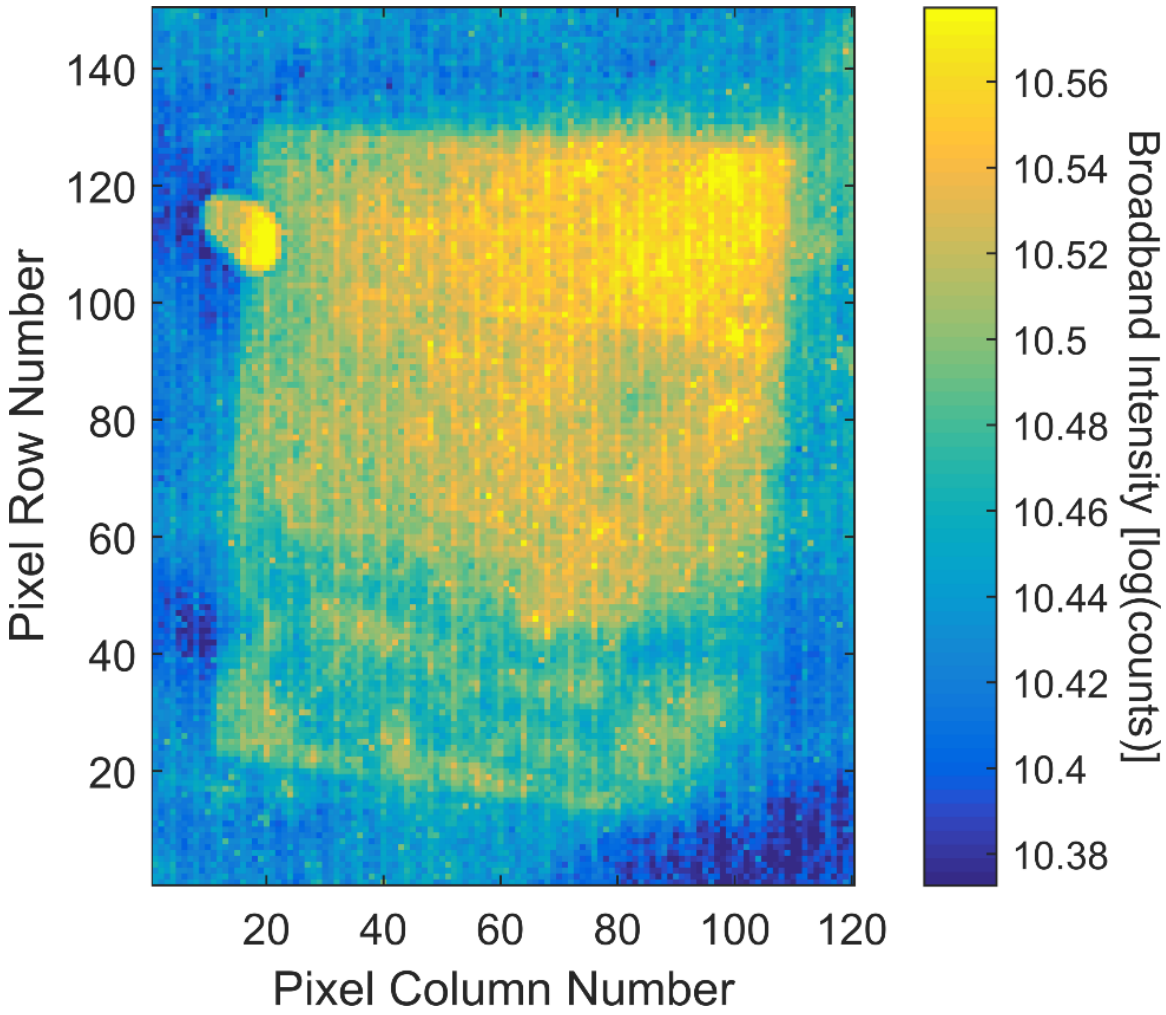

Figure 39 - Broadband image of stainless steel with 10µL DMMP applied by smearing.

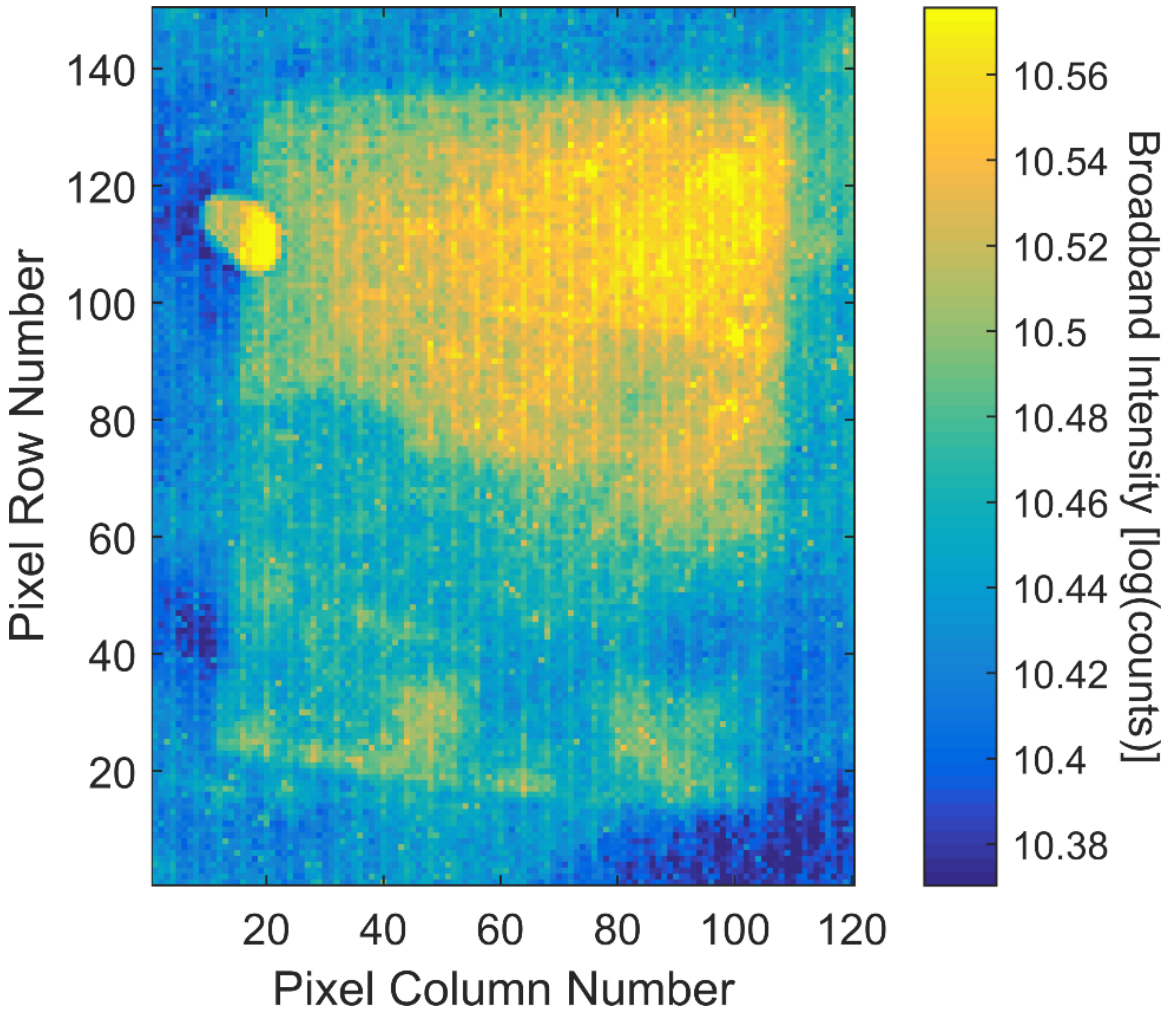

Figure 40 - Broadband image of stainless steel with 25µL DMMP applied.

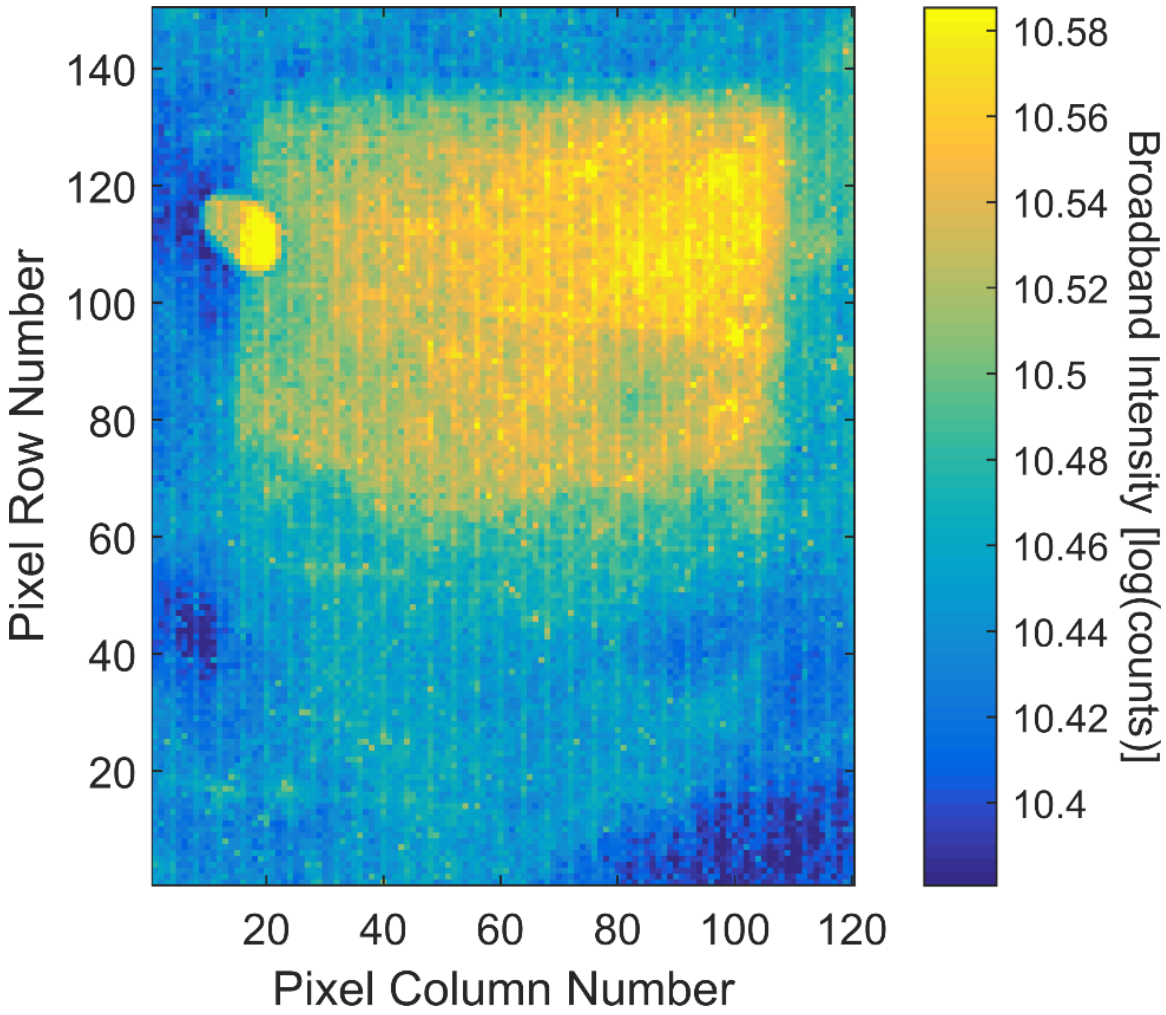

Figure 41 - Broadband image of stainless steel with 50µL DMMP applied.

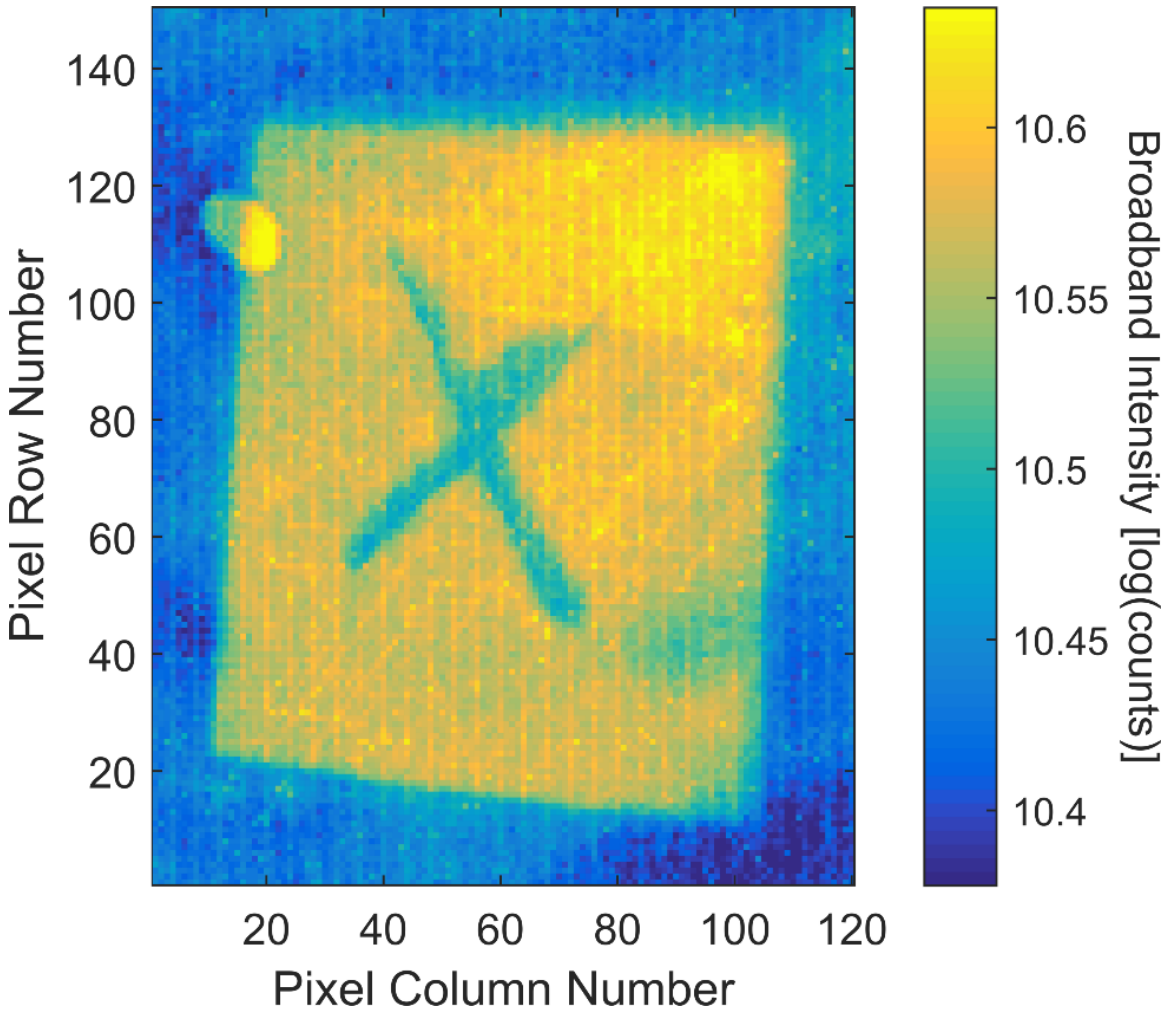

Figure 42 - Broadband image of stainless steel with 10µL DMMP applied in an "X" pattern.

The formica laminate scenes were collected in the same manner as the stainless steel ones. Since the formica laminate is much less reflective, the broadband images are much less clear and it would be difficult to identify any contamination from them.

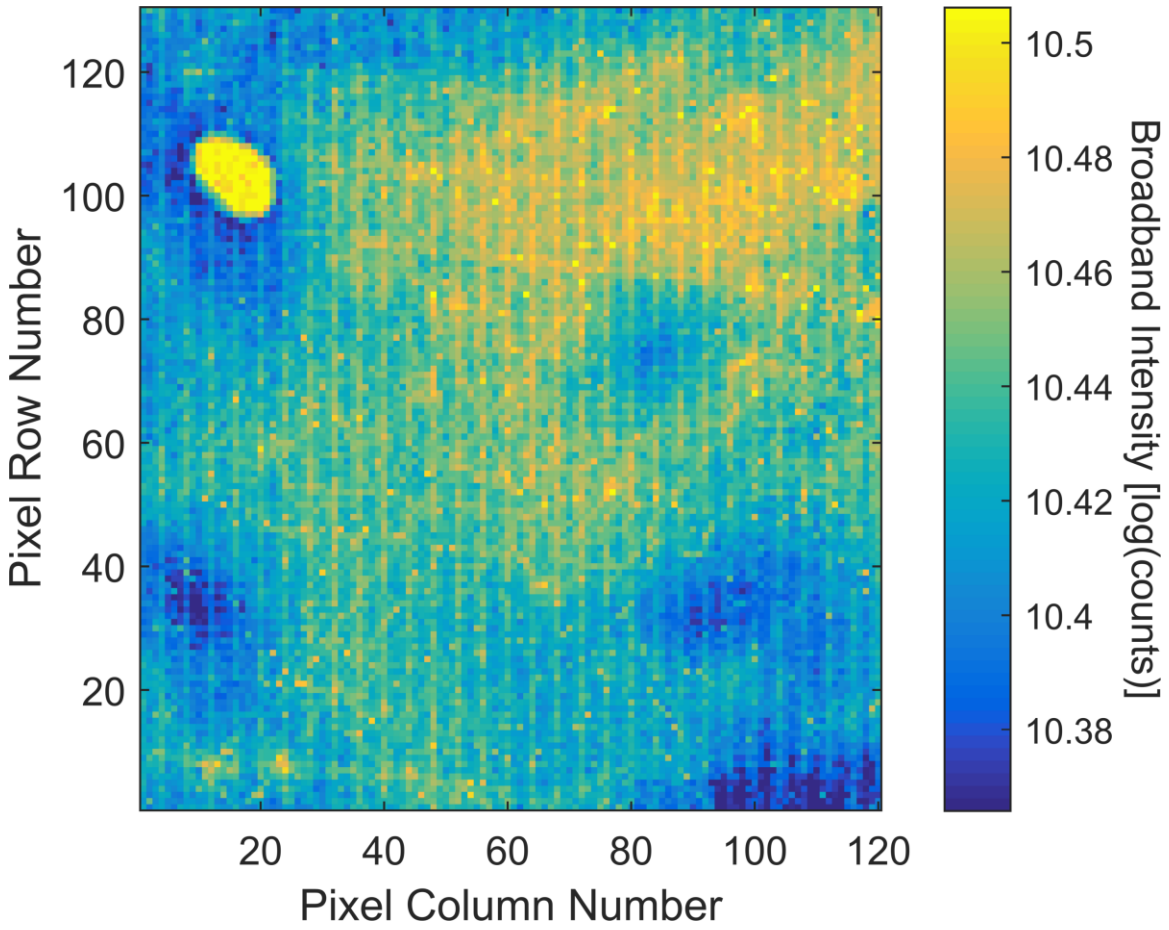

Figure 43 - Broadband image of bare laminate.

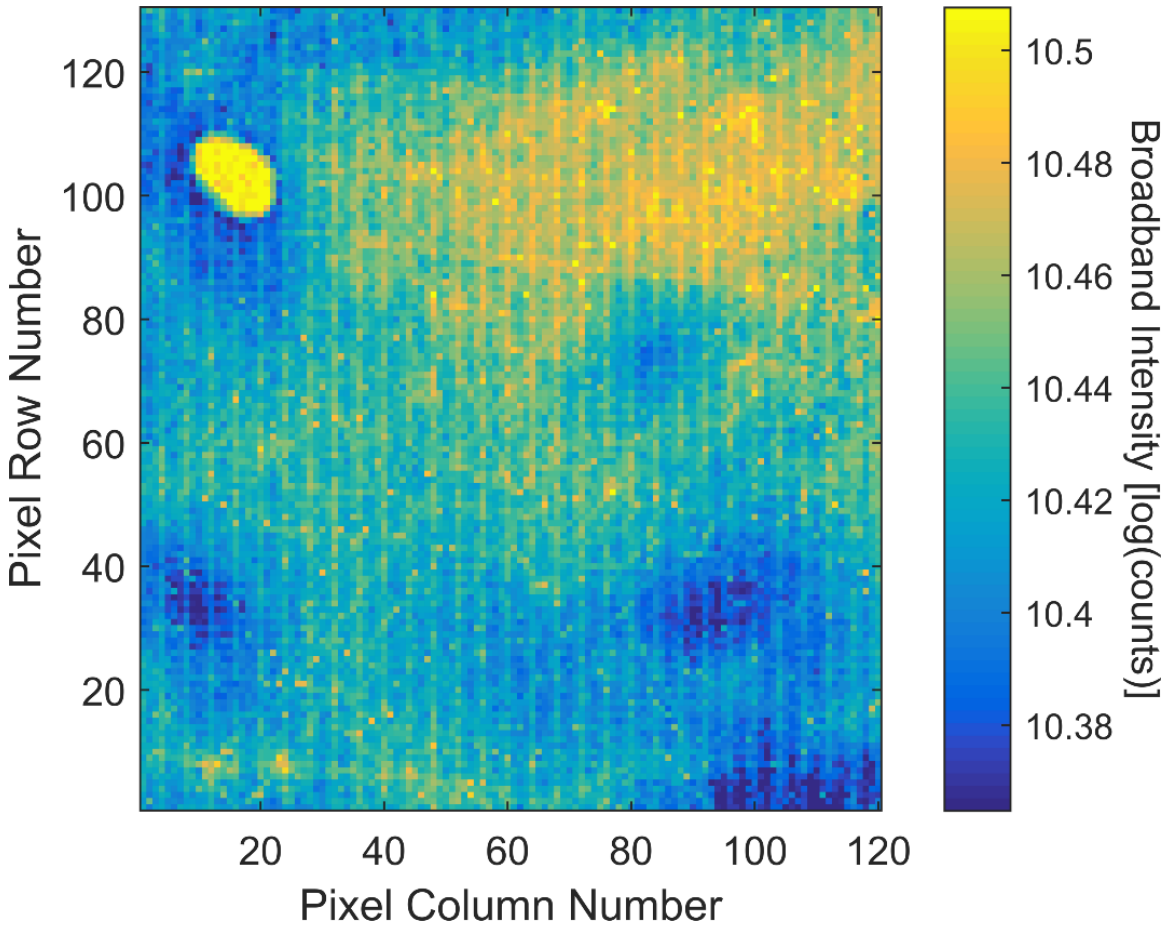

Figure 44 - Broadband image of laminate with 1µL DMMP applied.

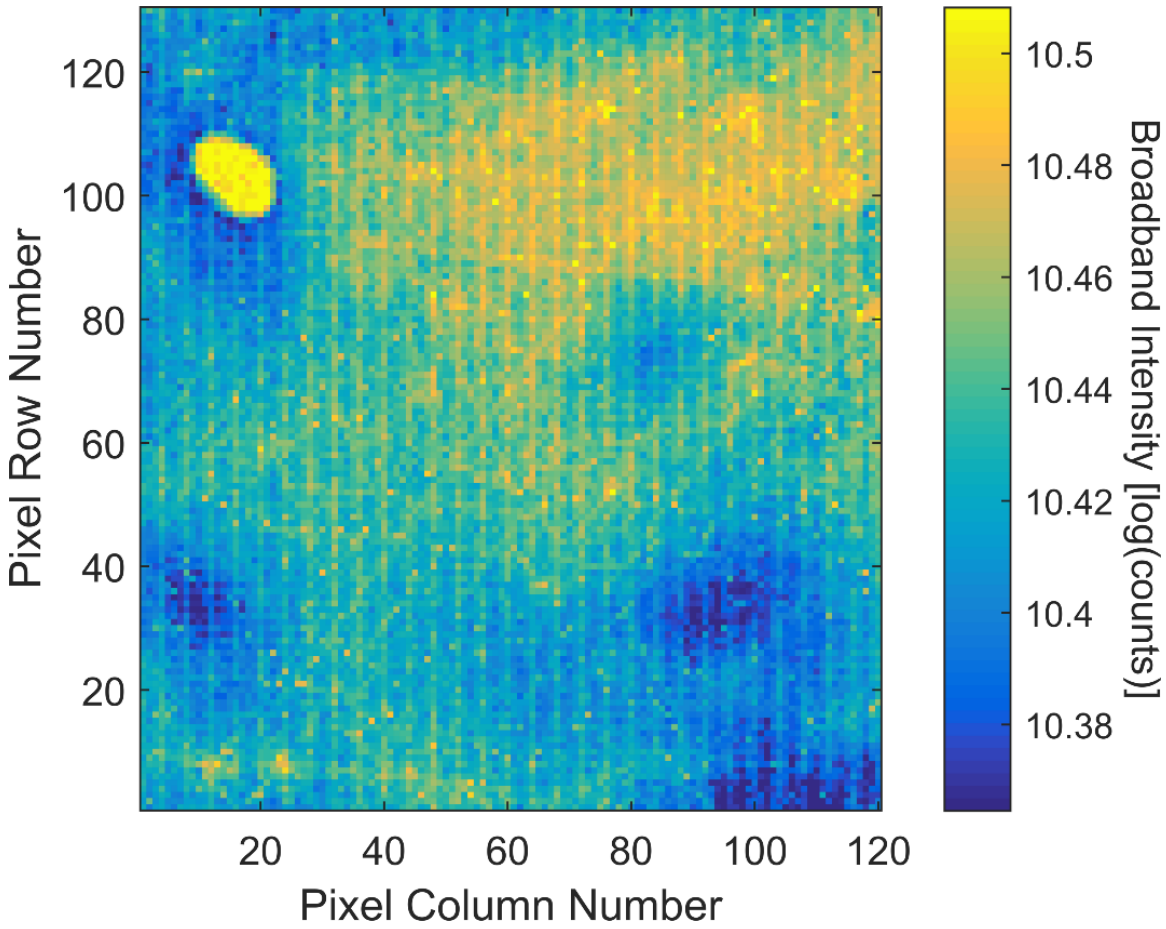

Figure 45 - Broadband image of laminate with 5µL DMMP applied.

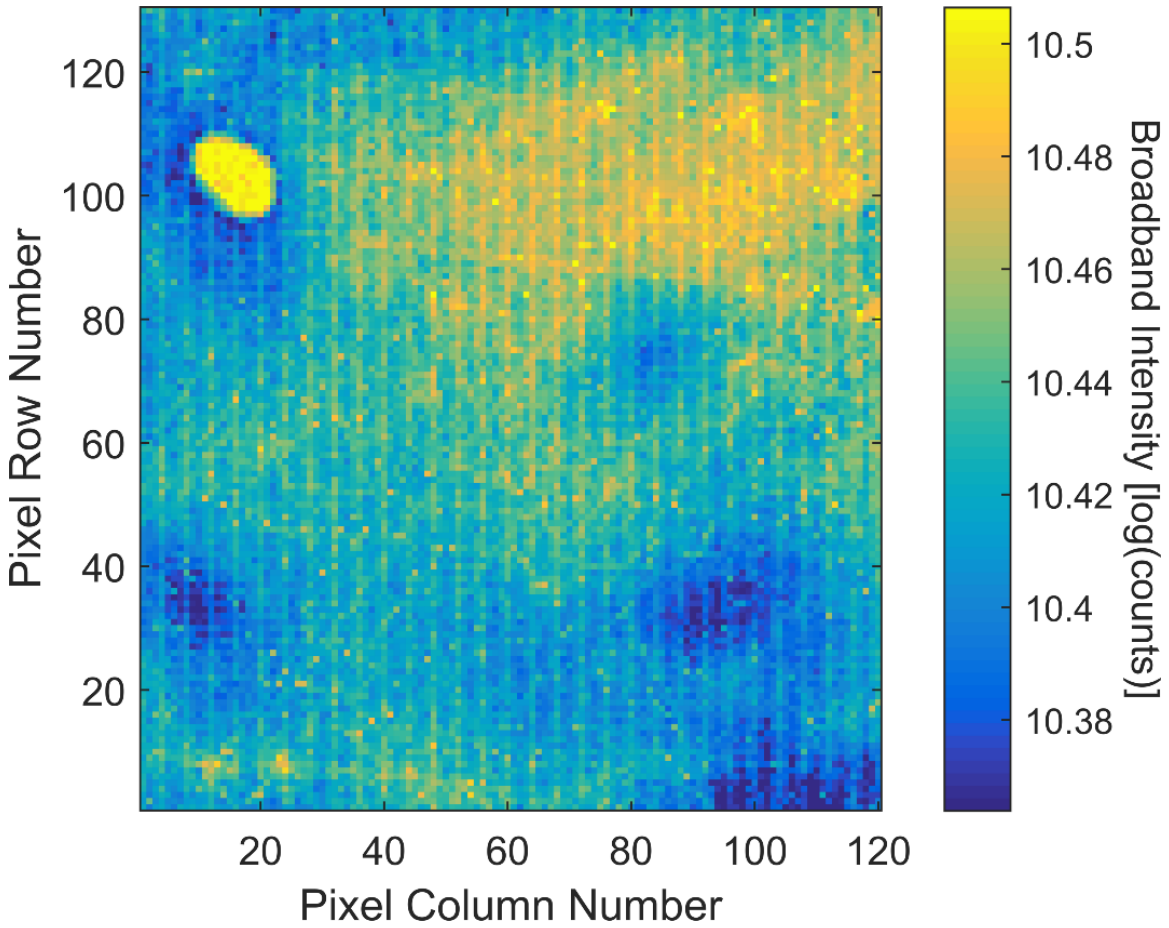

Figure 46 - Broadband image of laminate with 10µL DMMP applied by solution.

Again, another bare scene was collected for the scenes with higher concentration because it was done at a different time. The formica laminate scenes are still very unclear and difficult to get any meaningful information from.

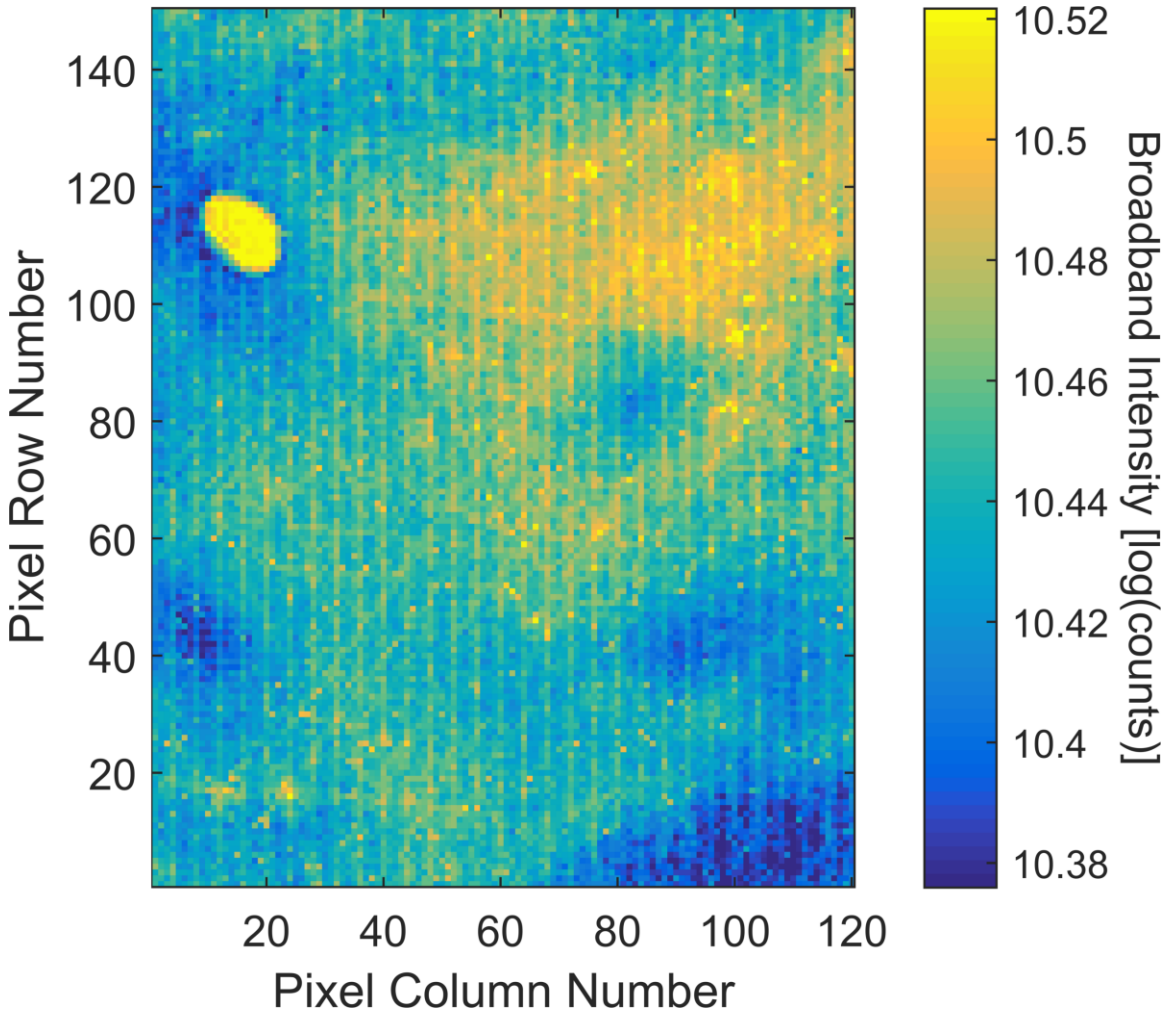

Figure 47 - Broadband image of bare laminate.

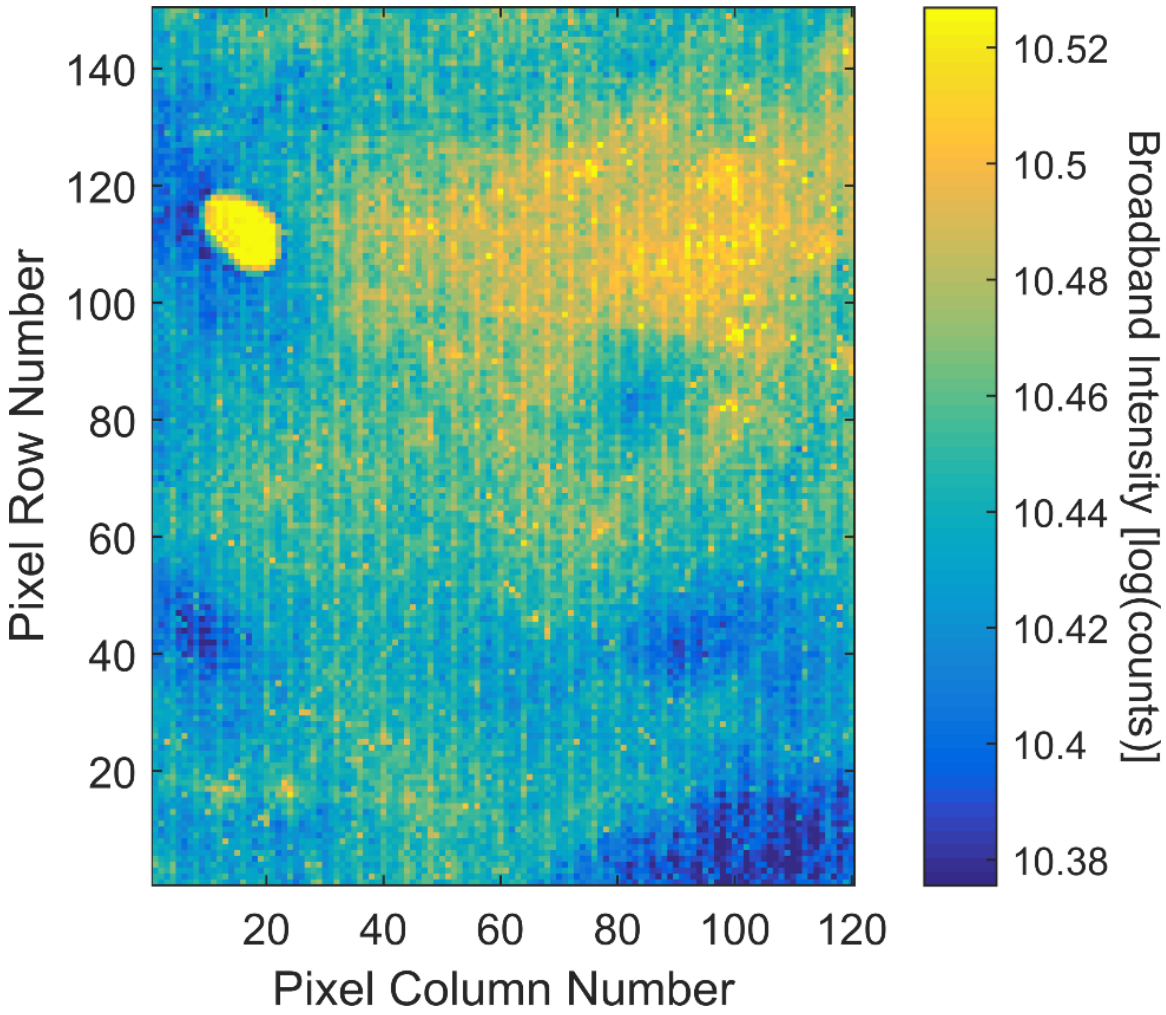

Figure 48 - Broadband image of laminate with 10µL DMMP applied by smearing.

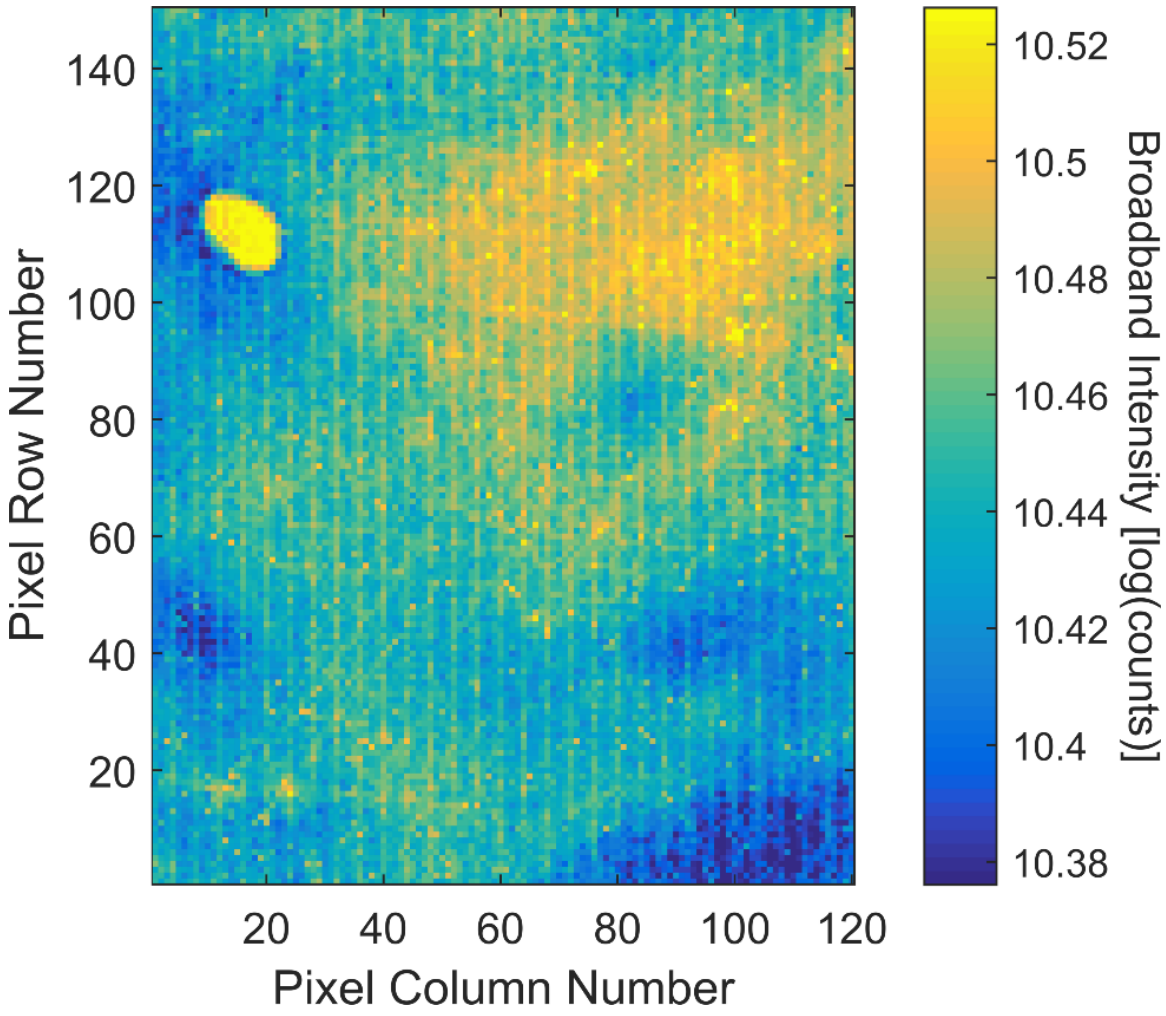

Figure 49 - Broadband image of laminate with 25µL DMMP applied.

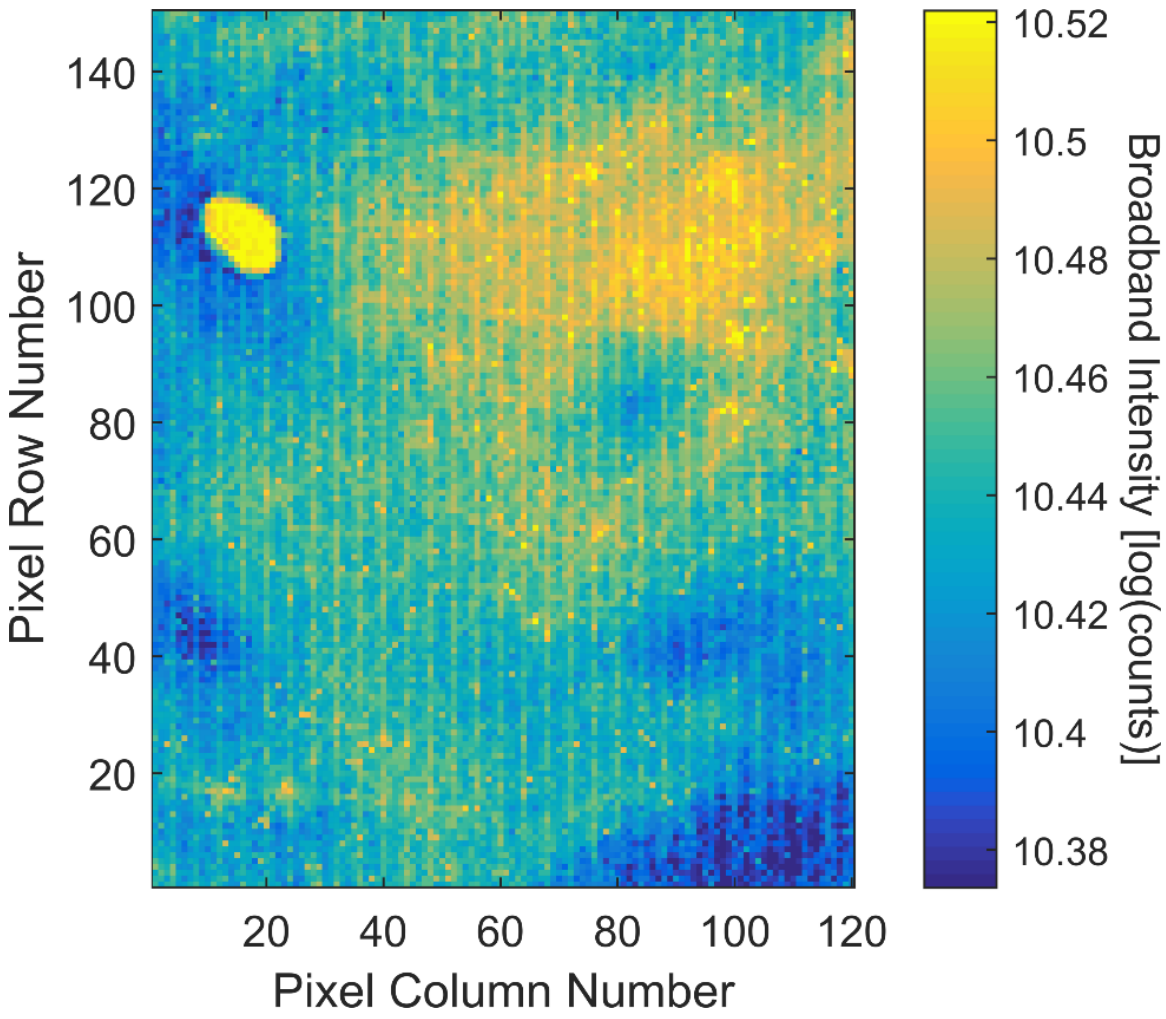

Figure 50 - Broadband image of laminate with 50µL DMMP applied.

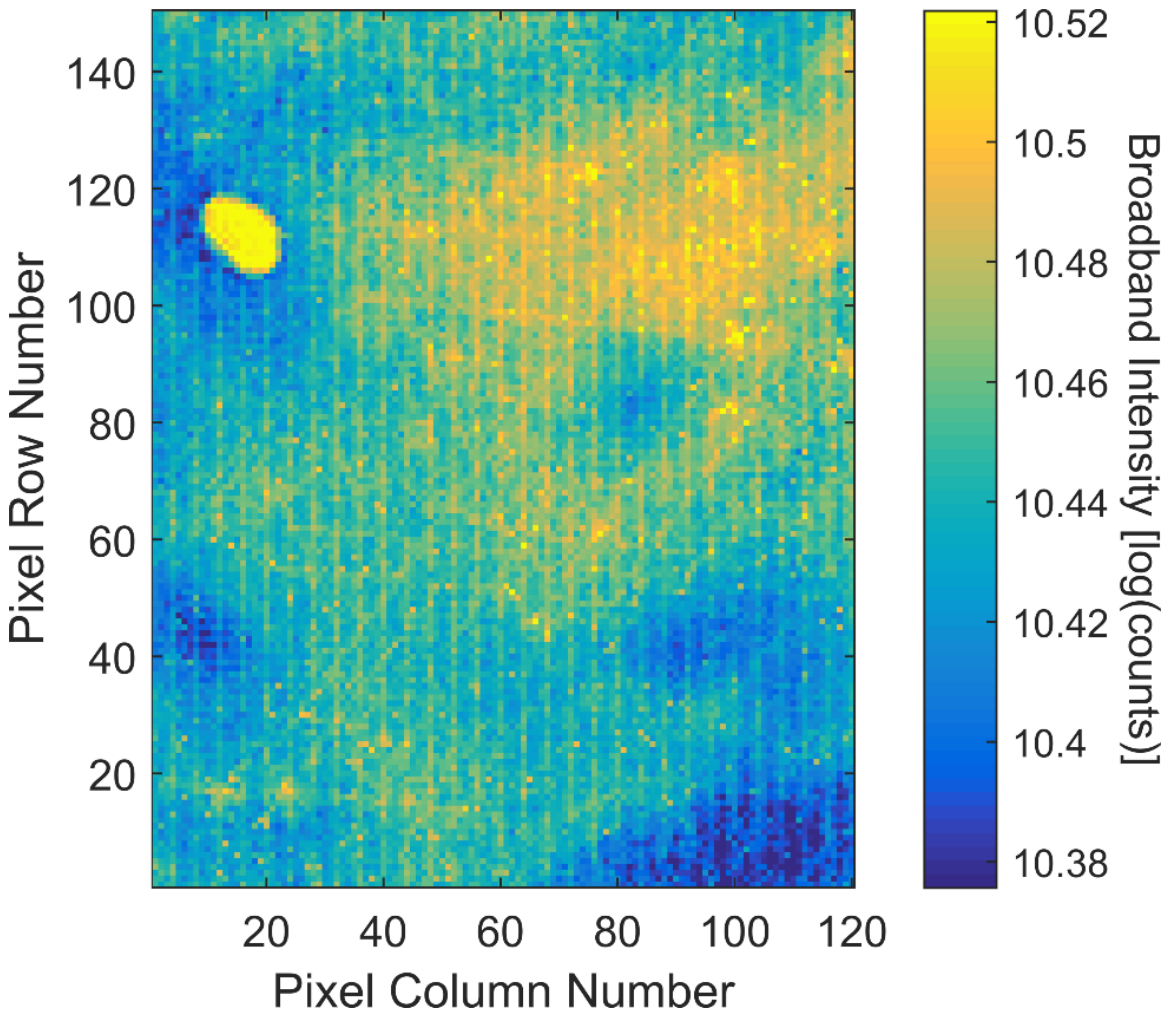

Figure 51 - Broadband image of laminate with 10µL DMMP applied in "X" pattern.

Appendix C – Calibrated Images

The calibration process was effective in removing the bad pixels seen in the broadband images. The intensities were used to calibrate to the known radiance of the two built-in black bodies. In these images, it can be seen that the scene was not completely illuminated, as there is a section about columns 90-110 that can be faintly seen.

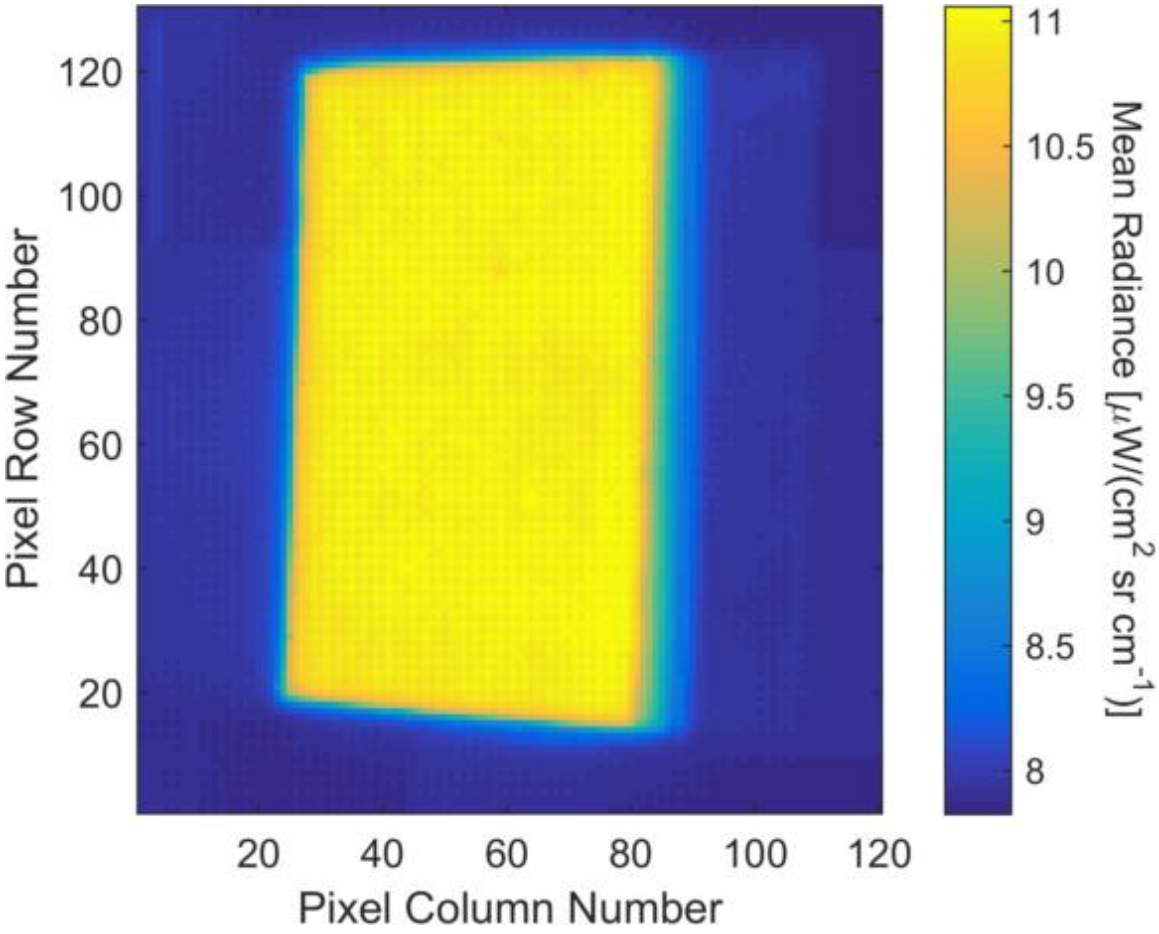

Figure 52 - Calibrated image of bare stainless steel.

In Figure 53, the contamination can be seen by a slightly darker yellow. With a highly reflective surface, even at this point in the data analysis, contamination can be seen at a fairly low concentration.

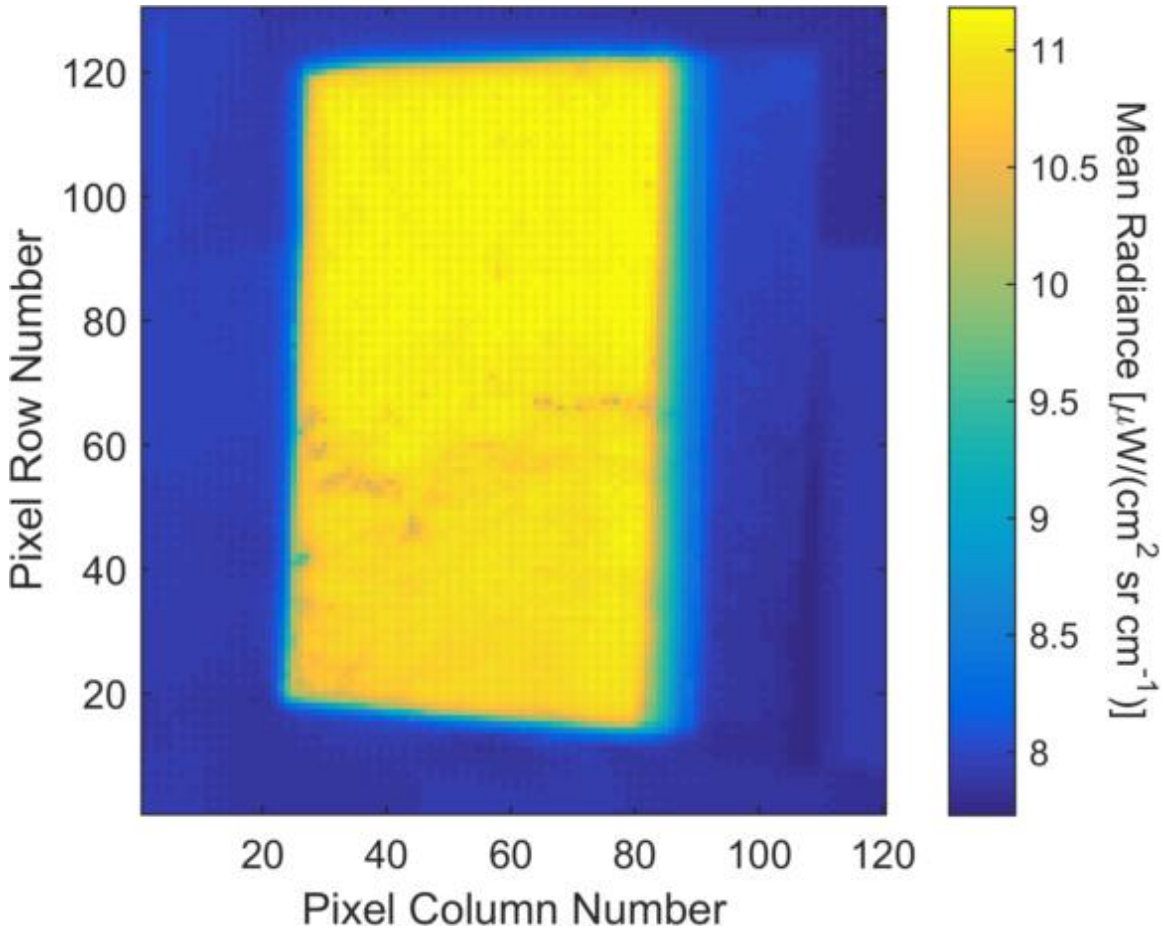

Figure 53 - Calibrated image of stainless steel with 1µL DMMP applied.

In Figure 54, the contamination becomes clearer as there is more dark yellow and now some blue areas on the coupon.

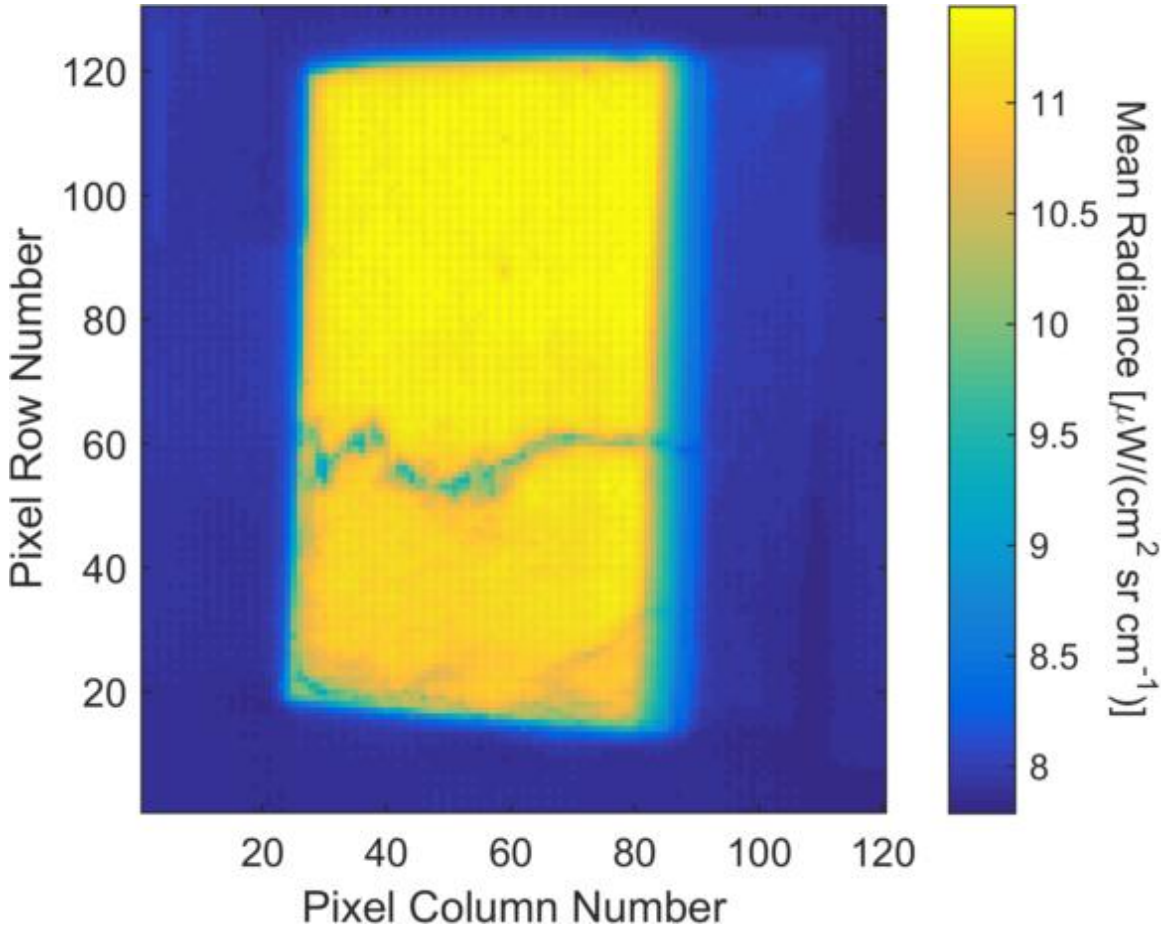

Figure 54 - Calibrated image of stainless steel with 5µL DMMP applied.

The contamination can be seen covering nearly all of the bottom half of the coupon in Figure 55. Again, it is signified by a dark yellow or blue color.

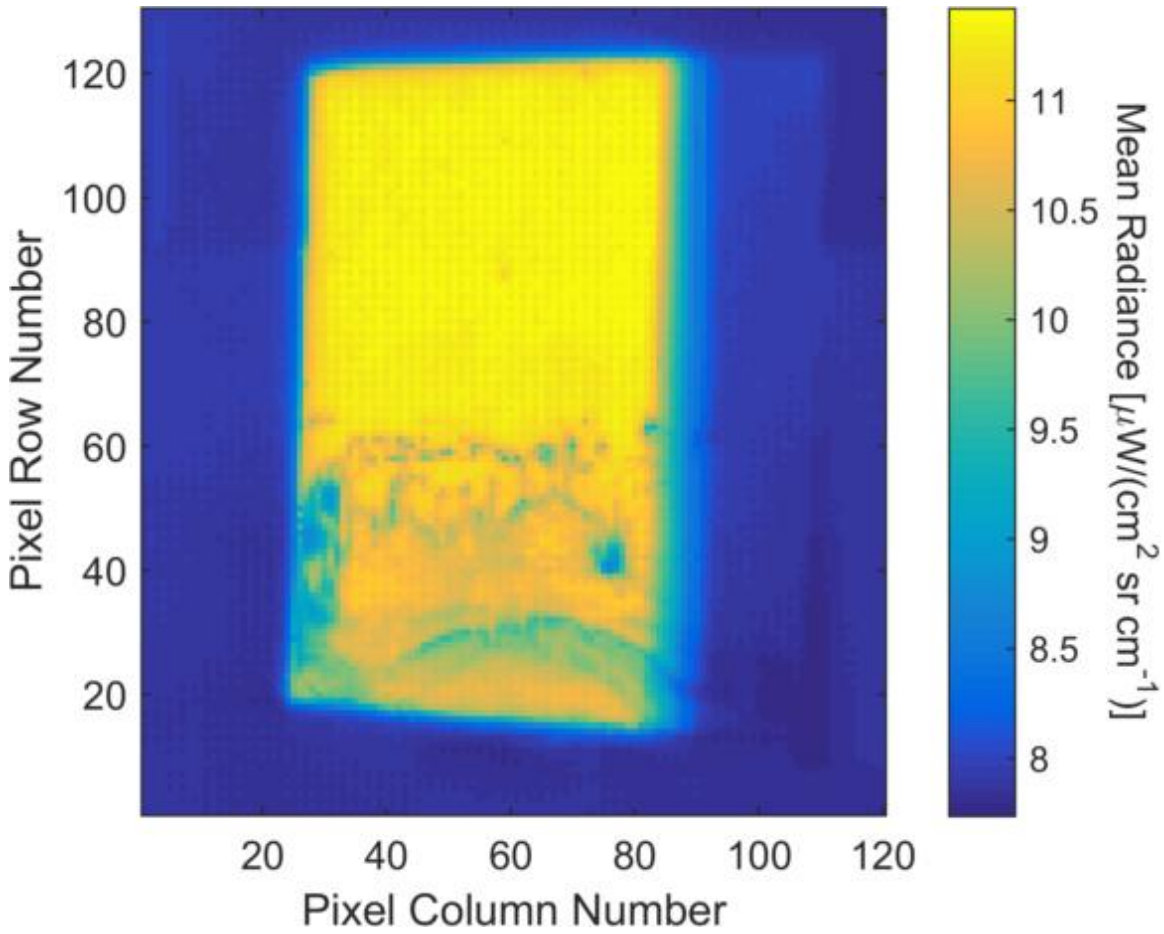

Figure 55 - Calibrated image of stainless steel with 10μL DMMP applied by solution.

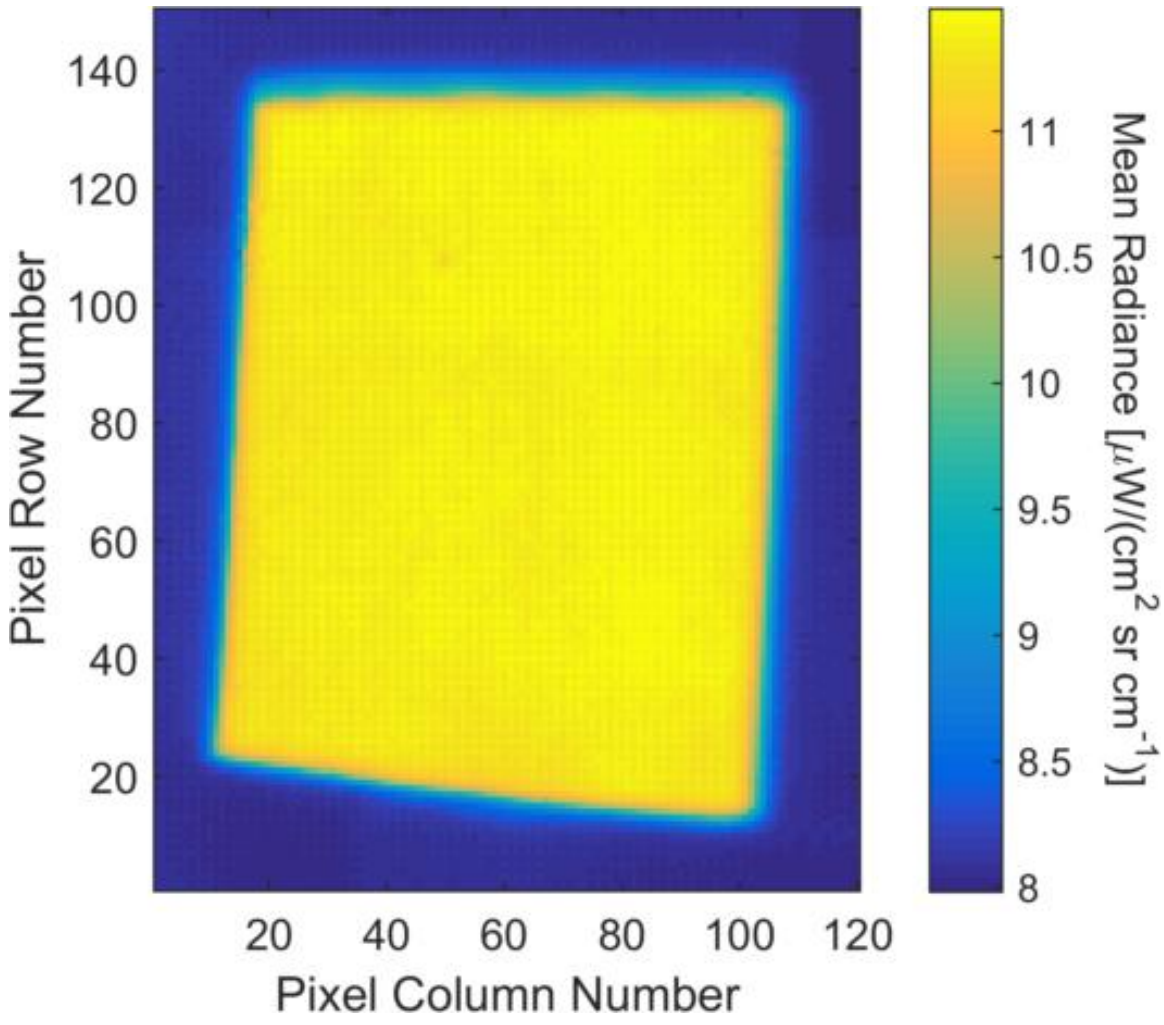

Figure 56 - Calibrated image of bare stainless steel.

As the surface concentration increases, the contamination gets easier to see in the calibrated images. The X pattern becomes more distinct in the calibrated image in Figure 60.

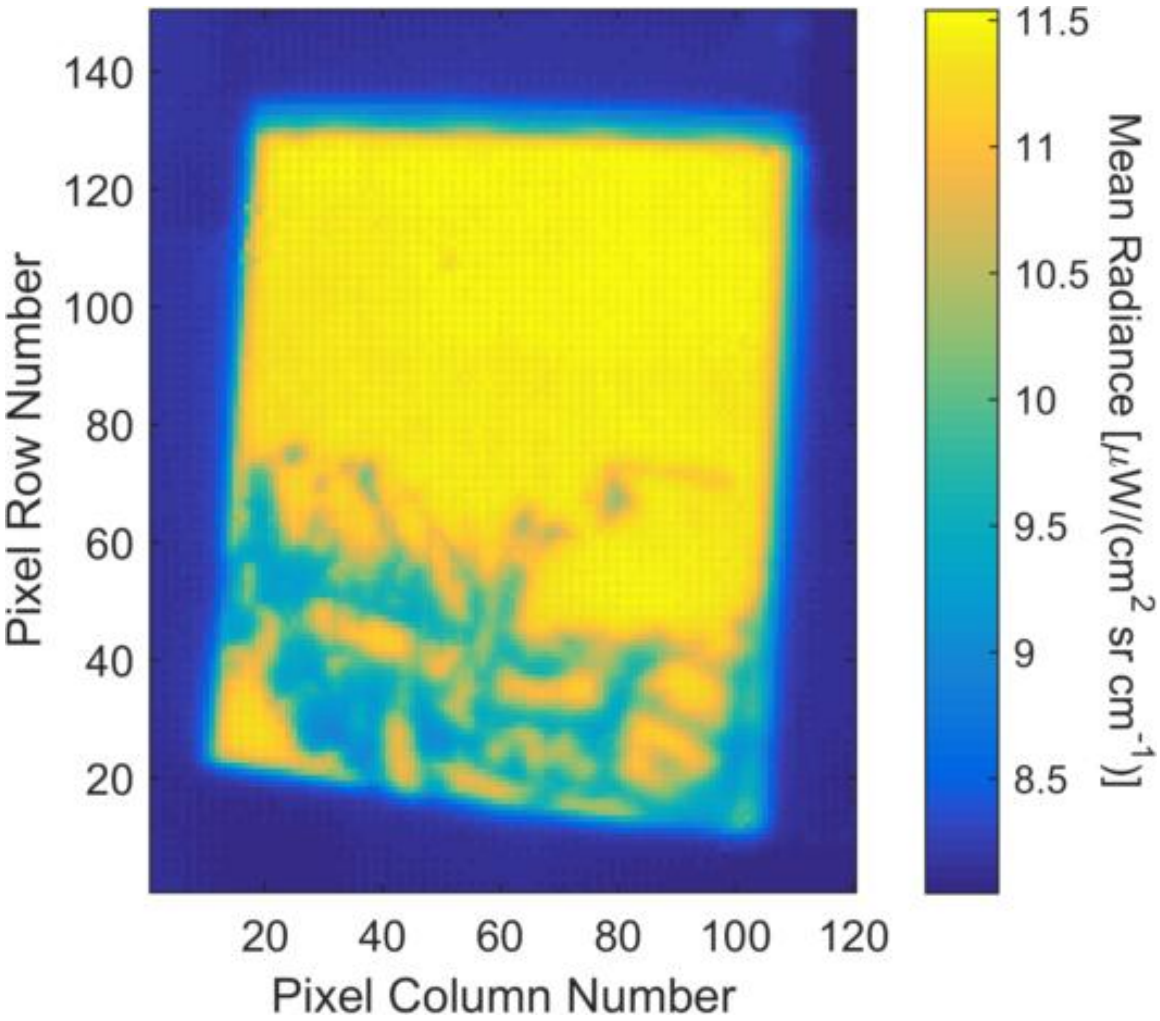

Figure 57 - Calibrated image of stainless steel with 10μL DMMP applied by smearing.

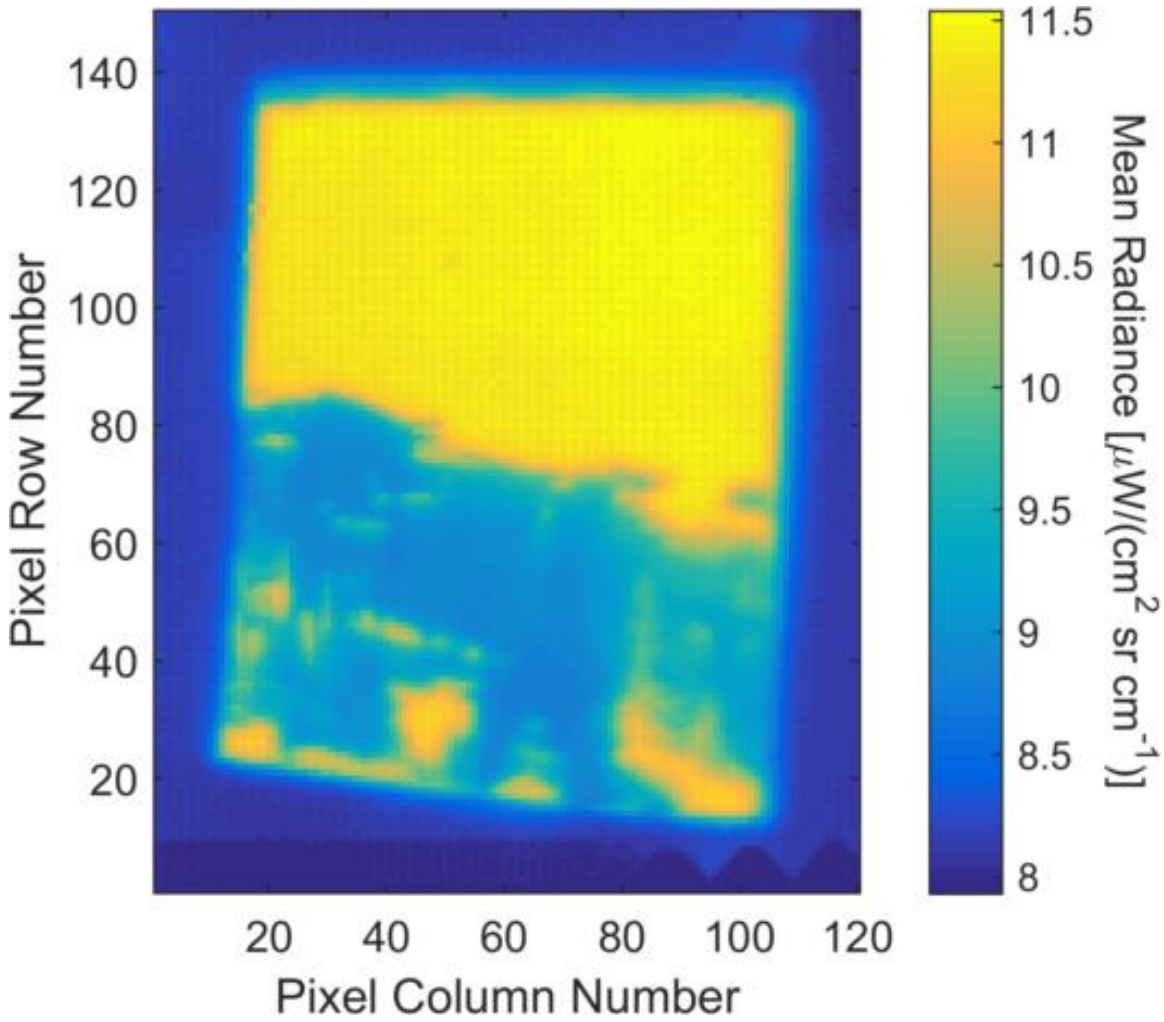

Figure 58 - Calibrated image of stainless steel with 25µL DMMP applied.

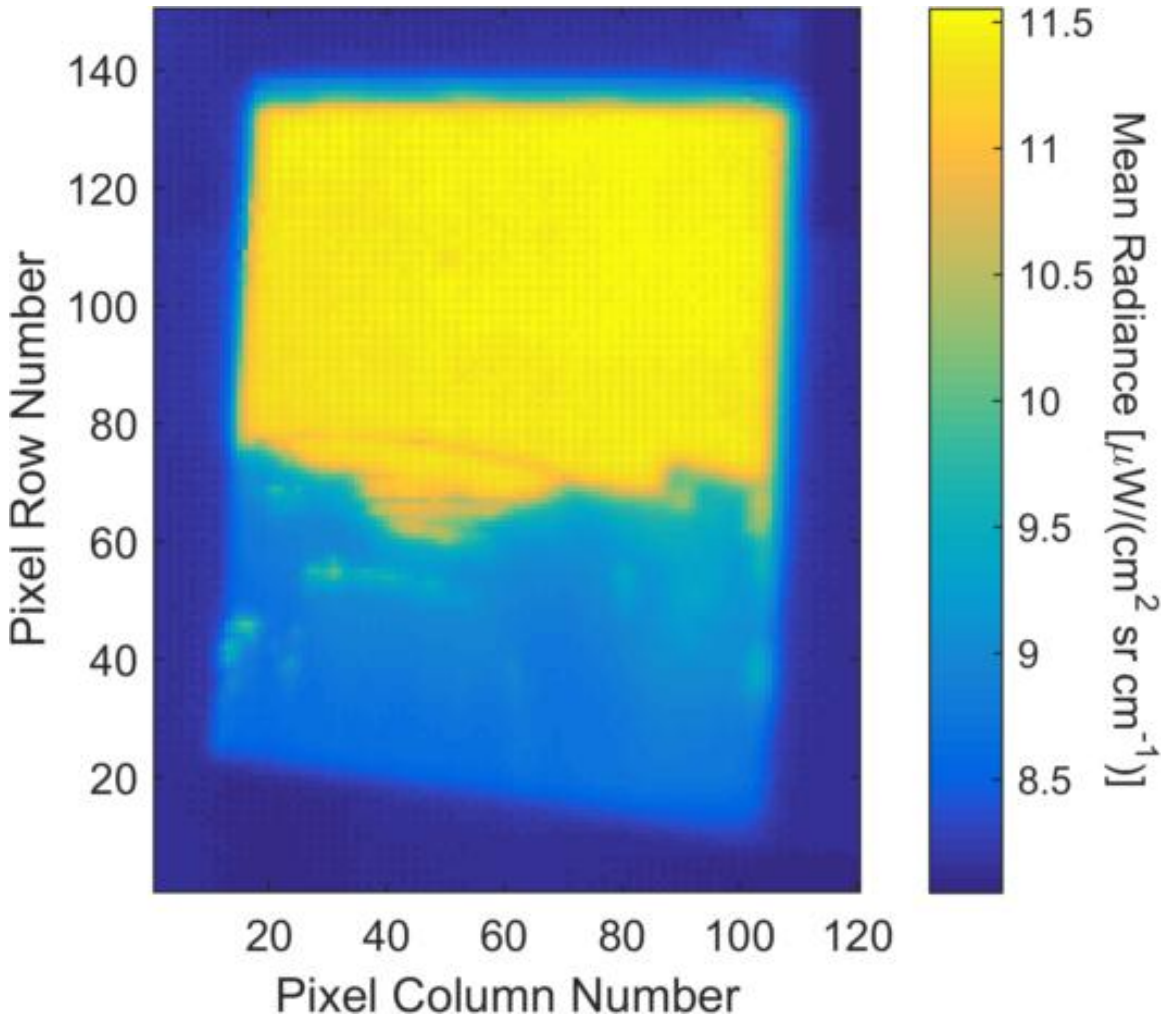

Figure 59 - Calibrated image of stainless steel with 50µL DMMP applied.

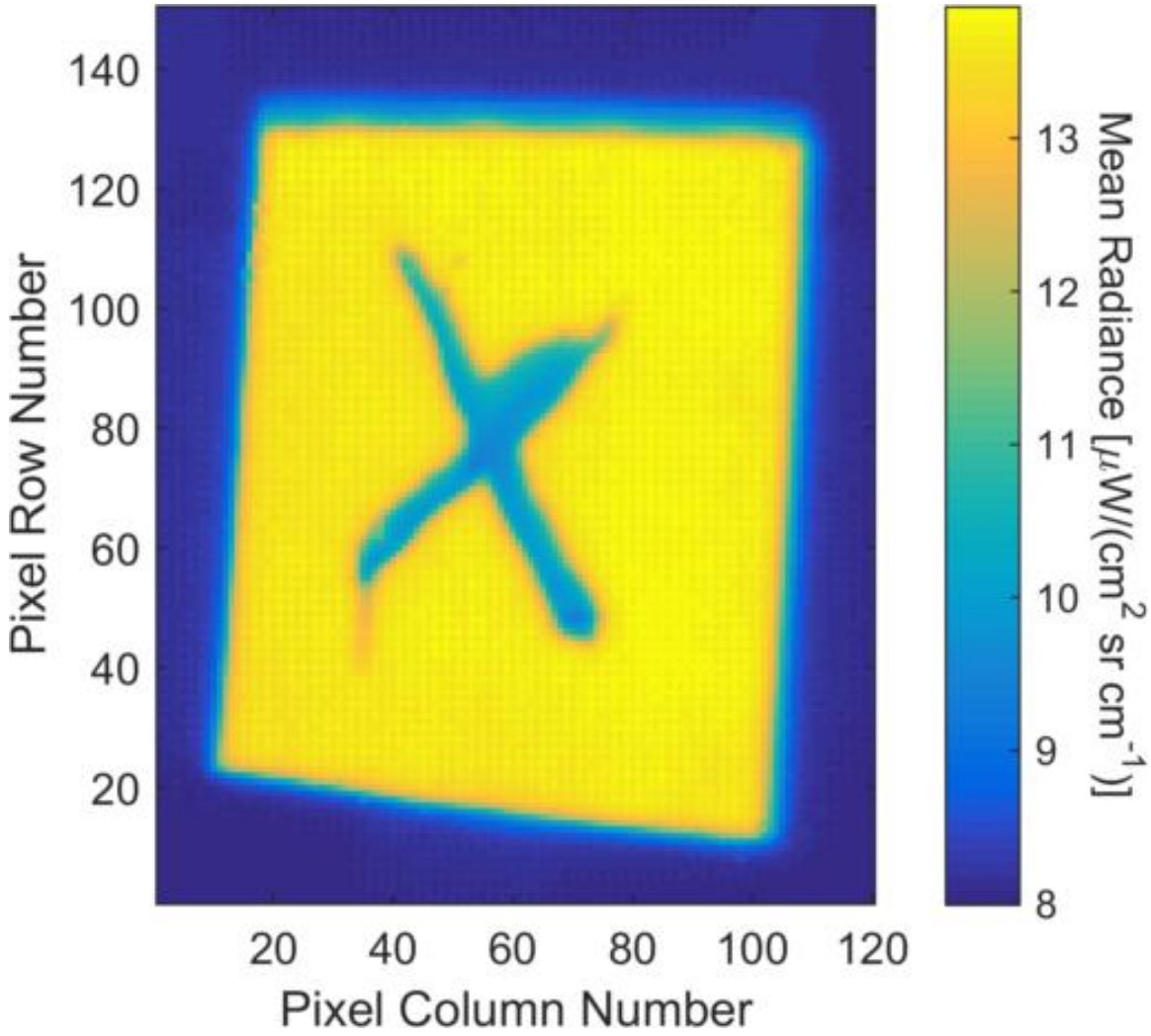

Figure 60 - Calibrated image of stainless steel with 10μL DMMP applied in "X" pattern.

The illumination can be seen to be off-center in the calibrated image of bare formica laminate in Figure 61.

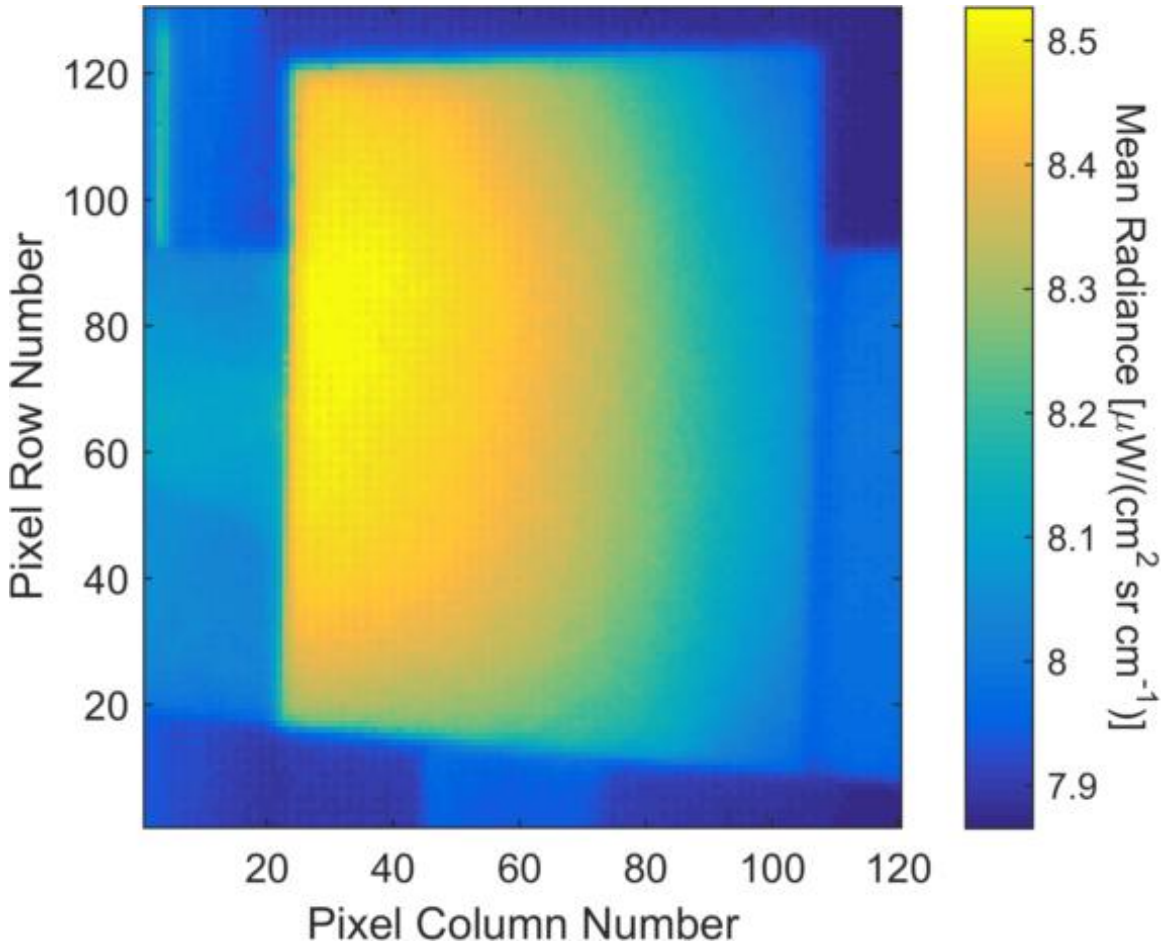

Figure 61 - Calibrated image of bare laminate.

In Figure 62, the non-illuminated bottom right seems to get darker, but there is no clear deposition pattern visible. There is also little difference in Figure 63 as the amount of DMMP applied goes up from 1 to 5µL.

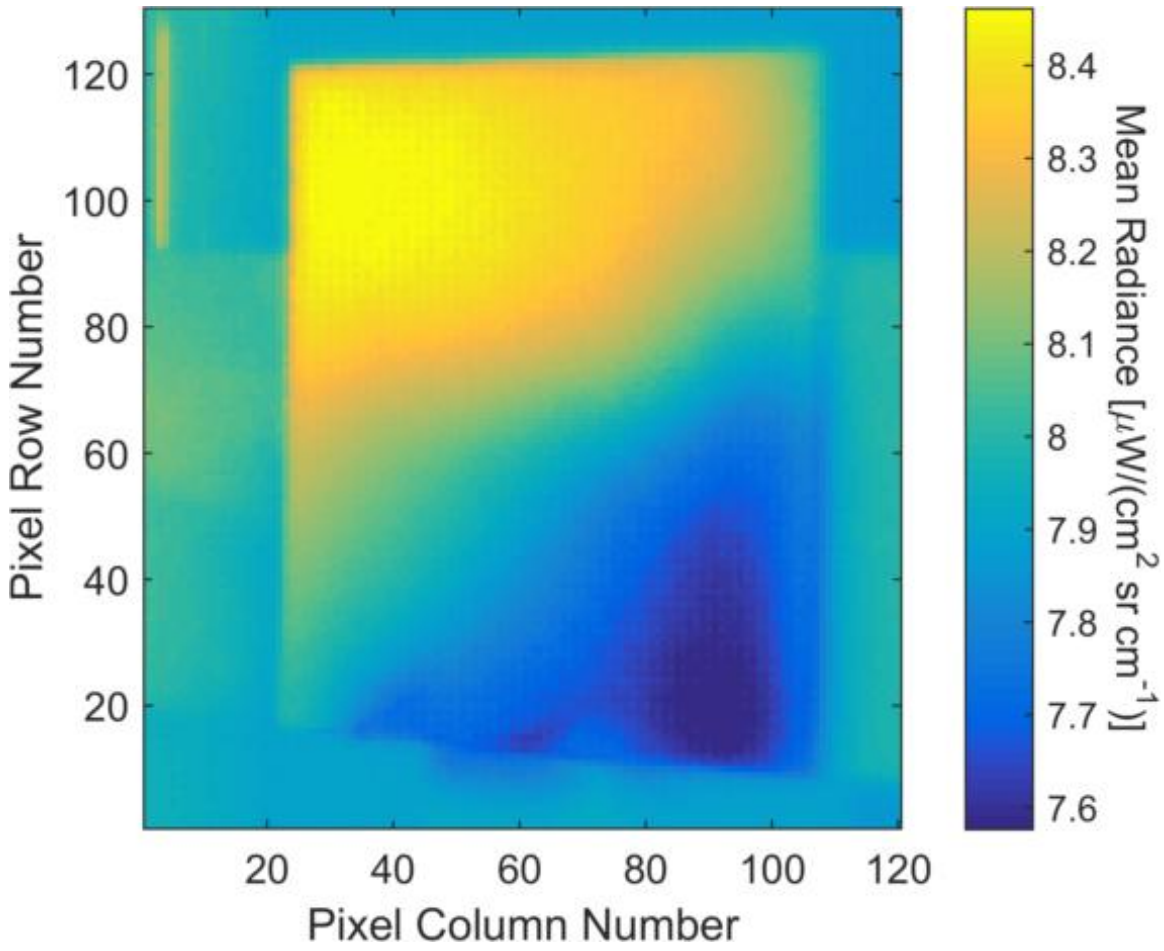

Figure 62 - Calibrated image of laminate with 1µL DMMP applied.

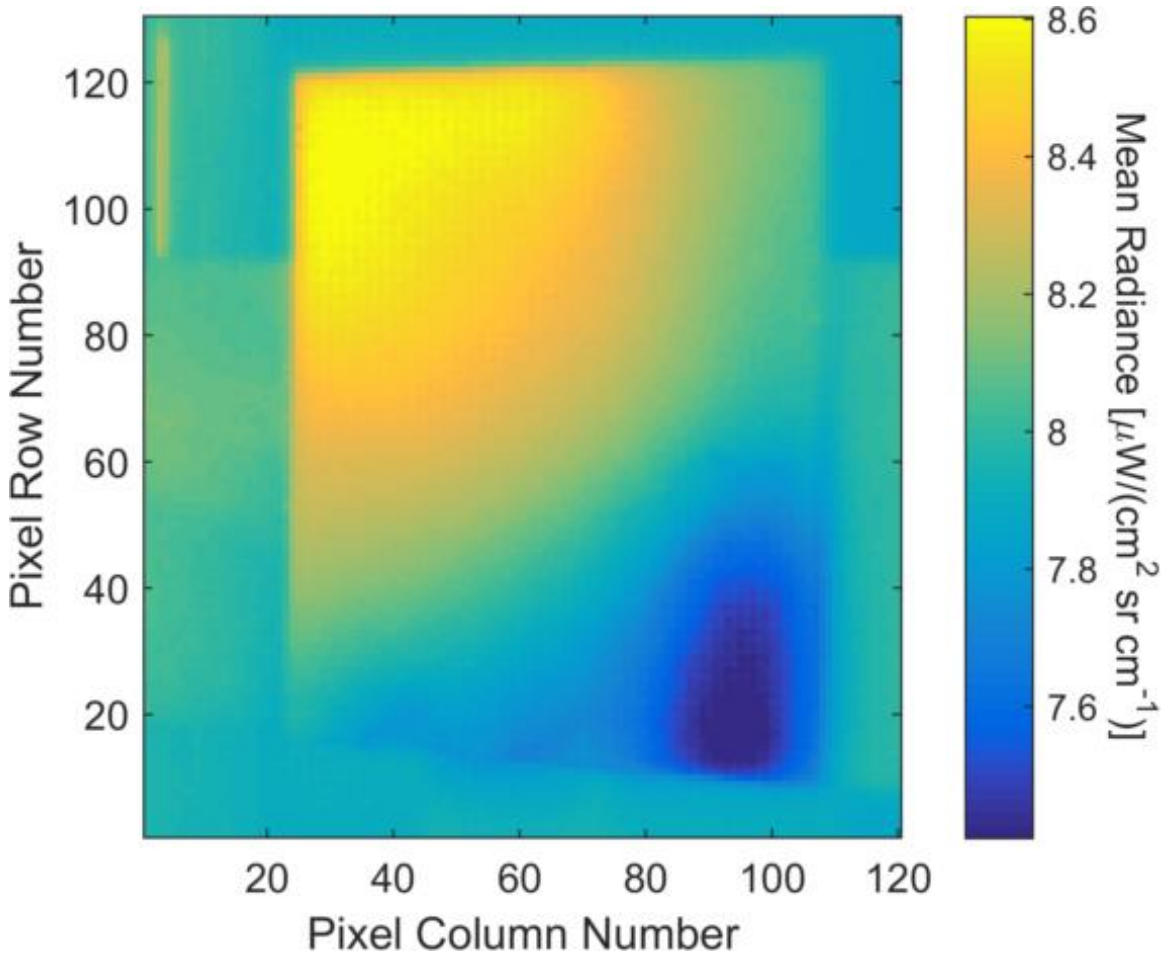

Figure 63 - Calibrated image of laminate with 5µL DMMP applied.

Some deposition is becoming visible in the calibrated image of 10µL DMMP applied to formica laminate. The blue area of the image now takes up the left side of the coupon as well.

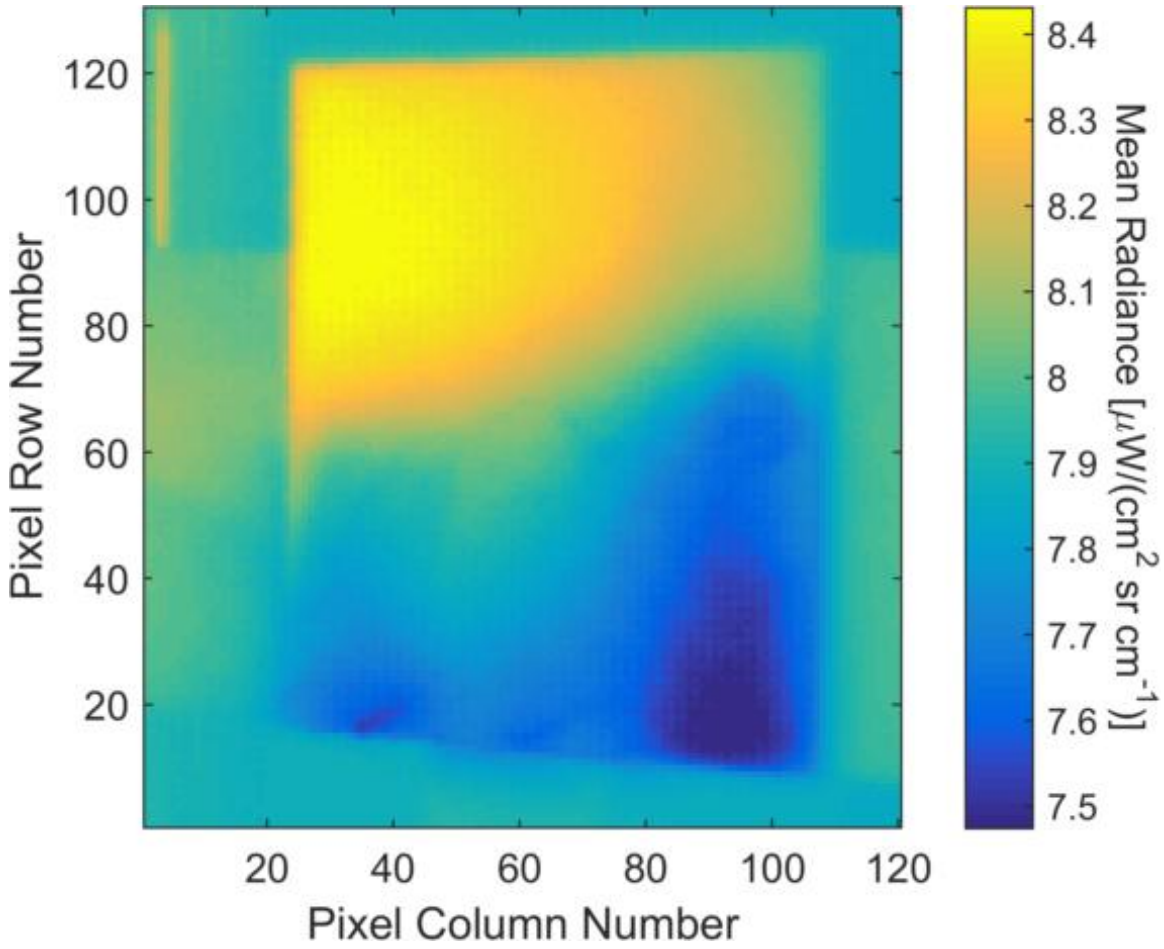

Figure 64 - Calibrated image of laminate with 10µL DMMP applied by solution.

In this blank, which was used to process the higher concentration scenes, it can be seen that the illumination is properly centered.

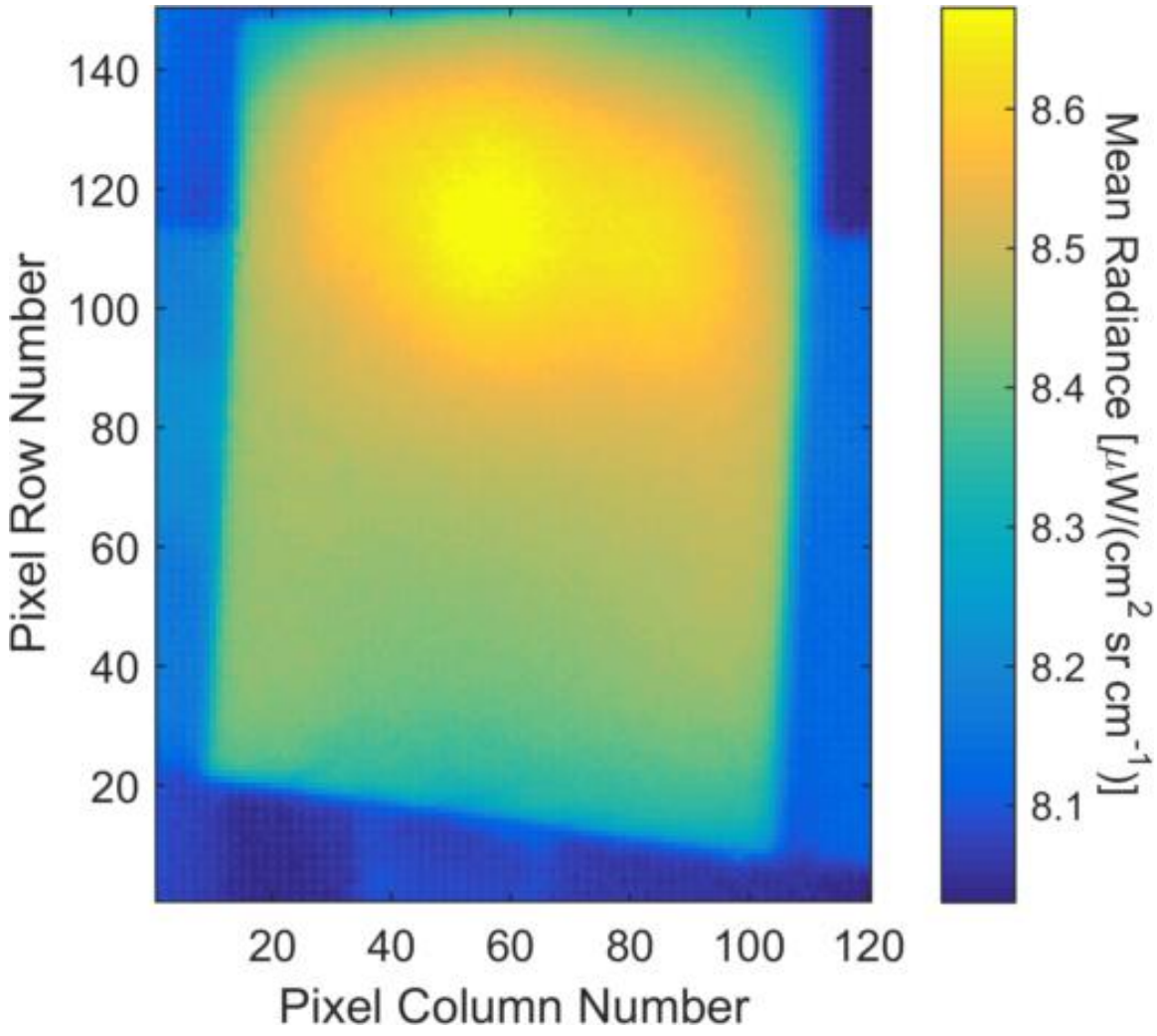

Figure 65 - Calibrated image of bare laminate.

The contaminated areas are much easier to see as concentration increases as seen in Figures 66-68. When compared to the bare sample, the blue area on the bottom half of the coupon stands out. In Figure 69, the X pattern, which was not visible on the broadband image, can now be faintly seen.

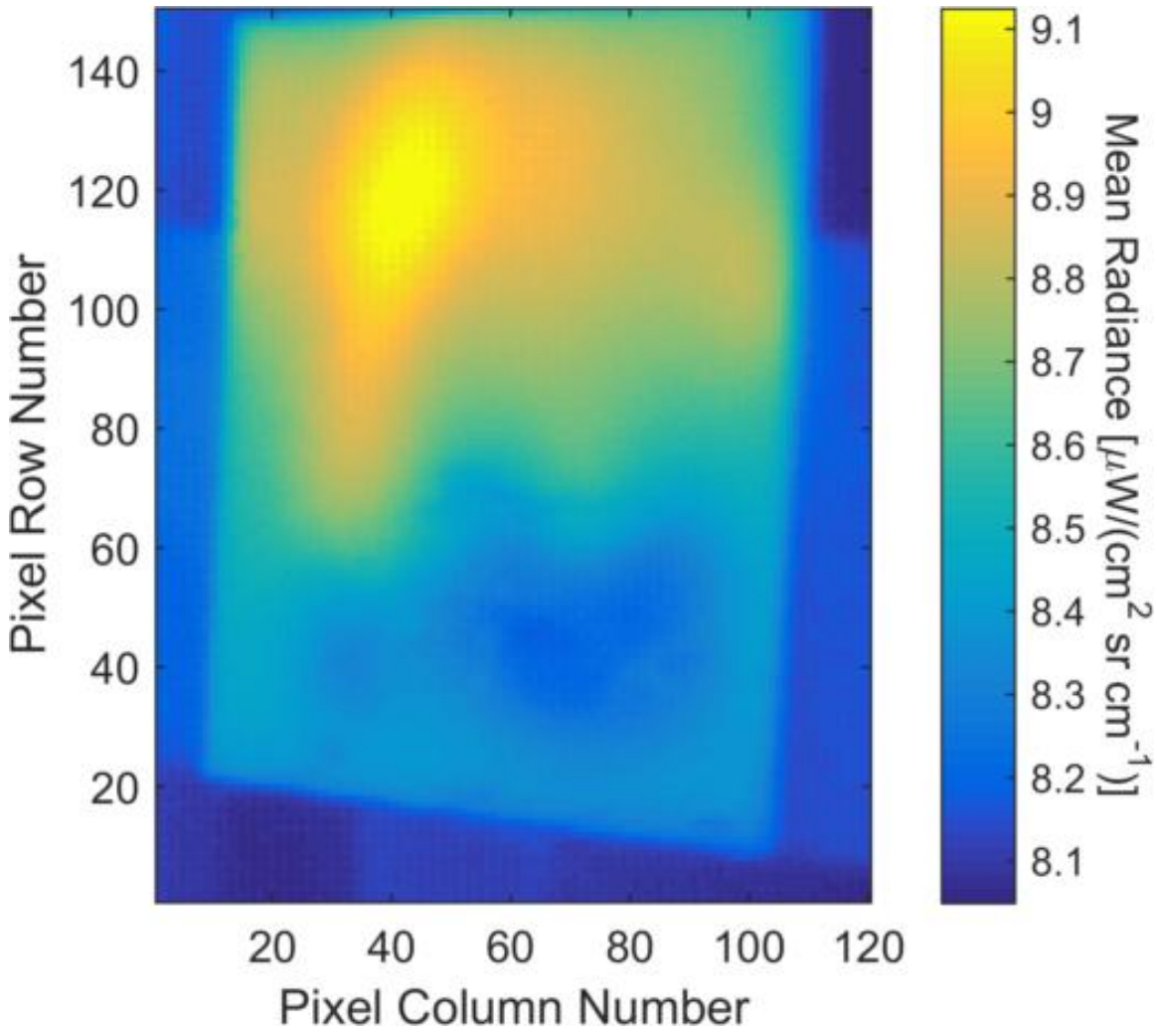

Figure 66 - Calibrated image of laminate with 10μL DMMP applied by smearing.

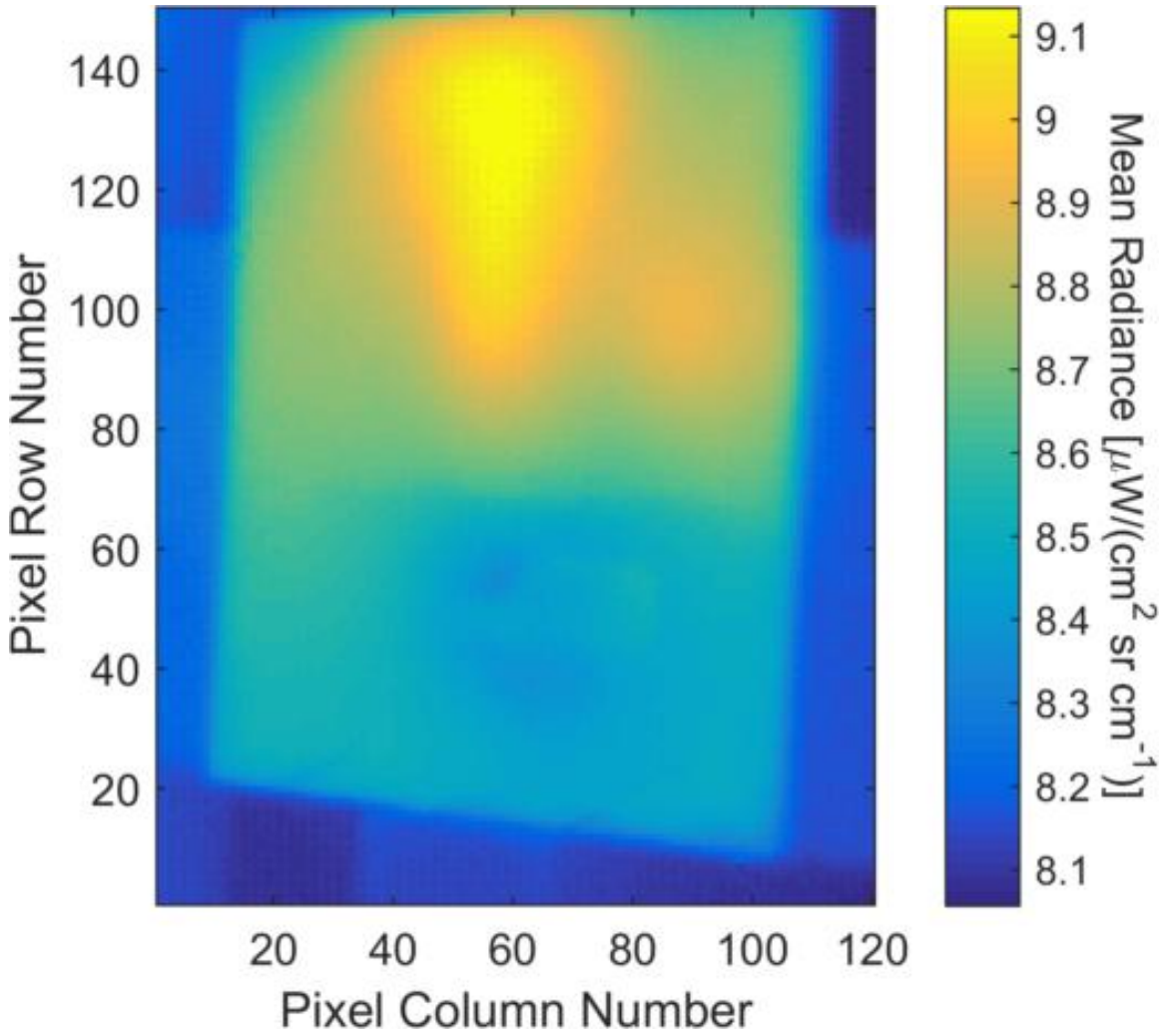

Figure 67 - Calibrated image of laminate with 25µL DMMP applied.

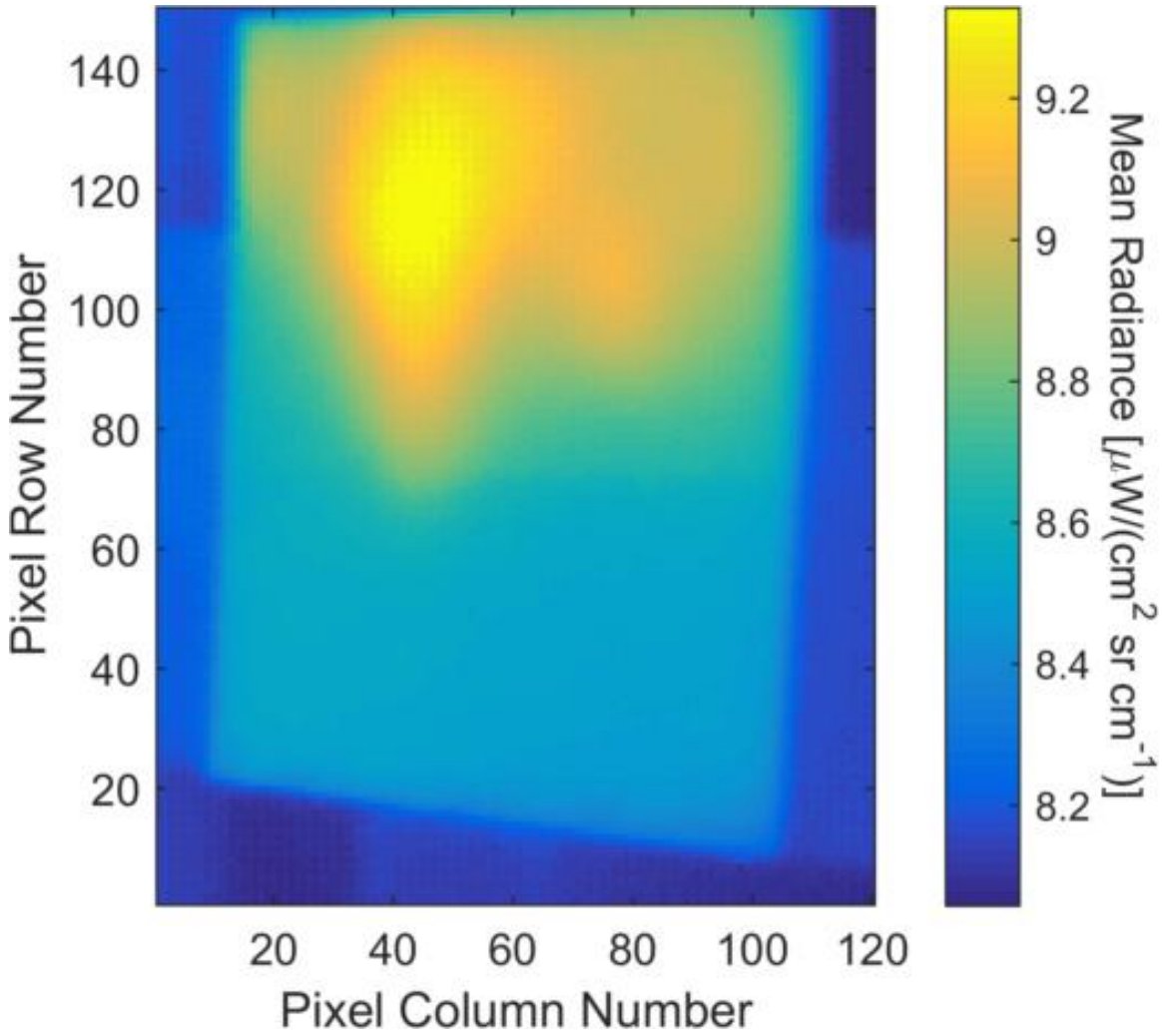

Figure 68 - Calibrated image of laminate with 50µL DMMP applied.

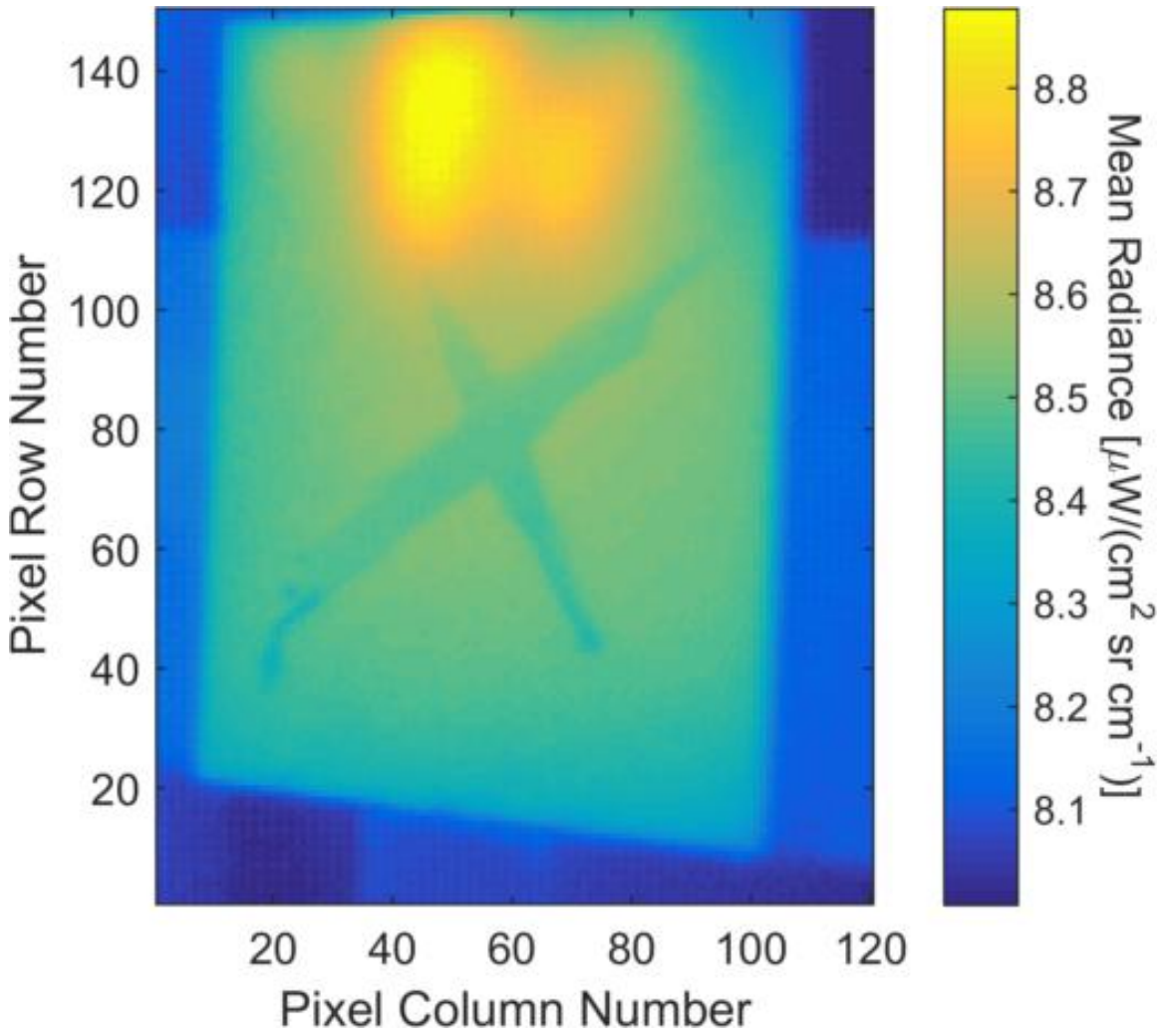

Figure 69 - Calibrated image of laminate with 10µL DMMP applied in "X" pattern.

Appendix D – Spectral Angle Plots

The spectral angle plots were generated to clarify where contamination with a spectrum similar to a DMMP reference spectrum exists. In Figure 70, it can be seen that some of the noise does give a fairly low angle, but there is no discernable pattern to it.

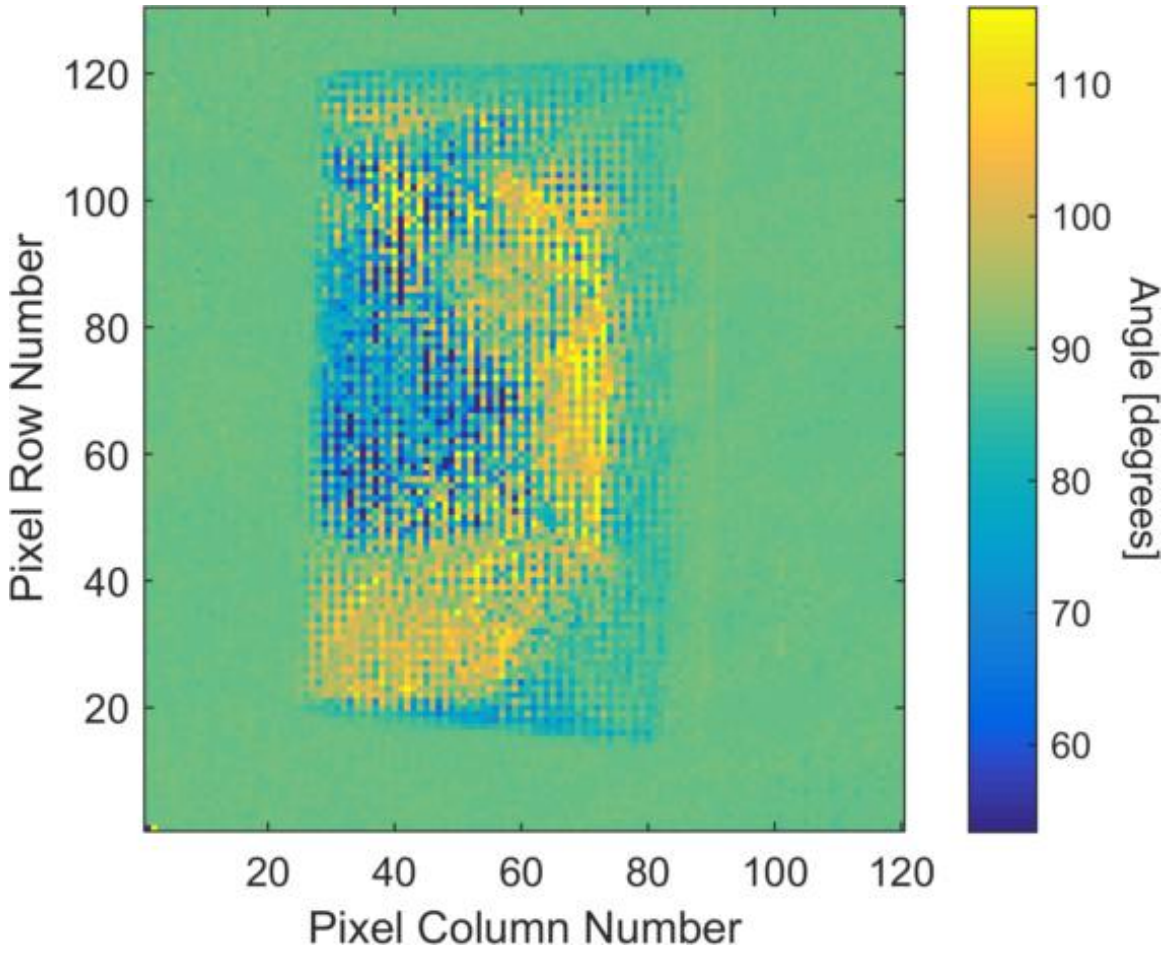

Figure 70 - Spectral angle plot of bare stainless steel.

In Figure 71, we can clearly see the deposition across the bottom half of the coupon. This is much clearer than the calibrated image (Figure 53) where there was only slightly darker yellow sections in this area.

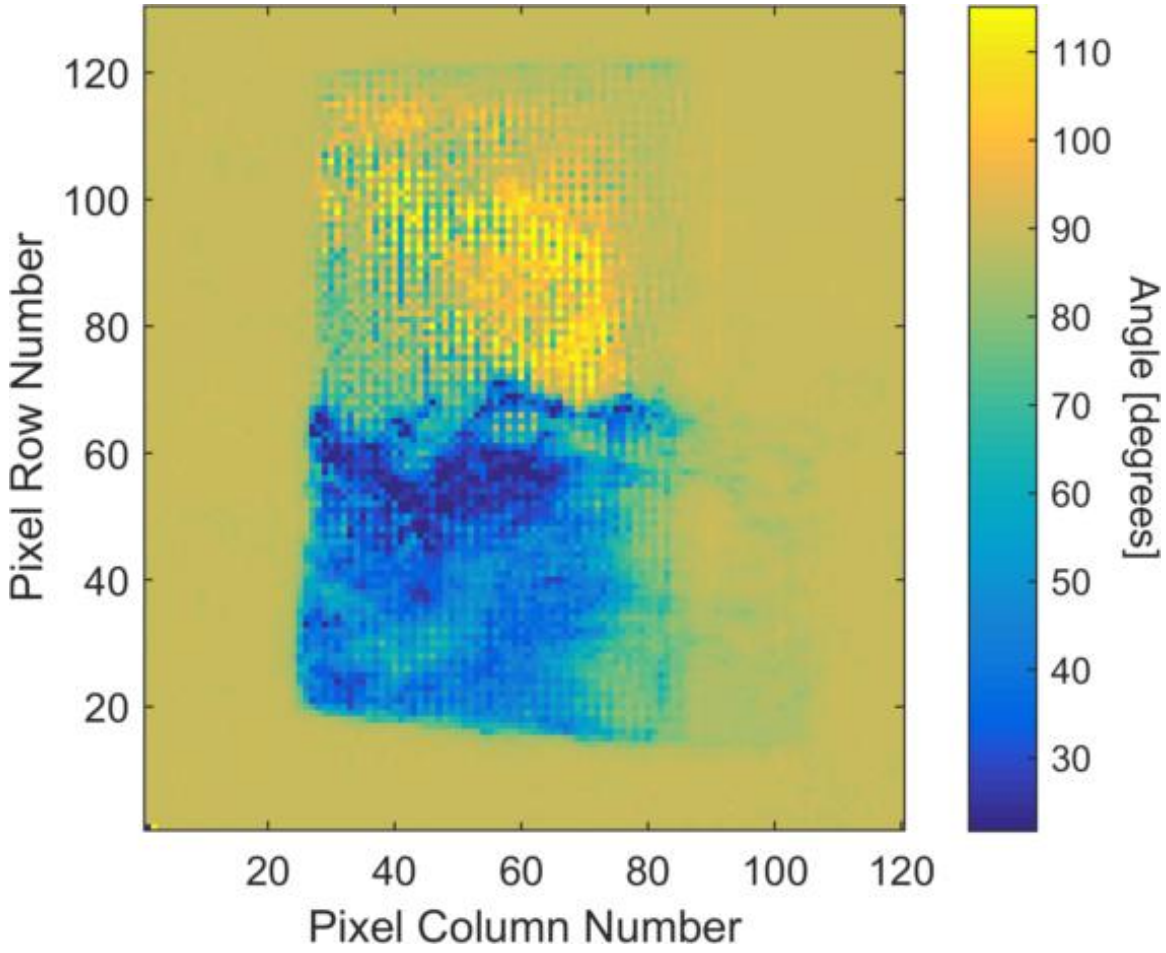

Figure 71 – Spectral angle plot of stainless steel with 1µL DMMP applied.

Again, Figure 72 shows the chemical deposition much better than the calibrated image. In Figure 54, the only clear contamination was along row 60. Here varying concentrations can also be seen as the darker portions are more similar to the reference, and therefore of higher concentration.

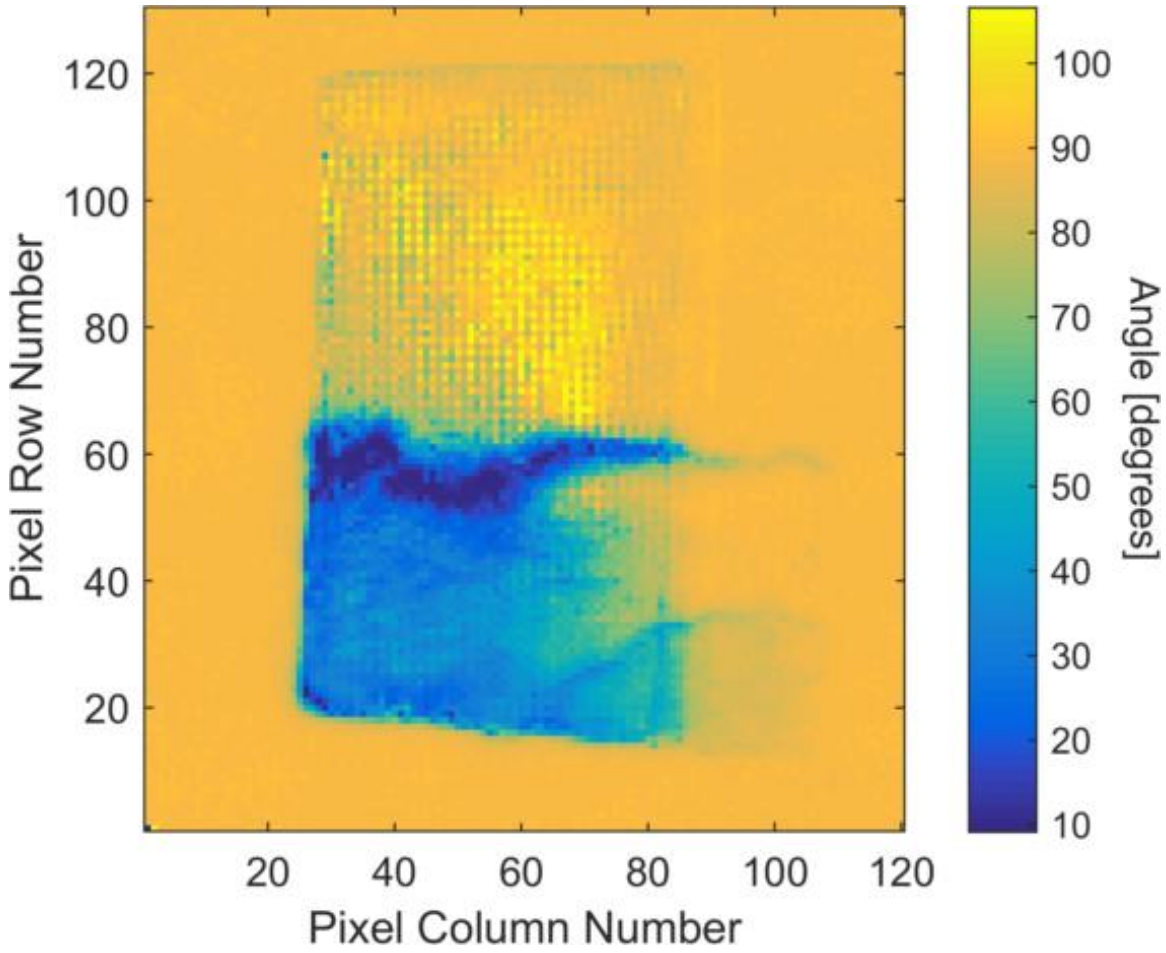

Figure 72 - Spectral angle plot of stainless steel with 5µL DMMP applied.

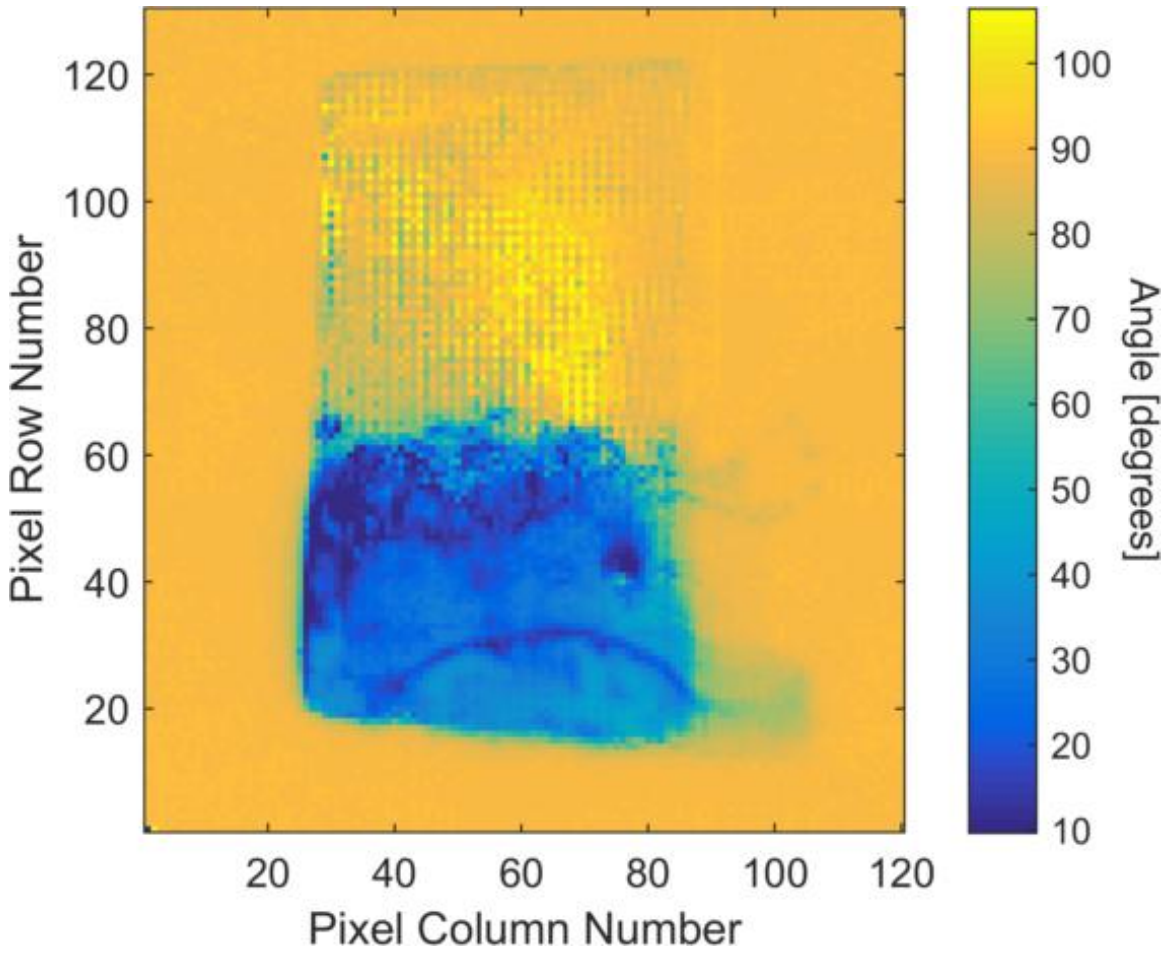

Figure 73 - Spectral angle plot of stainless steel with 10µL DMMP applied by solution.

In Figure 74, there is no discernable patter to the angles and it appears as just noise. The color scale shifted up, as there were pixels with a very high angle from the reference. This accounts for the darker colors overall. As the concentrations increase in Figures 75-77, the deposition becomes ever clearer.

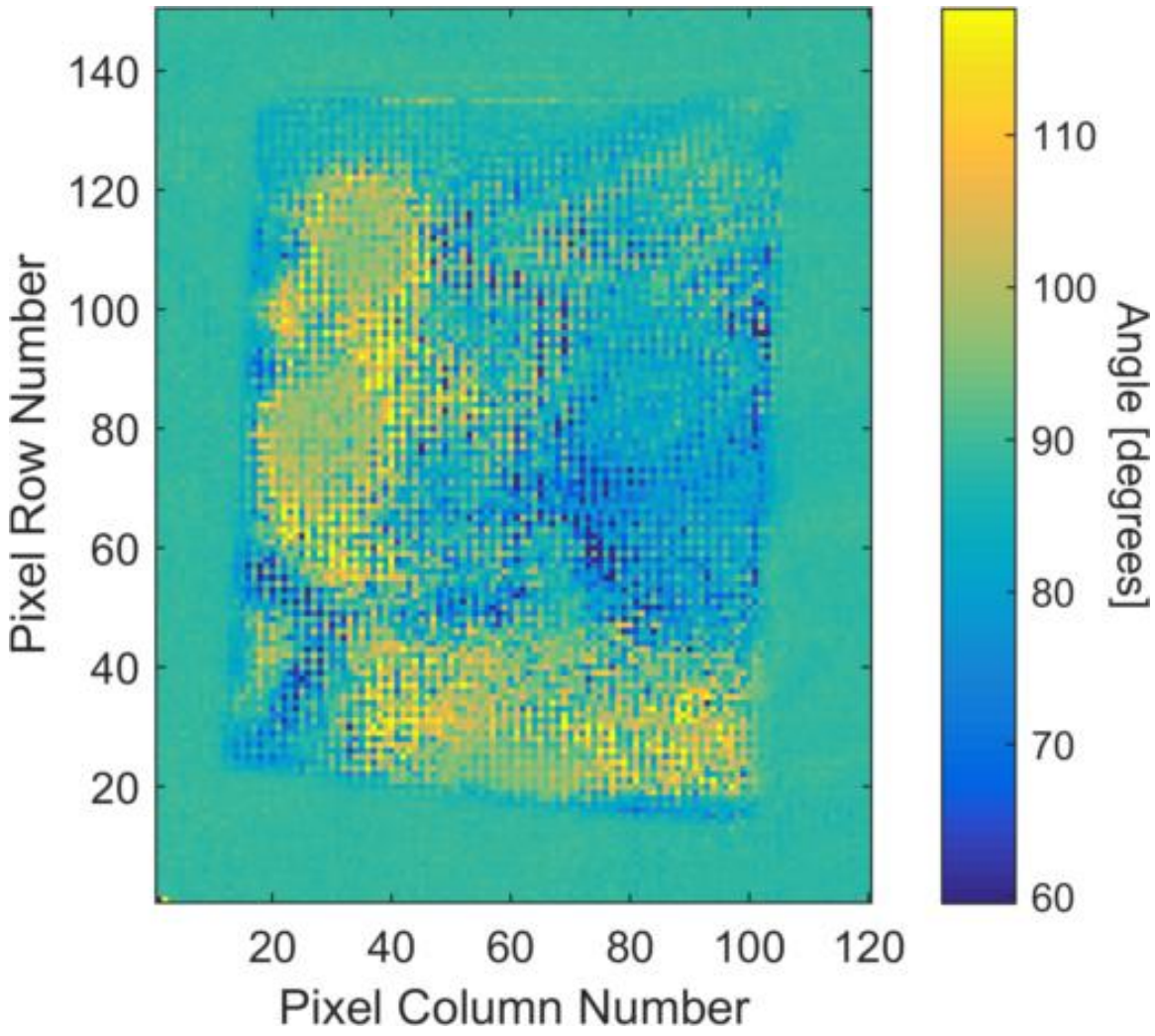

Figure 74 - Spectral angle plot of bare stainless steel.

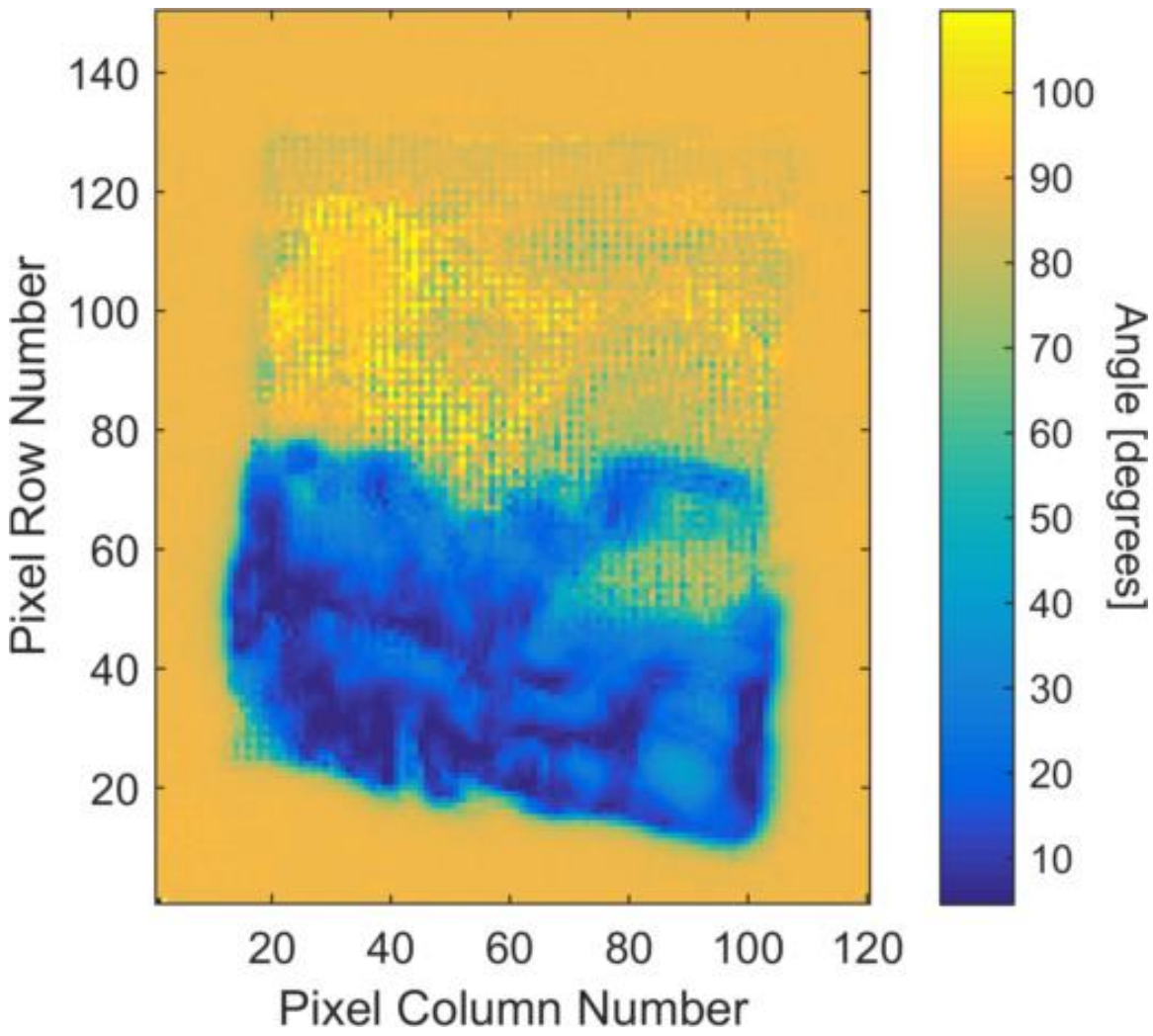

Figure 75 - Spectral angle plot of stainless steel with 10µL DMMP applied by smearing.

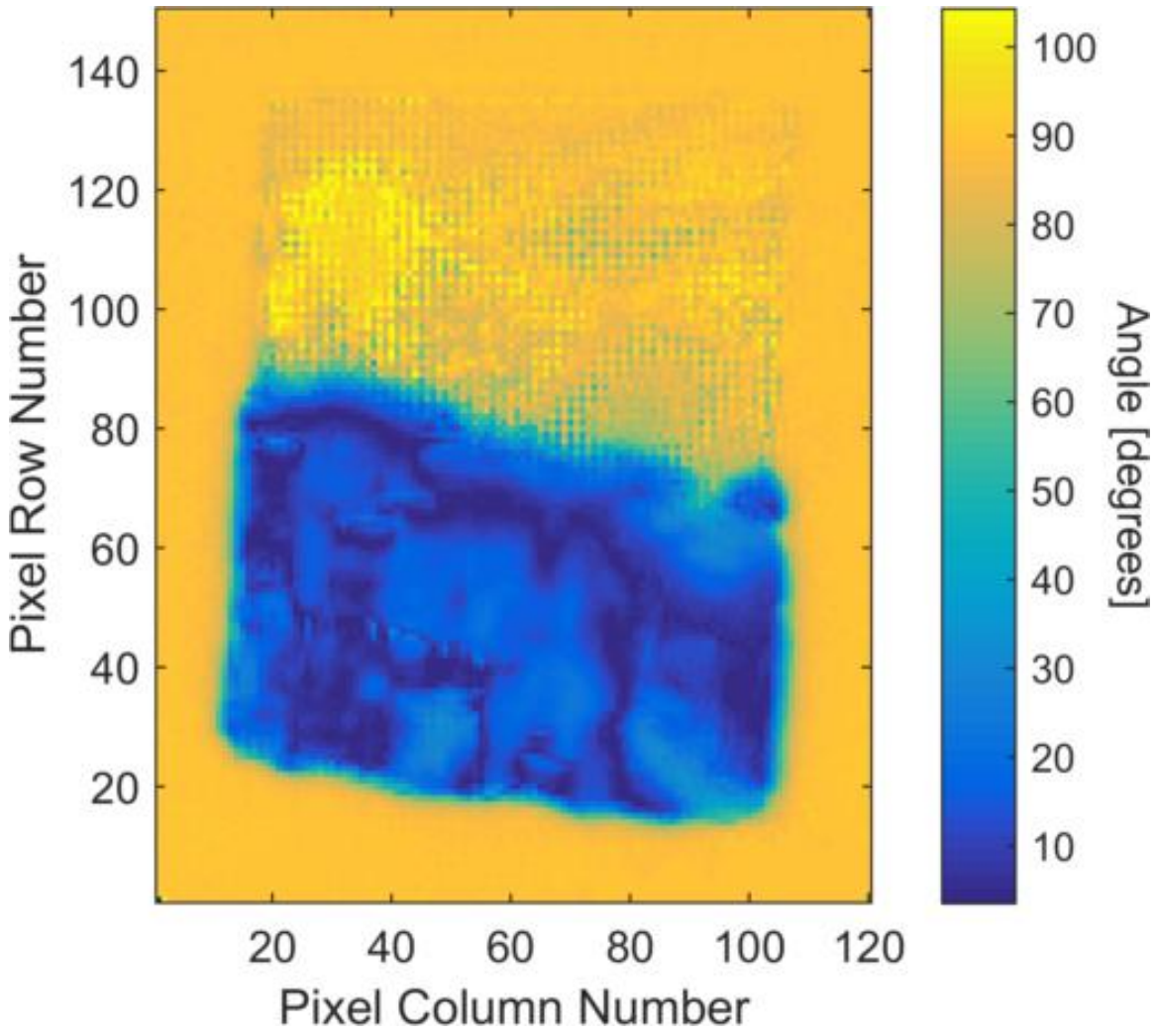

Figure 76 - Spectral angle plot of stainless steel with 25µL DMMP applied.

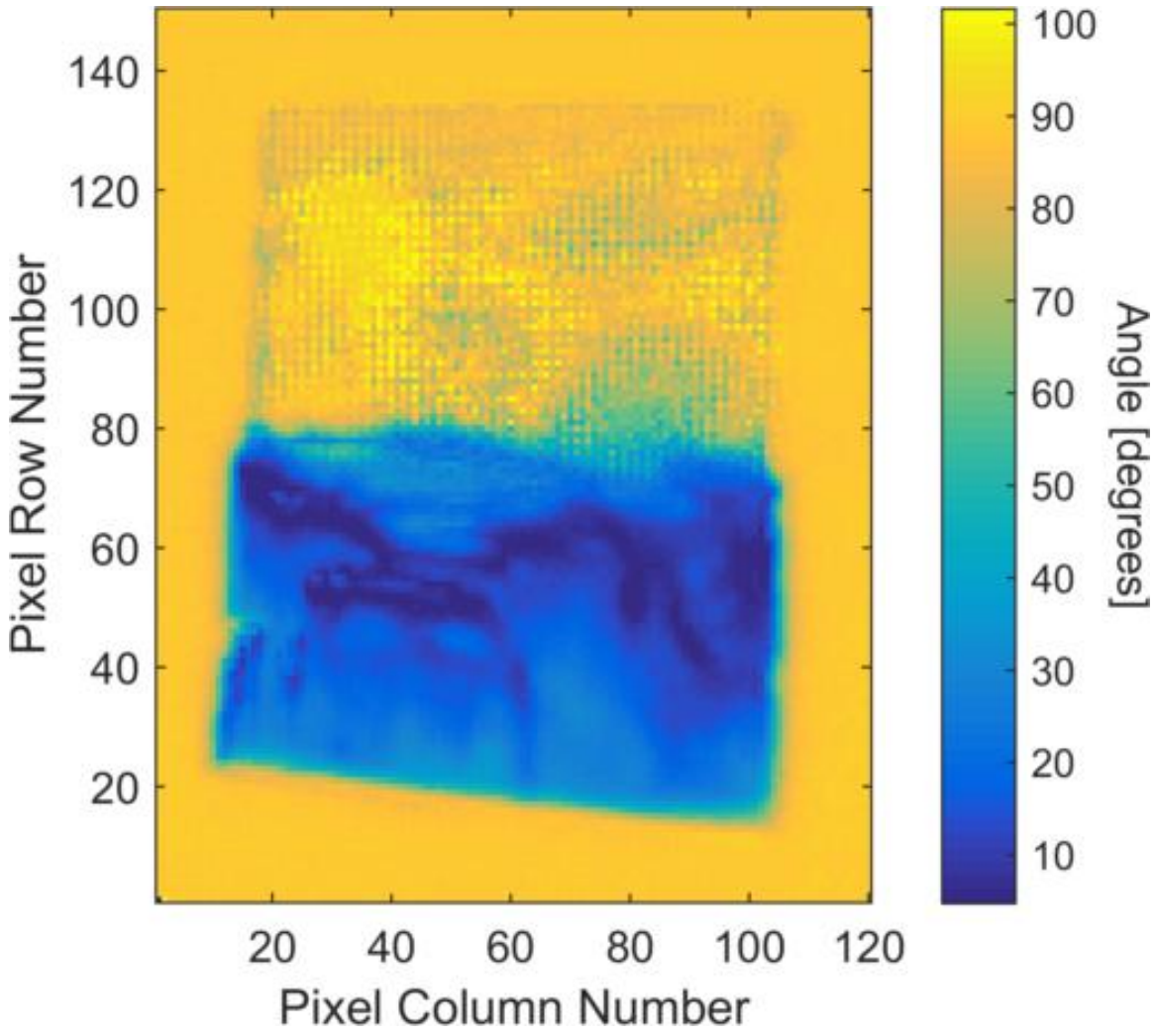

Figure 77 - Spectral angle plot of stainless steel with 50µL DMMP applied.

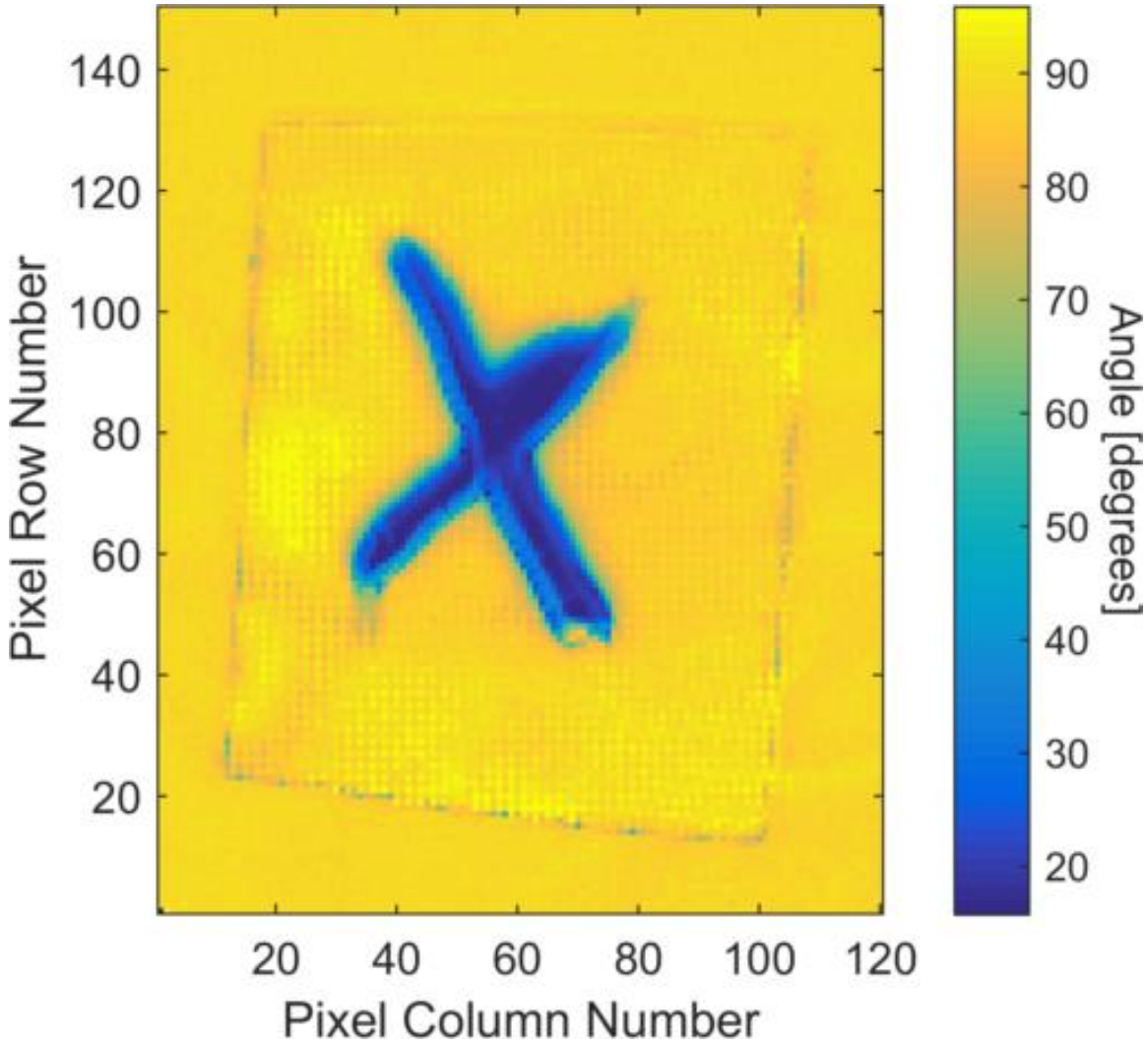

Figure 78 - Spectral angle plot of stainless steel with 10µL DMMP applied in "X" pattern.

The bare formica laminate scene again has some lower angles, but appears as noise. In Figure 80, it can be seen that the deposition of 1μL DMMP did not result in good coverage of the coupon. This led to problems with the quantification later on in data processing. The deposition in Figure 81 was also not ideal.

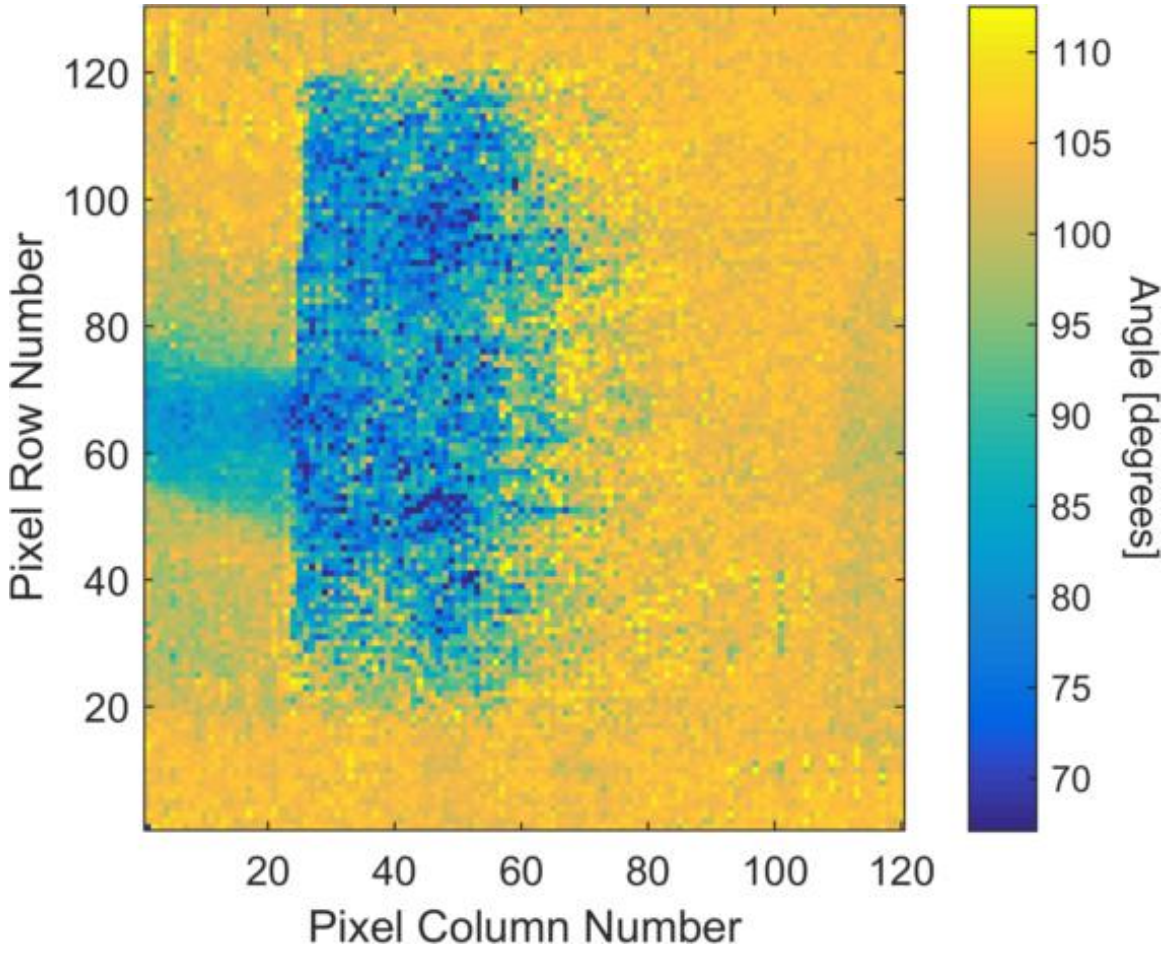

Figure 79 - Spectral angle plot of bare laminate.

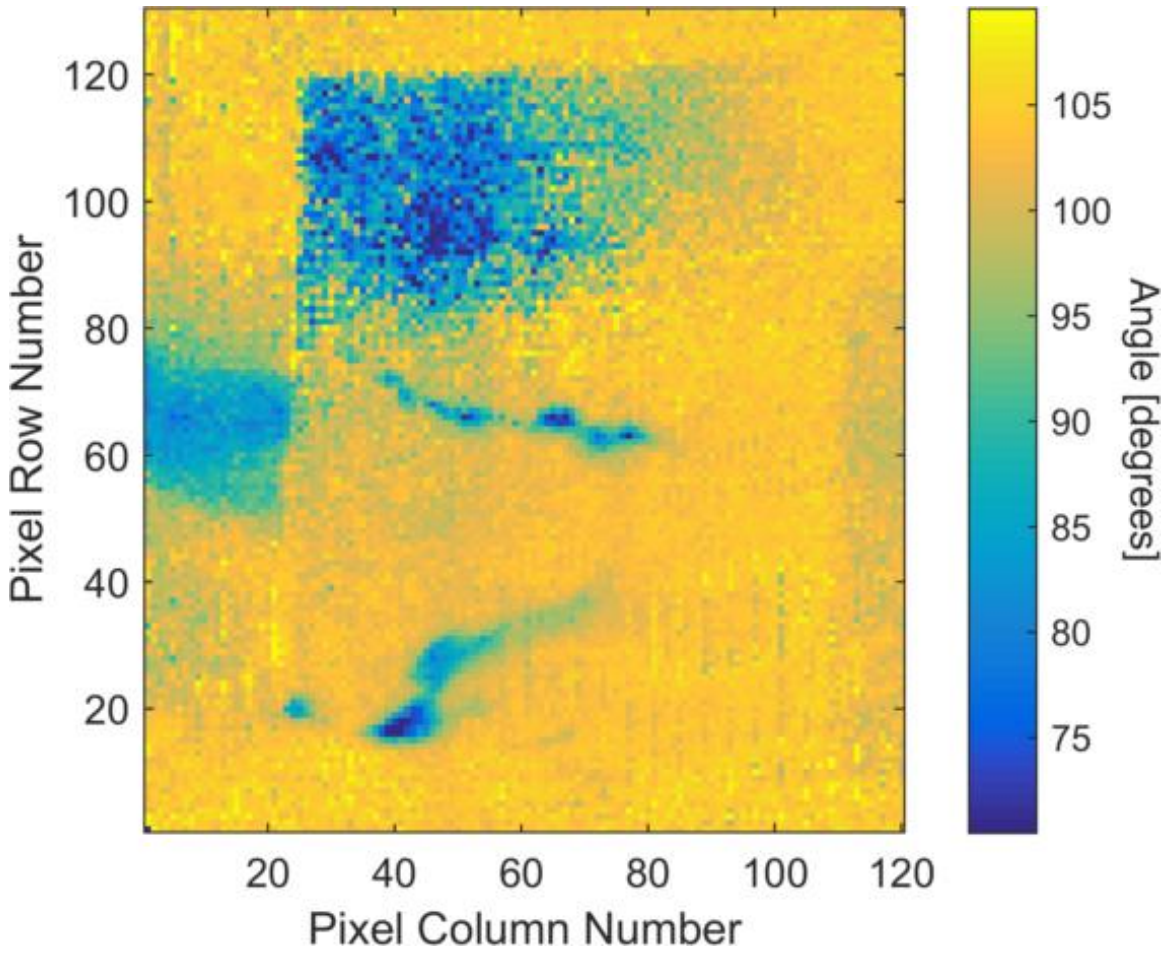

Figure 80 - Spectral angle plot of laminate with 1µL DMMP applied.

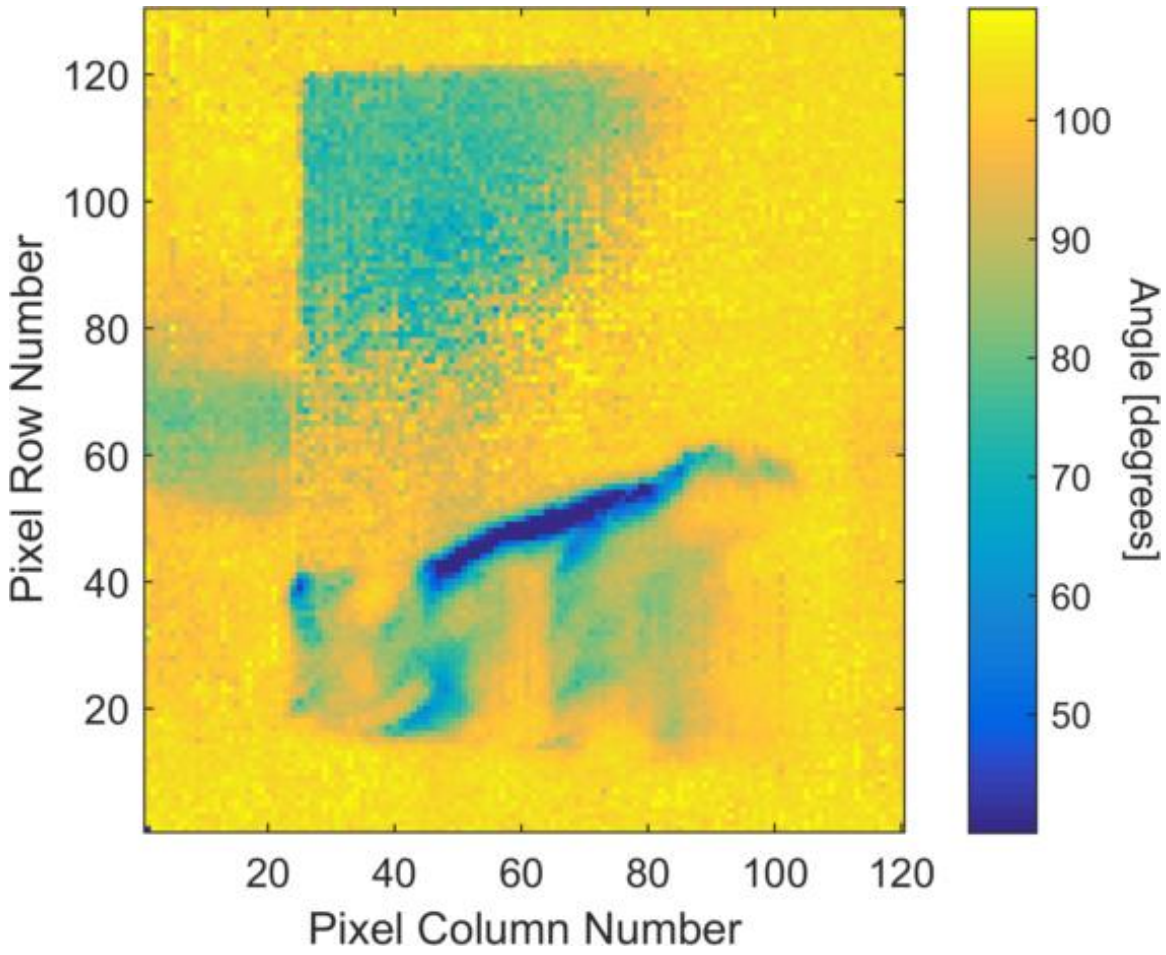

Figure 81 - Spectral angle plot of laminate with 5µL DMMP applied.

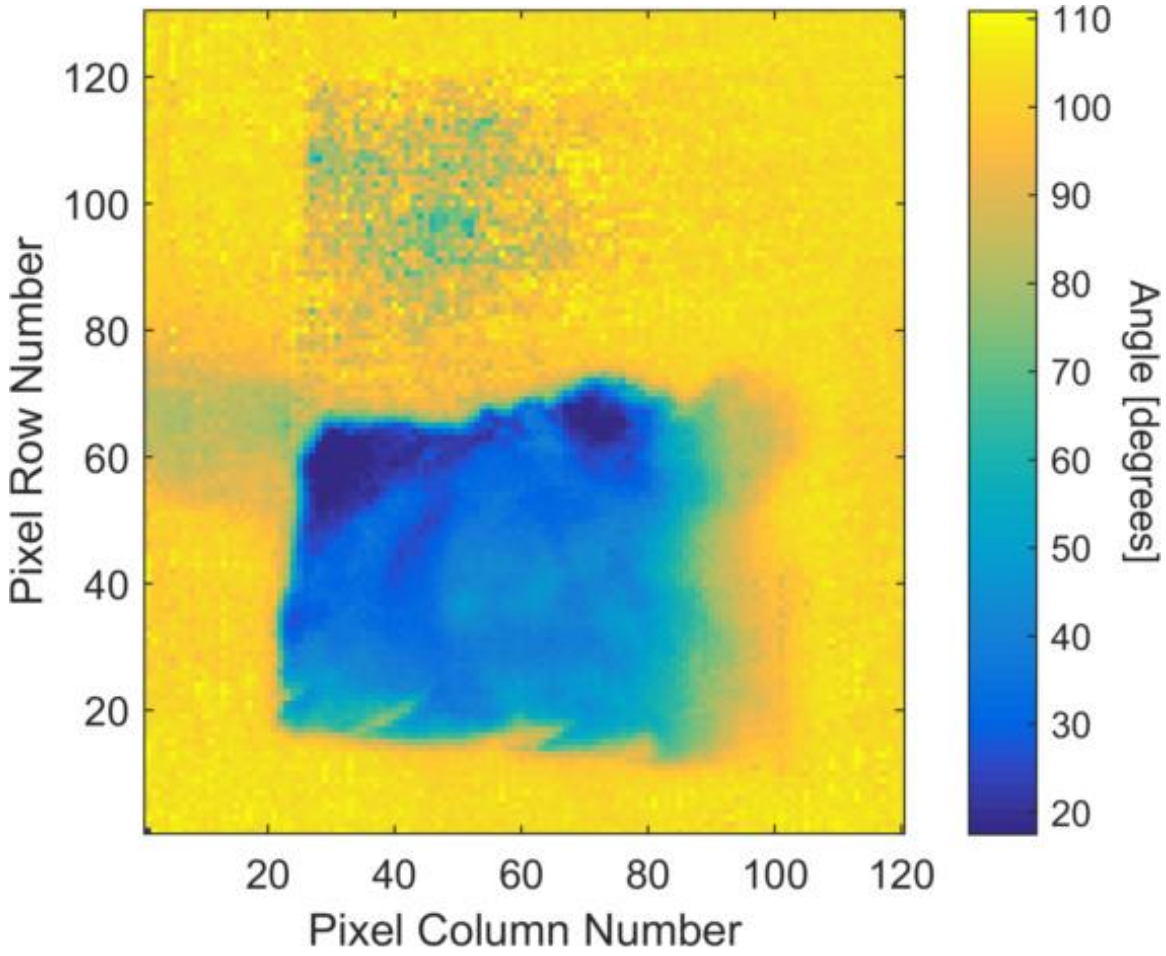

Figure 82 - Spectral angle plot of laminate with 10µL DMMP applied by solution.

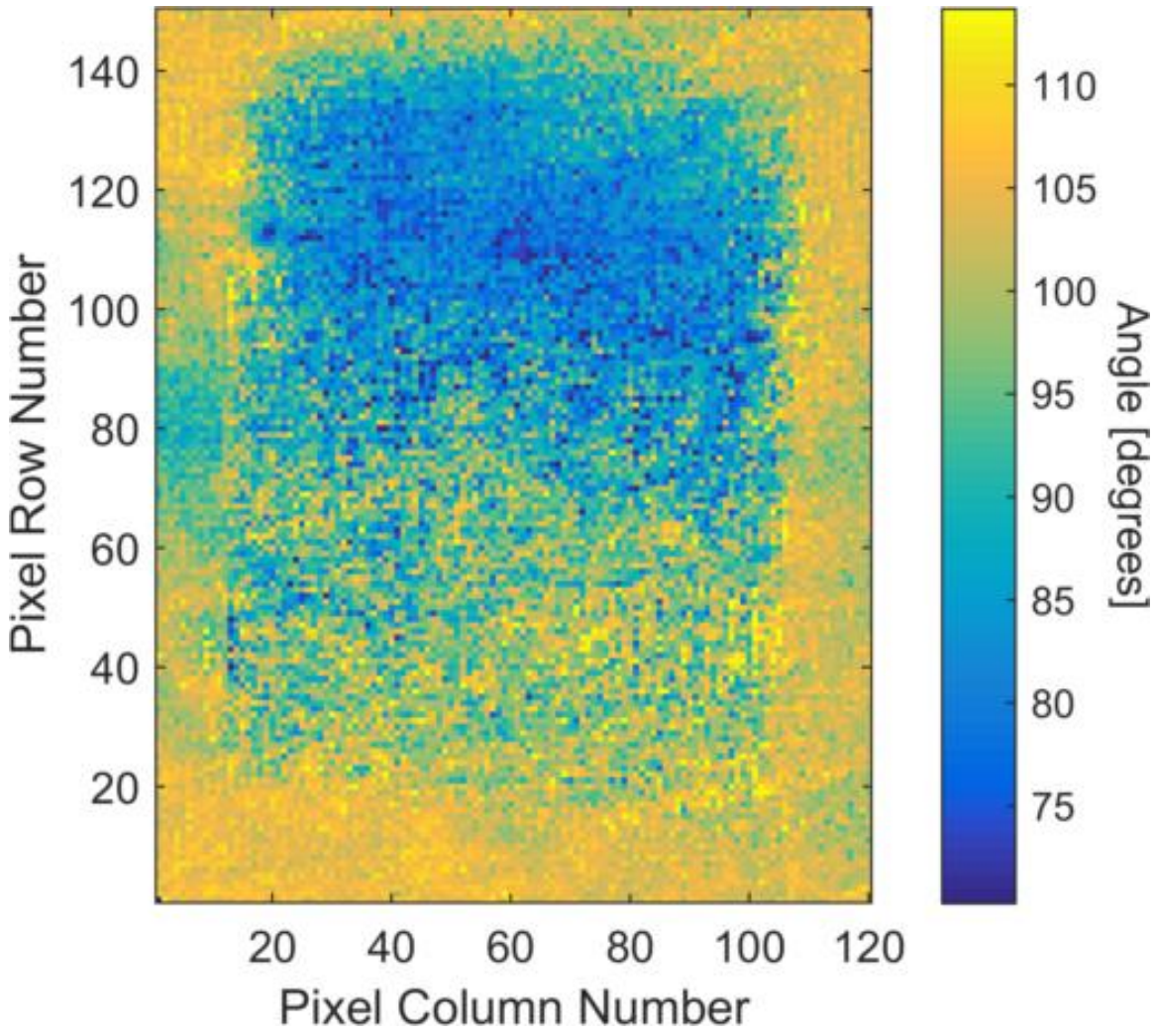

Figure 83 - Spectral angle plot of bare laminate.

As the concentrations increase, the deposition also becomes clearer on the formica laminate. Figure 87 shows the X pattern, which was faint in the calibrated image (Figure 69), is much clearer.

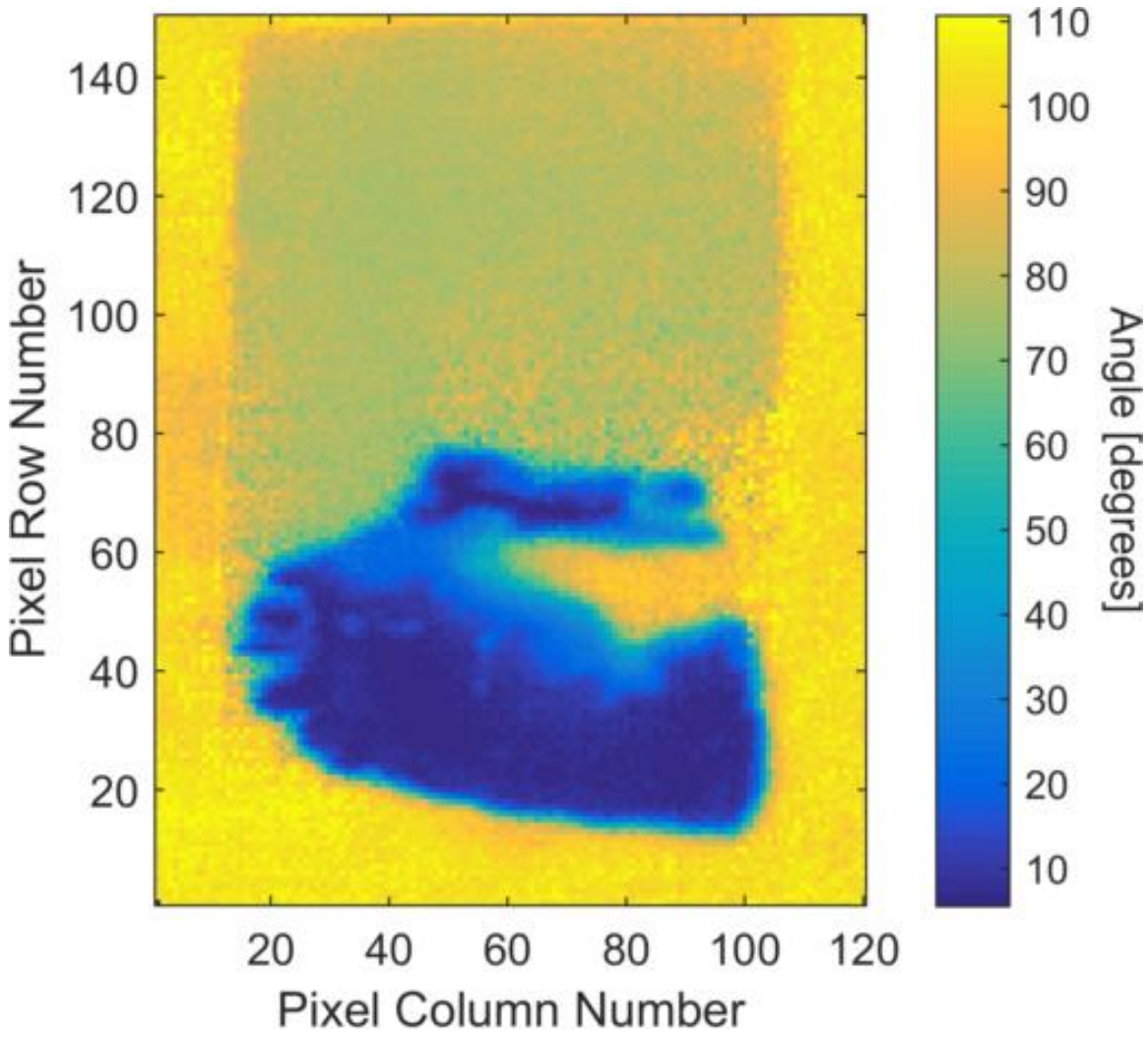

Figure 84 - Spectral angle plot of laminate with 10µL DMMP applied by smearing.

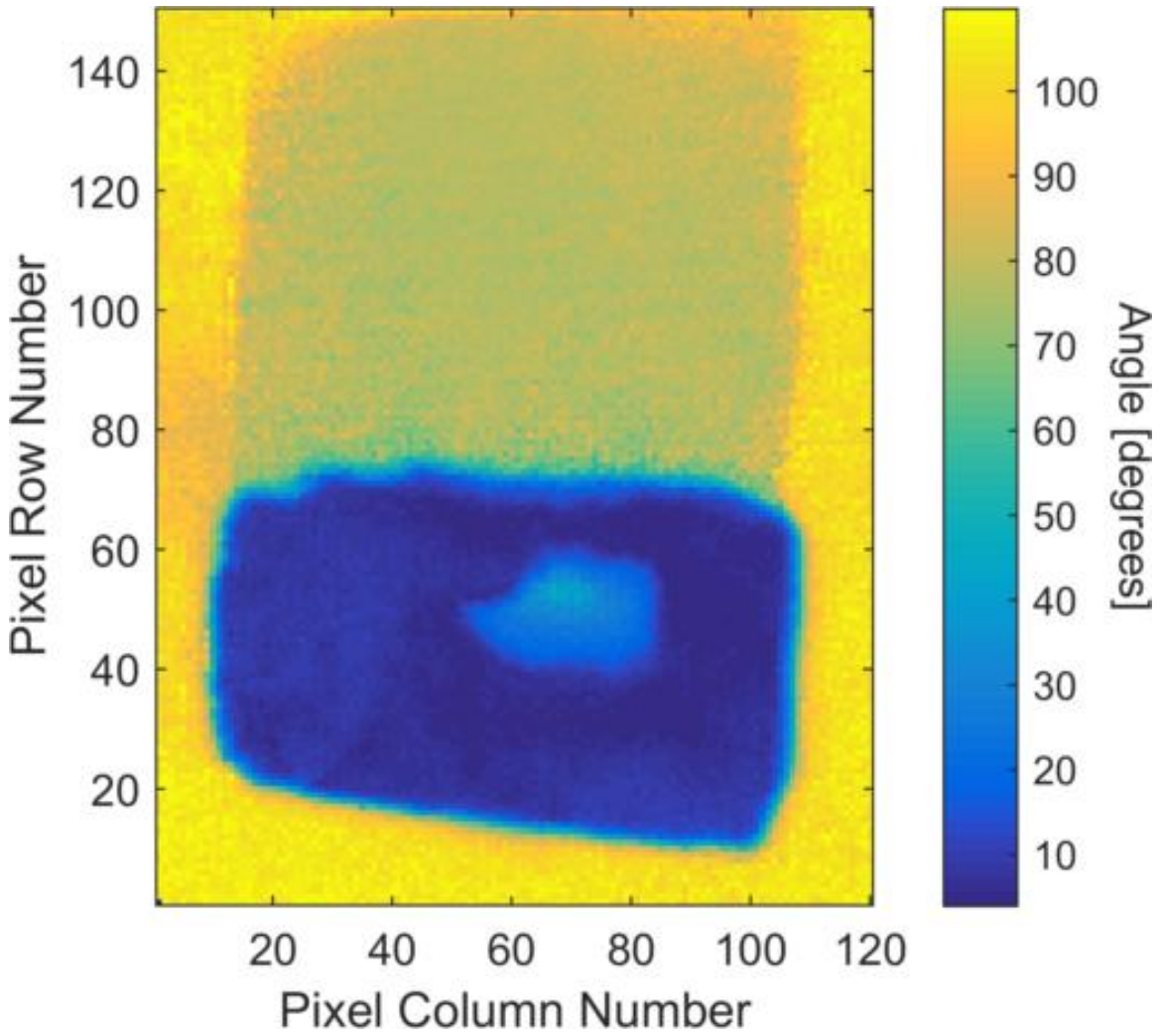

Figure 85 - Spectral angle plot of laminate with 25µL DMMP applied.

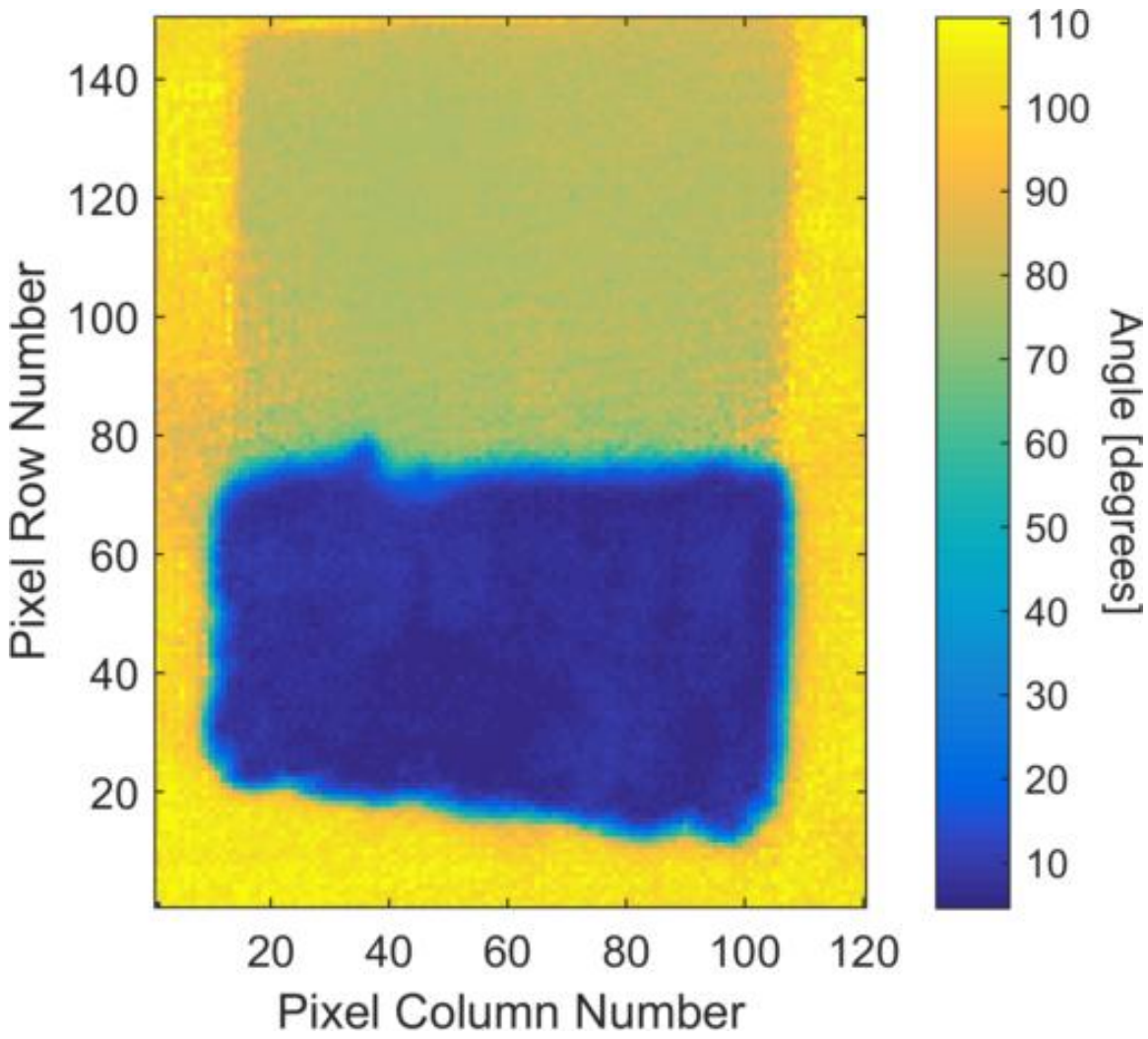

Figure 86 - Spectral angle plot of laminate with 50µL DMMP applied.

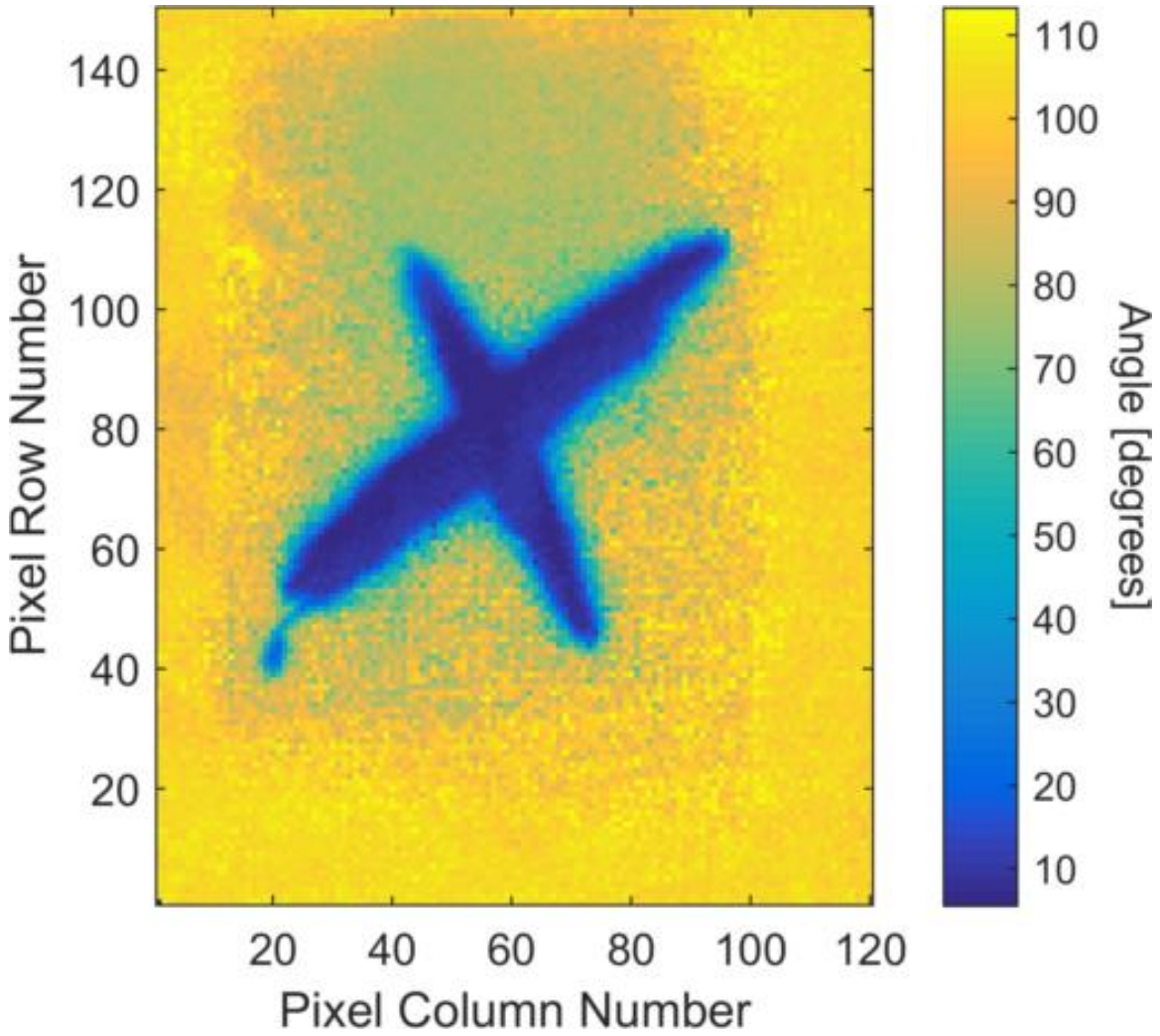

Figure 87 - Spectral angle plot of laminate with 10µL DMMP applied in "X" pattern.

Appendix E – Averaged Spectra

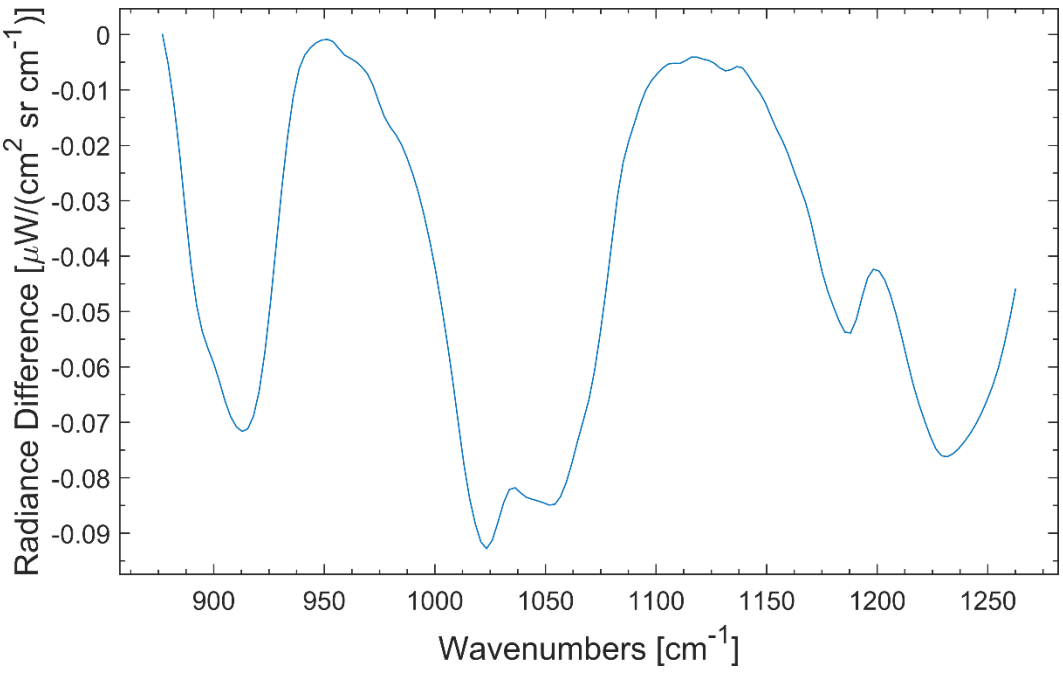

Figure 88 - Averaged spectra for 1µL DMMP applied to stainless steel (22µg/cm2).

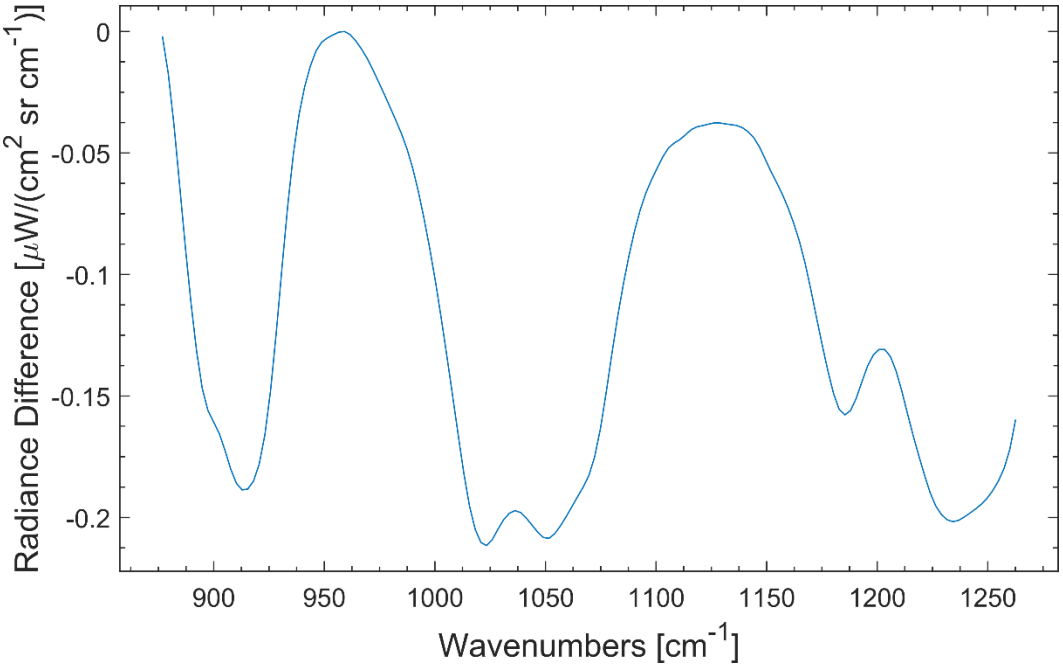

Figure 89 - Averaged spectra for 5µL DMMP applied to stainless steel (110µg/cm2).

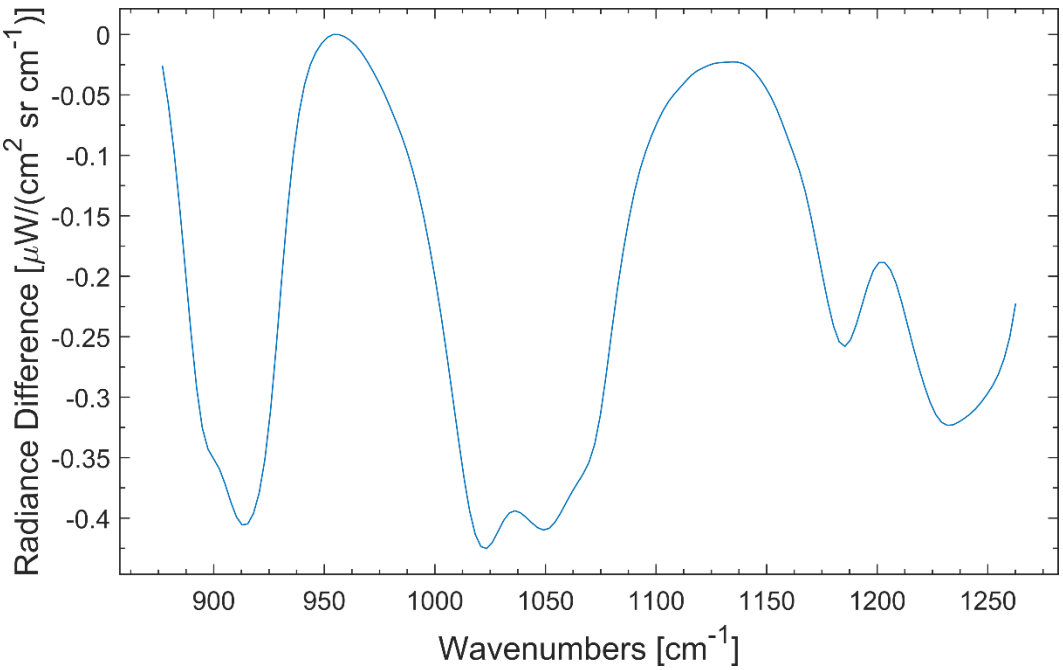

Figure 90 - Averaged spectra for 10µL DMMP applied to stainless steel by solution (222µg/cm2).

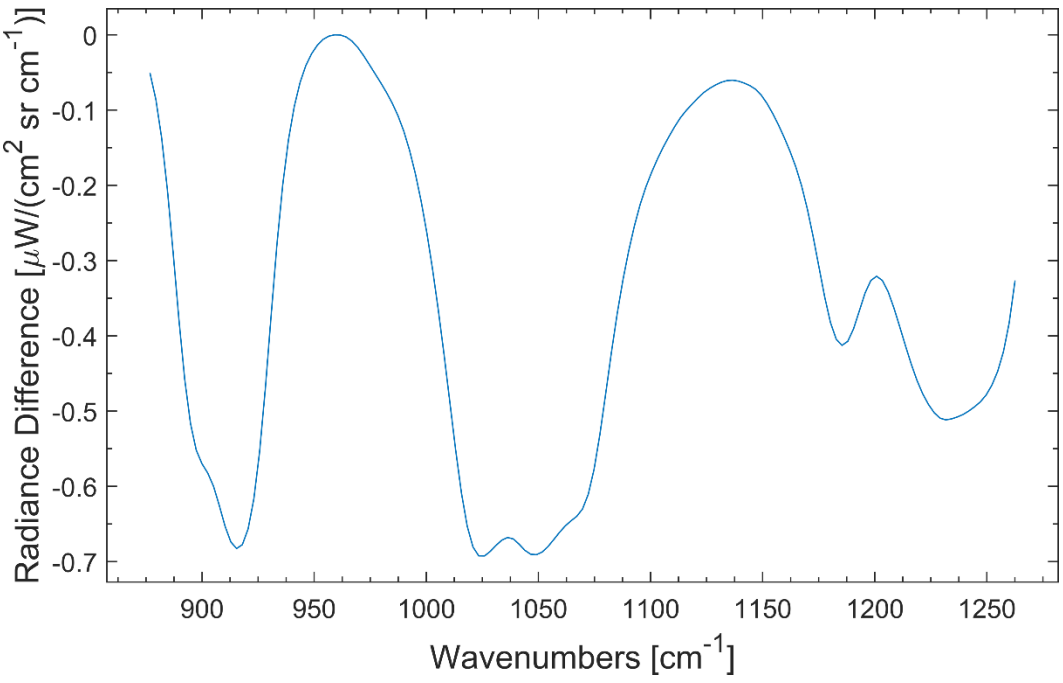

Figure 91 - Averaged spectra for 10µL DMMP applied to stainless steel by smearing (222µg/cm2).

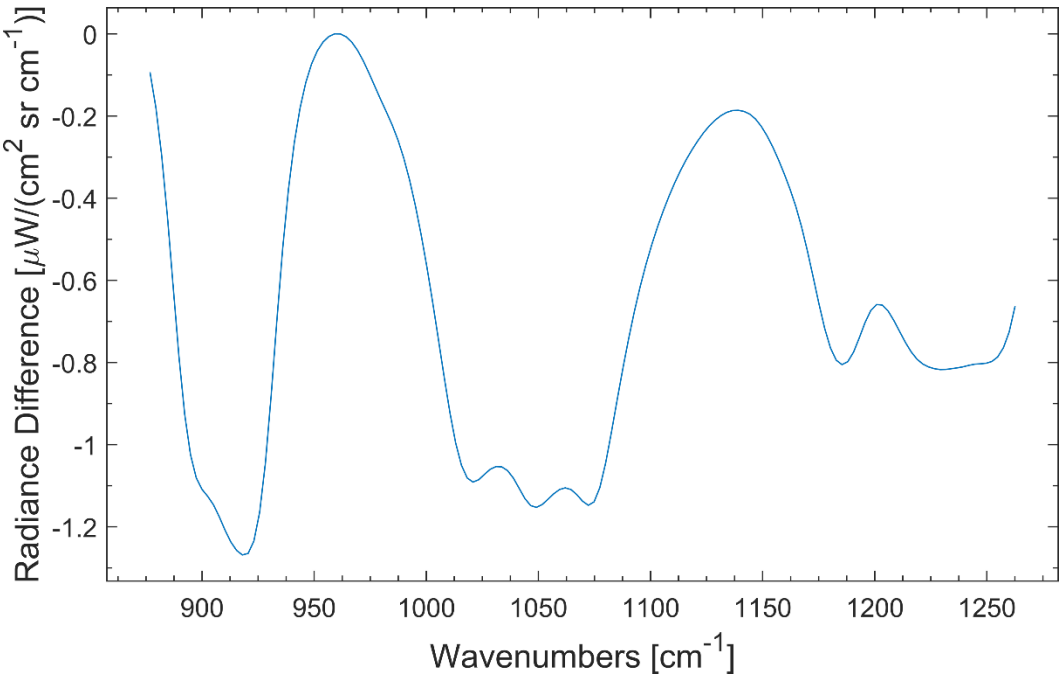

Figure 92 - Averaged spectra for 25µL DMMP applied to stainless steel (555µg/cm2).

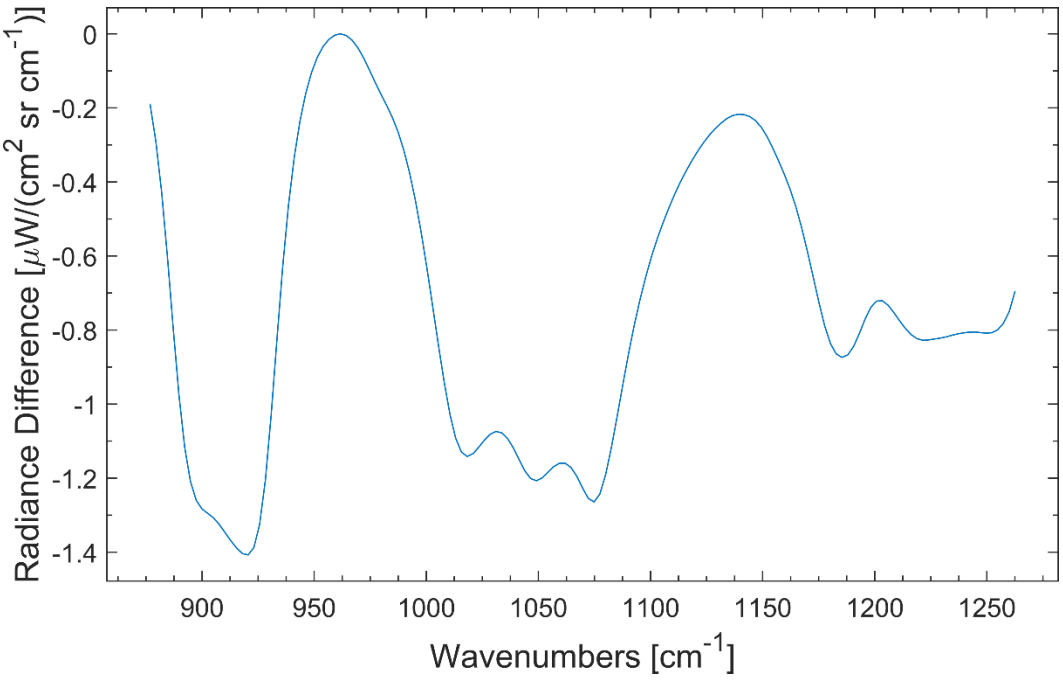

Figure 93 - Averaged spectra for 50µL DMMP applied to stainless steel (1110µg/cm2).

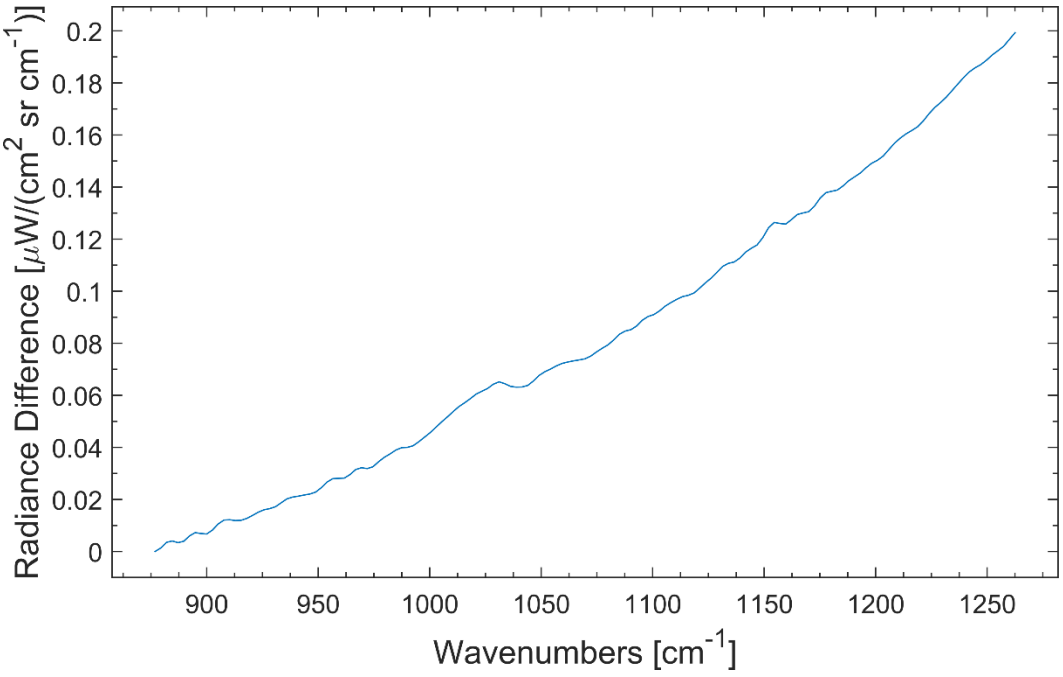

Figure 94 - Averaged spectra for 1µL DMMP applied to laminate (22µg/cm2).

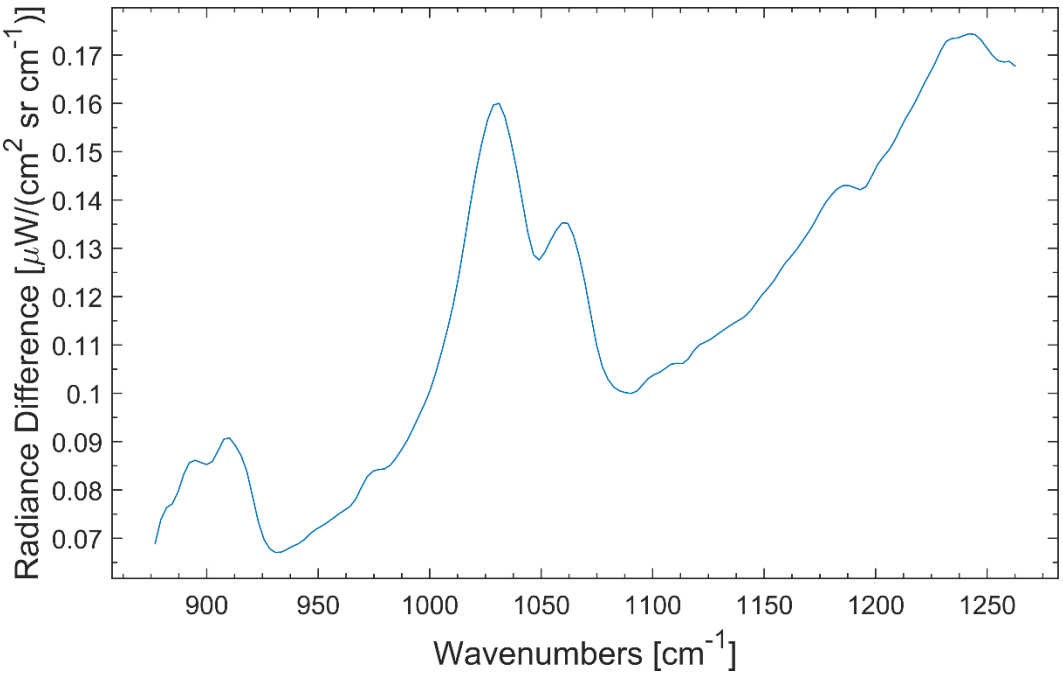

Figure 95 - Averaged spectra for 5µL DMMP applied to laminate (111µg/cm2).

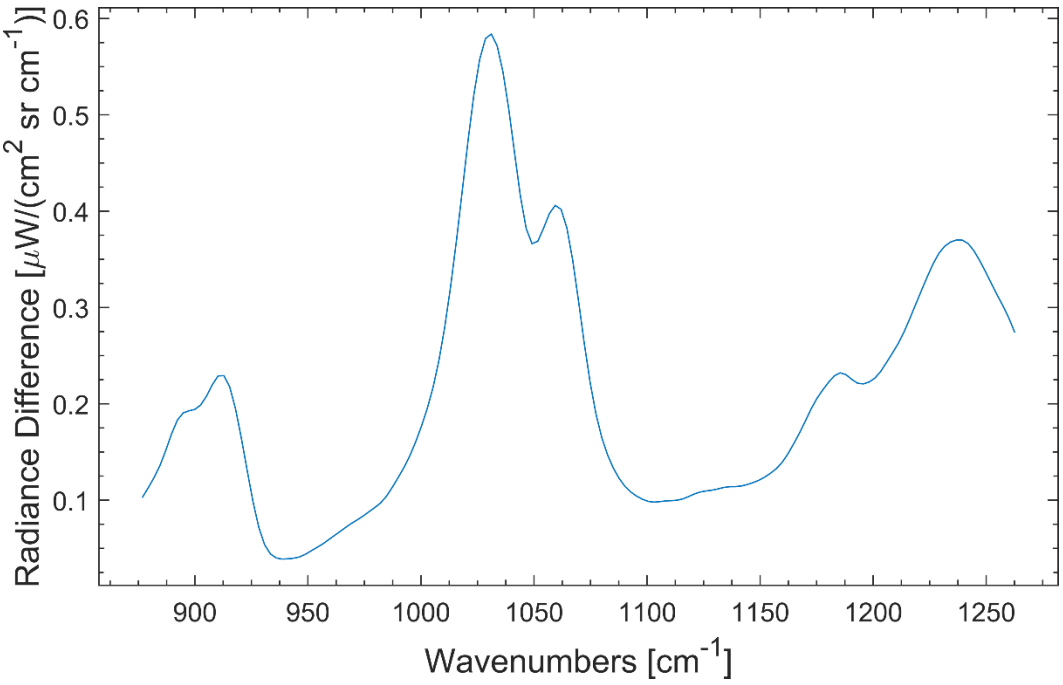

Figure 96 - Averaged spectra for 10µL DMMP applied to laminate by solution (222µg/cm2).

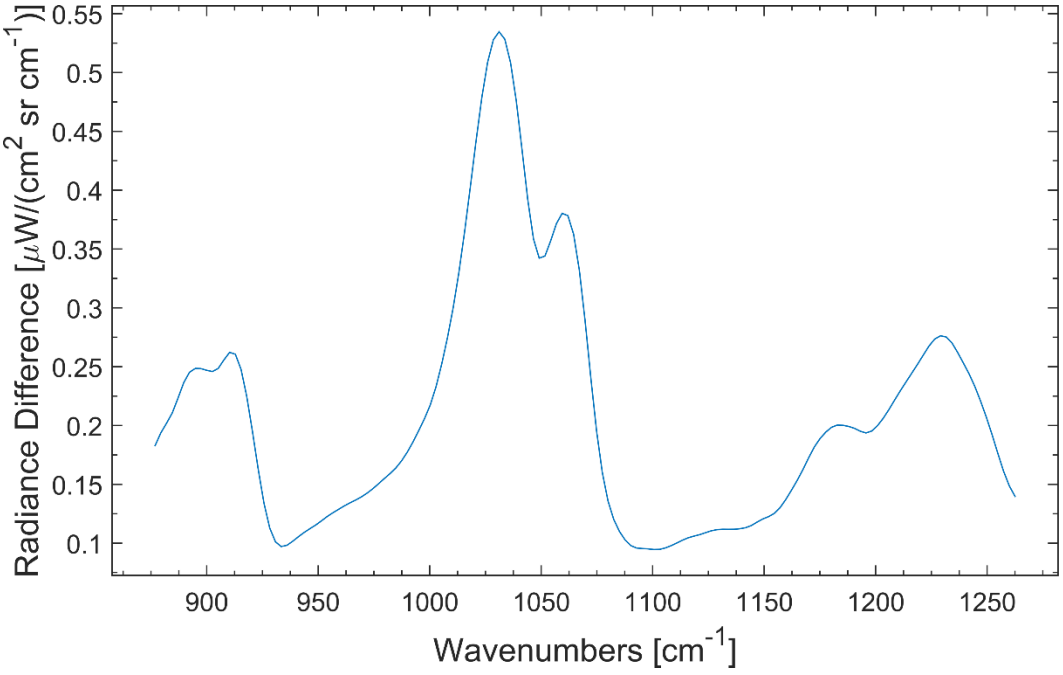

Figure 97 - Averaged spectra for 10µL DMMP applied to laminate by smearing (222µg/cm2).

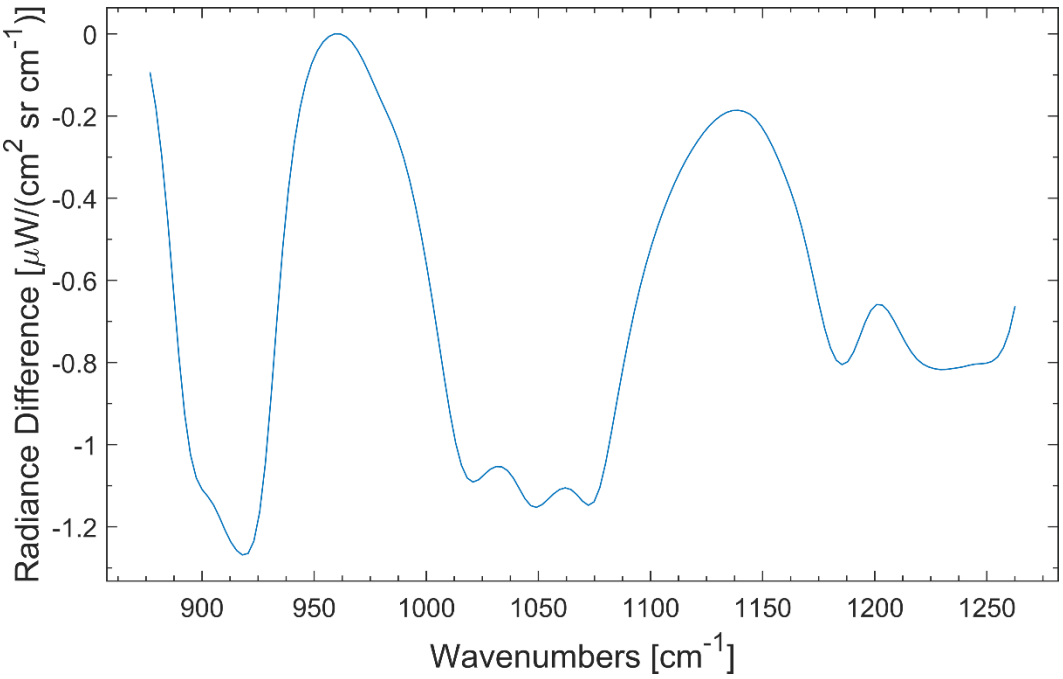

Figure 98 - Averaged spectra for 25µL DMMP applied to laminate (555µg/cm2).

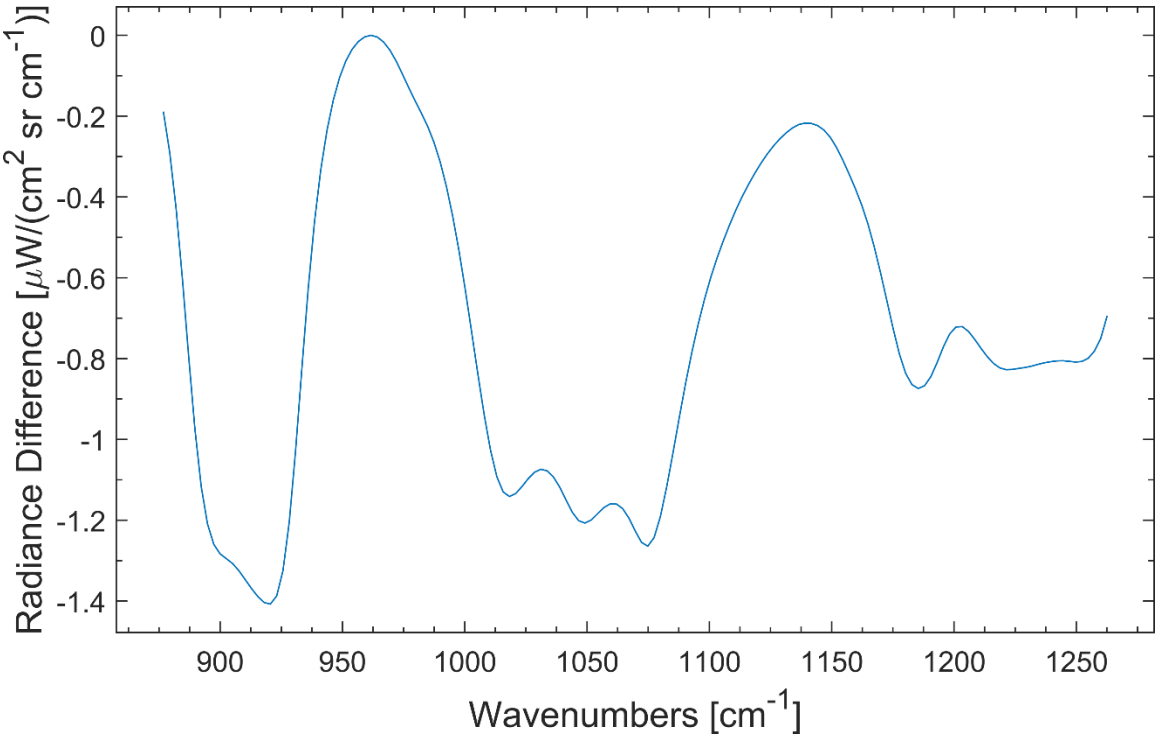

Figure 99 - Averaged spectra for 50µL DMMP applied to laminate (1110µg/cm2).

Bibliography

Carey, J. L., Dunn, C., & Gaspari, R. J. (2013). Central respiratory failure during acute organophosphate poisoning. *Respiratory Physiology & Neurobiology*, *189*(2), 403-410. doi:http://dx.doi.org/10.1016/j.resp.2013.07.022

Dutta, R. R., & Puzari, P. (2014). Amperometric biosensing of organophosphate and organocarbamate pesticides utilizing polypyrrole entrapped acetylcholinesterase electrode. *Biosensors and Bioelectronics*, *52*(0), 166-172. doi:http://dx.doi.org.wrs.idm.oclc.org/10.1016/j.bios.2013.08.050

Edelman, G. J., Gaston, E., van Leeuwen, T. G., Cullen, P. J., & Aalders, M. C. G. (2012). Hyperspectral imaging for non-contact analysis of forensic traces. *Forensic Science International*, *223*(1–3), 28-39. doi:http://dx.doi.org.wrs.idm.oclc.org/10.1016/j.forsciint.2012.09.012

Fu, G., Chen, W., Yue, X., & Jiang, X. (2013). Highly sensitive colorimetric detection of organophosphate pesticides using copper catalyzed click chemistry. *Talanta*, *103*(0), 110-115. doi:http://dx.doi.org.wrs.idm.oclc.org/10.1016/j.talanta.2012.10.016

Goltz, Mark, N.Dong Shik, Kim, Racz, LeeAnn. (2011). Using nanotechnology to detect nerve agents. *Air & Space Power Journal*, *25*(2), 56. Retrieved from http://search.ebscohost.com/login.aspx?direct=true&db=f5h&AN=64285931&site=ehost-live

Lee, J. H., Park, J. Y., Min, K., Cha, H. J., Choi, S. S., & Yoo, Y. J. (2010). A novel organophosphorus hydrolase-based biosensor using mesoporous carbons and carbon black for the detection of organophosphate nerve agents. *Biosensors and Bioelectronics, 25*(7), 1566-1570. doi:http://dx.doi.org.wrs.idm.oclc.org/10.1016/j.bios.2009.10.013

Liu, S., Yuan, L., Yue, X., Zheng, Z., & Tang, Z. (2008). Recent advances in nanosensors for organophosphate pesticide detection. *Advanced Powder Technology, 19*(5), 419-441. doi:http://dx.doi.org.wrs.idm.oclc.org/10.1016/S0921-8831(08)60910-3

Luckarift, H. R., Greenwald, R., Bergin, M. H., Spain, J. C., & Johnson, G. R. (2007). Biosensor system for continuous monitoring of organophosphate aerosols. *Biosensors and Bioelectronics, 23*(3), 400-406. doi:http://dx.doi.org/10.1016/j.bios.2007.04.023

Muñoz-Quezada, M. T., Lucero, B. A., Barr, D. B., Steenland, K., Levy, K., Ryan, P. B., . . . Vega, C. (2013). Neurodevelopmental effects in children associated with exposure to organophosphate pesticides: A systematic review. *Neurotoxicology, 39*(0), 158-168. doi:http://dx.doi.org/10.1016/j.neuro.2013.09.003

Musameh, M., Notivoli, M. R., Hickey, M., Huynh, C. P., Hawkins, S. C., Yousef, J. M., & Kyratzis, I. L. (2013). Carbon nanotube-web modified electrodes for ultrasensitive detection of organophosphate pesticides. *Electrochimica Acta, 101*(0), 209-215. doi:http://dx.doi.org.wrs.idm.oclc.org/10.1016/j.electacta.2012.11.030

Qin, J., Chao, K., Kim, M. S., Lu, R., & Burks, T. F. (2013). Hyperspectral and multispectral imaging for evaluating food safety and quality. *Journal of Food Engineering, 118*(2), 157-171. doi:http://dx.doi.org.wrs.idm.oclc.org/10.1016/j.jfoodeng.2013.04.001

Reusch, Willam (2013). "Infrared Spectroscopy." Michigan State University. Web. 18 Feb. 2015. <http://www2.chemistry.msu.edu/faculty/reusch/VirtTxtJml/Spectrpy/InfraRed/infrared.htm>.

SDBSWeb. *SDBS, Spectral Database for Organic Compounds,* AIST. Web. 18 Feb. 2015. <http://sdbs.db.aist.go.jp/>.

Simonian, A. L., Good, T. A., Wang, S., & Wild, J. R. (2005). Nanoparticle-based optical biosensors for the direct detection of organophosphate chemical warfare agents and pesticides. *Analytica Chimica Acta, 534*(1), 69-77. doi:http://dx.doi.org.wrs.idm.oclc.org/10.1016/j.aca.2004.06.056

Smith, Brian C. (2011). *Fundamentals of Fourier Transform Infrared Spectroscopy*. Boca Raton, FL: CRC Press.

Stout, D. M., Bradham, K. D., Egeghy, P. P., Jones, P. A., Croghan, C. W., Ashley, P. A., Pinzer, E., Friedman, W., Brinkman, M. C., Nishioka, M. G., and Cox, D. C. (2009). "American Healthy Homes Survey: A National Study of Residential Pesticides

Measured from Floor Wipes." *Environmental Science & Technology* 43(12), 4294-4300. doi:http://pubs.acs.org/doi/abs/10.1021/es8030243

Stuart, Barbara. (1996). *Modern Infrared Spectroscopy*. David J. Ando (Ed.). New York: Published on Behalf of ACOL (U of Greenwich) by Wiley.

White, B. J., & Harmon, H. J. (2005). Optical solid-state detection of organophosphates using organophosphorus hydrolase. *Biosensors and Bioelectronics, 20*(10), 1977-1983. doi:http://dx.doi.org.wrs.idm.oclc.org/10.1016/j.bios.2004.08.019

REPORT DOCUMENTATION PAGE

Form Approved
OMB No. 074-0188

1. REPORT DATE *(DD-MM-YYYY)*	2. REPORT TYPE	3. DATES COVERED *(From – To)*
26-03-2015	Master's Thesis	October 2013– March 2015

TITLE AND SUBTITLE

Hyperspectral Imagery for Large Area Survey of Organophosphate Pesticides

5a. CONTRACT NUMBER

5b. GRANT NUMBER

5c. PROGRAM ELEMENT NUMBER

6. AUTHOR(S)

Baseley, Daniel R., Captain, USAF

5d. PROJECT NUMBER
15V110

5e. TASK NUMBER

5f. WORK UNIT NUMBER

7. PERFORMING ORGANIZATION NAMES(S) AND ADDRESS(S)
Air Force Institute of Technology
Graduate School of Engineering and Management (AFIT/ENV)
2950 Hobson Way, Building 640
WPAFB OH 45433-7765

8. PERFORMING ORGANIZATION REPORT NUMBER

AFIT-ENV-MS-15-M-203

9. SPONSORING/MONITORING AGENCY NAME(S) AND ADDRESS(ES)
Environmental Protection Agency
National Homeland Security Research Center
26 West Martin Luther King Drive
Cincinnati, OH 45268
Matthew Magnuson
513-569-7321, magnuson.matthew@epa.gov

10. SPONSOR/MONITOR'S ACRONYM(S)

EPA/NHSRC

11. SPONSOR/MONITOR'S REPORT NUMBER(S)

12. DISTRIBUTION/AVAILABILITY STATEMENT
DISTRUBTION STATEMENT A. APPROVED FOR PUBLIC RELEASE; DISTRIBUTION UNLIMITED.

13. SUPPLEMENTARY NOTES
This material is declared a work of the U.S. Government and is not subject to copyright protection in the United States.

14. ABSTRACT

Current detection of organophosphate pesticides in residential settings involves taking swipe samples at locations of potential contamination and conducting lab analysis. This method provides results that are applicable only to the points where samples were taken. A standoff detection method utilizing hyperspectral imaging would allow for analysis of a larger area without the need for lab analysis. This report demonstrates a proof of concept experiment that shows the applicability of hyperspectral imaging for the detection of organophosphates. The differences in detection on reflective and non-reflective surfaces are also explored. To the author's knowledge, this research is the first to use the Telops longwave infrared hyperspectral imager to positively identify and locate dimethyl methylphosphonate on both reflective and non-reflective surfaces.

15. SUBJECT TERMS
(Fill in with pertinent terminology related to the topic of your thesis.)

16. SECURITY CLASSIFICATION OF:			17. LIMITATION OF ABSTRACT	18. NUMBER OF PAGES	19a. NAME OF RESPONSIBLE PERSON
a. REPORT	b. ABSTRACT	c. THIS PAGE			Willie F. Harper, AFIT/ENV
U	U	U	UU	113	19b. TELEPHONE NUMBER *(Include area code)* (937) 255-6565, ext xxxx (NOT DSN) (emailname@afit.edu)

Standard Form 298 (Rev. 8-98)
Prescribed by ANSI Std. Z39-18